THE UNIVERSITY *of* EDINBURGH

Cell patterning and neuronal network engineering on parylene-C:SiO_2 substrates

Mark A. Hughes

Doctor of Philosophy – The University of Edinburgh – 2014

Contents

Figures

Preface

The work contained within this thesis is my own and has not been done in collaboration, except where otherwise stated. No part of this thesis has been submitted to any other university in application for a higher degree.

Acknowledgements

I would like to thank my supervisors Professors Mike Shipston and Alan Murray for their enthusiastic guidance throughout. The Wellcome Trust funded this project via their clinical PhD program; itself delivered by the Edinburgh Clinical Academic Training (ECAT) program led by Professors Iredale, Walker, and Jackson.

Dr Andy Bunting was generous with his time and expertise regarding silicon semiconductor fabrication processes at the Scottish Micro-electronics Centre. Trudi Gillespie provided invaluable help, guidance, and advice regarding fluorescence microscopy. Andy Downes helped by performing atomic force microscopy and Raman spectroscopy measurements. Peter Duncan, Kyla Brown, Paul Brennan, Javier Tello, Alun Williams, and Neil Henderson helped by providing access to cell lines. The Shipston group at large, together with fellow ECAT trainees, provided advice, practical help, and encouragement.

Abbreviations

AFM	Atomic Force Microscopy
Ara-C	Arabinofuranoside
ATCC	American Type Culture Collection
BBB	Blood-Brain Barrier
BCI	Brain Computer Interface
Bio-MEM	Bio-microelectromechanical system
BSA	Bovine Serum Albumin
CAD	Computer Aided Design
CAM	Cell Adhesion Molecule
CELSRs	Cadherin EGF LAG seven-pass G-type receptor
CIF	Caltech Intermediate Form
CNS	Central Nervous System
CNT	Carbon Nanotube
CPU	Central Processing Unit
CVD	Chemical Vapour Deposition
DARPA	Defence Advanced Research Projects Agency
DC	Direct Current
DCC	Deleted in Colorectal Carcinoma protein (UNC-40/DCC)
DF	Differentiated
DIV	Days *in vitro*
DMEM	Dulbecco's Modified Eagle Medium
ECM	Extracellular matrix
EEG	Electroencephalogram
EGF	Epidermal Growth Factor
EGT	Evolutionary Game Theory
ES	Embryonic Stem
eV	Electron Volt
FBS	Foetal Bovine Serum
FGF	Fibroblast Growth Factor
FN	Fibronectin
FNIII	Fibronectin type 3
GDS II	Graphic Database System-II
GEO	Gene Expression Omnibus
GFAP	Glial Fibrillary Acidic Protein
GPa	Gigapascal
GSC	Glioma Stem Cell
HBEC-5i	Human Brain Endothelial Cell type 5i
HBSS	Hanks Balanced Salt Solution
HEK 293	Human Embryonic Kidney 293
HEPES	4-(2-hydroxyethyl)-1-piperazineethanesulfonic acid, buffering agent
HMDS	Hexamethyldisilazane
HRSEM	High Resolution Scanning Electron Microscopy
Ig	Immunoglobulin
IGF	Insulin-like Growth Factor
Ig SF	Immunoglobulin Super Family

ITGAV	Integrin αV gene
KS	Kolmogorov-Smirnov
LREC	Lothian Research Ethics Committee
LUHMES	Lund Human Mesencephalic cell line
MEA	Multi-electrode array
MECP2	Methyl CpG binding protein 2
MEMs	Microelectromechanical systems
mHypo-E N7	Embryonic Mouse Hypothalamus Cell Line N7
MAP2	Microtubule-Associate Protein 2
MSC	Mesenchymal Stem Cell
N2a	Neuro 2a cell line
NCAM	Neuronal Cell Adhesion Molecule
NEMs	Nanoelectromechanical systems
PAGE	Polyacrylamide Gel Electrophoresis
PAI	Parylene-C Adhesion Index
PDL	Poly-D- lysine
PDMS	Poly(dimethyl)-siloxane
PEG	Polyethylene glycol
PLL	Poly-L-lysine
PLO	Poly-L-ornithine
PNS	Peripheral Nervous System
RAM	Random Access Memory
RGD	Arginylglycylaspartic acid
ROI	Region of Interest
RPM	Revolutions Per Minute
SEM	Scanning Electron Microscopy
SEM	Standard error of the mean
siRNA	Small Interfering RNA
SRI	SiO_2 Repulsion Index
T3	Triiodothyronine
T4	Thyroxine
UCLA	University of California, Los Angeles
UD	Undifferentiated
UV	Ultraviolet
VN	Vitronectin
WT	Wild Type
XPS	X-ray Photoelectron Spectroscopy

Abstract

Cell patterning platforms support diverse research goals including tissue engineering, the study of cell physiology, and the development of biosensors. Patterning and interfacing with *neurons* is a particular challenge, being approached via various bioengineering approaches. Such constructs, when optimised, can inform our understanding of neuronal computation and learning, and ultimately aid the development of intelligent neuroprostheses. A fundamental pre-requisite is the ability to dictate the spatial organization and topography of patterned neuronal cells. This thesis details efforts to pattern neurons using photolithographically defined arrays of the polymer parylene-C, printed upon oxidised silicon wafers.

Initial work focused on exploring the parylene-C:SiO_2 construct as a wide-ranging cell-patterning platform, assessing cell adhesion from both substrate- and cell-centric perspectives. Next, the LUHMES (Lund Human Mesencephalic) cell line was used to explore the potential for construction of interrogatable, topographically-defined neuronal networks. In isolation, LUHMES neurons failed to pattern and did not show any morphological signs of cellular differentiation. However, in the context of a cellular template (the HEK 293 cell line which was found to pattern reliably), LUHMES were able to adhere secondarily on-chip. This co-culture environment promoted morphological differentiation of neurons. As such, HEK 293 cells fulfilled a role analogous to glia, dictating neuronal cell adhesion and generating an environment conducive to neuronal survival.

Neurites extended between islands of adherent cell somata. The geometry and configuration of parylene-C influenced the organisation of neurites. With appropriate designs, orthogonal neuronal networks could be created. The dominant guidance cue for neurite growth direction appears to be a diffusible chemotactic agent. HEK 293 cells were later replaced with slower growing human glioma-derived precursors, extracted during tumour debulking surgery. These primary cells patterned accurately on parylene-C and provided a similarly effective, and longer lasting, scaffold for neuronal adhesion.

Chapter 1 Introduction

1.1 Motivations for cell patterning

Cell adhesion is a critically important, multifaceted process that informs numerous functions necessary for life. Understanding and manipulating the mechanisms that dictate cell adhesion and behaviour on *synthetic* materials is similarly important. Cell patterning platforms, informed by (and informing) this understanding, support work in diverse research domains. For example, they facilitate the development of micro-scale biosensors and implantable bioelectronics (1), aid the investigation of fundamental aspects of cellular physiology (2), and can be adapted for tissue engineering purposes (3).

Why pattern *neurons*?

Interacting with engineered *in vitro* neuronal networks represents a unique opportunity to approach an exciting array of research questions. Engineered networks provide a platform to explore theories regarding information processing and computation in nervous systems (4), and have translational potential as lab-on-chip platforms for drug discovery (5). They are also relevant to neuroprosthetics, which are built on a foundation of sympathetic interaction between nervous systems and microelectronics (6,7). The fidelity of such interactions is enhanced as *in vitro* neuronal network engineering research progresses. Beyond neuroscience, insights derived from engineered neuronal networks serve to inspire novel biomimetic or heterotic[*] computing paradigms (8); potentially informing new computer architectures capable, for example, of sidestepping the Von Neumann bottleneck[†] by operating in a neuromorphic, asynchronous, parallel, and fault tolerant mode.

---

[*] Heterotic computing refers broadly to the concept of hybrid, mixed mode systems deployed for the purpose of unconventional computation.

[†] The von Neumann model describes an architecture for electronic digital computers in which an instruction fetch and a data operation cannot occur simultaneously because they share a common data communication system (bus). This shared bus between data memory and program memory results in a bottleneck which limits data transfer between the CPU and memory.

1.2 Cell adhesion

A balance between specific competitive binding, and non-specific repulsion, governs cell adhesion to an adjacent substrate. Specificity of cellular adhesion is controlled biologically by expression of cell surface receptors that bind with reciprocal ligands. In parallel, certain generic physico-chemical forces also inform and modulate adhesion (9).

1.2.1 Biological factors

Families of transmembrane cell adhesion molecules (CAMs) govern cell-specific mechanisms of adhesion. CAMs typically have three domains: an extracellular domain that interacts either with components of the extracellular matrix (ECM) or other CAMs, a transmembrane domain, and an intracellular domain that interacts with the cell's own cytoskeleton (see Figure 1-1).

Integrins, cadherins, selectins and the immunoglobulin superfamily (Ig SF) constitute the four primary classes of CAMs (with selectins found only on circulating cells and endothelium). CAMs can be modified by endo/exocytosis, by proteolytic mechanisms, or by conformational change of an adhesion receptor. Initially, CAMs are distributed randomly in the plasma membrane. Upon adhesion, receptor segregation results in formation of tight adhesive zones. Adhesion is modulated either by mobilizing receptors from cytoplasmic storage compartments or *de novo* formation of new receptors. Membrane receptors or ligands are often hidden within the glycocalyx[‡] and other membrane-anchored molecules can act either to attract or repel a cell from a given substrate. As such, the net effect of the glycocalyx is modulated by the presence of giant macromolecules in the ECM (such as fibronectin or hyaluronic acid) (10).

Integrins are the dominant group of transmembrane receptors mediating cell:ECM interactions (11,12). Expressed in most cell types, including neurons, they consist of non-covalently linked α and β subunits. Twenty-four different $\alpha\beta$ heterodimers are

[‡] Glycocalyx is a term describing all extra-cellular membrane-bound polymeric proteoglycans.

possible, each with their own ligand-ECM specificity (13). Integrin-mediated cell adhesion involves recognition of, and binding to, adhesive protein ligands in the extra-cellular environment. Binding of ligand to integrin results in signal transduction cascades causing changes in cell motility, differentiation, gene expression, and cell process outgrowth (14,15). Integrin activation may occur externally (by changes in integrin-binding monoclonal antibodies or alterations in extracellular ion concentrations) or internally by, for example, over-expression of the ras-related GTPase R-ras, which has been shown to increase integrin-dependent attachment to ECM ligands (16). Other cell surface molecules (e.g. receptor tyrosine kinases, G-protein coupled receptors) can also bind to or associate with integrins, resulting in activation of intracellular signal transduction cascades (17).

Ig SF CAMs are evolutionarily ancient and widely expressed proteins that share structural features with immunoglobulins, each possessing an Ig domain. IgSF members include proteins of the T-cell receptor complex, virus receptors, tumour markers, major histocompatibility class I and II molecules, and glycoproteins found principally in the nervous system.

The cadherin superfamily comprises over 100 members sub-grouped into classic cadherins, protocadherins, desmosomal cadherins, flamingo/CELSRs (Cadherin EGF LAG seven-pass G-type receptors) and FAT. A role for cadherins has been described in regulating contacts and signalling between neurons (18). Neuronal cell adhesion molecule (NCAM) is a member of the IgSF. The FNIII portion of the NCAM extracellular domain has been implicated in neurite outgrowth mechanisms (19). A role for Ig SF CAMS during neuronal network development has also been illustrated. Specifically, the contactin subgroup is important in the development of cerebellar granule cell networks (20).

Figure 1-1 Integrin-mediated cell adhesion to the ECM

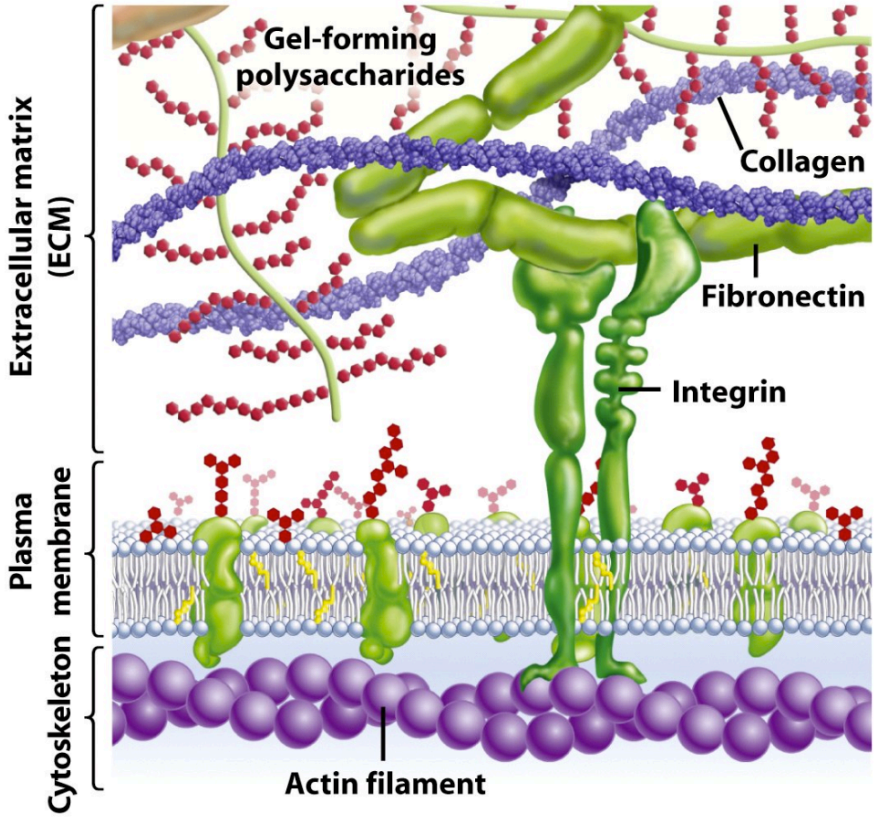

A transmembrane cell adhesion molecule (CAM, an integrin shown in this example) enables cell adhesion via binding to the ECM. Cell adhesion molecules typically consist of three domains. The extracellular component interacts either with other CAMs or with proteins in the ECM, whilst the intracellular component interacts with the cytoskeleton. Adapted from (21).

Extracellular matrix *versus* synthetic biomaterial

The ECM is a complex network of secreted proteins organized into a basement membrane or interstitial matrix. ECM proteins are multifunctional, providing structure and strength to a tissue and also informing cell behaviour via interactions with CAMs. Specific adhesion motifs (e.g. Arg-Gly-Asp [RGD]) on ECM molecules cooperate synergistically with other amino acid sequences (e.g. the PHSRN motif), to maintain effective spatial conformation of ligands and respective integrin receptors (22). The interface between a cell and an adjacent biomaterial is similarly dynamic and bi-directional. Receptor mediated cell adhesion to a biomaterial is also

mediated by CAM interactions (predominantly integrin) with absorbed ECM molecules such as vitronectin, collagen, or laminin (23-25).

1.2.2 Physico-chemical factors

Cell adhesion is also influenced more generically by surface energy, polarity, and 'wettability'. If a material is too hydrophobic, ECM molecules tend to be absorbed in a rigid denatured state. This conformation impairs access to specific binding sites (e.g. RGD-containing oligopeptides) and thereby impairs cell adhesion. Synthetic polymers used in medicine or biotechnologies are usually hydrophobic (with a contact angle ≥90°) so as to *intentionally* impair cellular colonization. A polymer surface can be rendered more hydrophilic by physical (e.g. irradiation by ions or ultraviolet light) or chemical (e.g. etching by treatment with acid or hydroxide) means (9). Such processes tend to increase the presence of oxygen-containing groups on the surface, increase surface free energy, and thereby enhance absorption of adhesion-mediating proteins. Complimentarily, such treatment can also result in a relative attenuation of the binding of characteristically cell repulsive proteins such as albumin, which preferentially adhere to less oxygenated and more hydrophobic substances (26).

Surface roughness

Macro-roughness (features ≥100 μm) can facilitate anchorage of a large implant in bone, for example. However, these irregularities are too large to be of consequence to an individual cell. Micro-scale roughness (1-100 μm) affects cells variably with no consensus as to whether the effects are positive or negative (27). Submicron surface roughness (100 nm-1 μm) also exerts variable effects, though positive pro-adhesive effects dominate. Nanoscale roughness (<100 nm), however, is considered to have a broadly positive effect on cell adhesion, growth, and differentiation; though specific findings remain cell and substrate specific (9,28,29). Synthetic materials fabricated so as to have nanoscale roughness closely resemble the structural scale and texture of the true ECM, mimicking the *in vivo* environment with its nanocrystals, nanofibers, and nano-sized folds of ECM molecules. As a consequence, cell-adhesion mediating molecules tend to absorb to these surfaces in a sympathetic geometric orientation,

giving cell adhesion receptors good access to binding sites. For example, carbon nanotubes (CNTs) are cylindrical carbon allotropes with diameter and length of the order of nanometres. CNT-coated surfaces have been shown to be highly biocompatible substrates, both in the context of biosensors and as a substrate for neuronal growth (30).

The characteristics of a synthetic substrate influence the formation of cell-to-substrate adhesion complexes, cell spreading, actin cytoskeleton arrangement, and downstream cell differentiation. As such, surfaces can be micro-patterned not only to inform cell adhesion, migration, and growth, but also to selectively induce differentiation into a given lineage. For example, mesenchymal stem cells (MSCs) cultured on different nano-patterned chemically modified gold surfaces can be directed towards a specific lineage. MSCs cultured on gold surfaces patterned with methyl groups (using dip pen nanolithography) remain undifferentiated, those on hydroxyl or carboxyl groups differentiate towards a chondrogenic (cartilaginous) phenotype, whilst those on amino groups are directed towards an osteogenic phenotype (31).

Cell behaviour is also impacted by the stiffness of a synthetic surface. Rat vascular smooth muscle cells are unable to form adhesion complexes when cultured on extremely soft matrices, whilst stiffer matrices promoted cell adhesion and actin cytoskeleton formation (32). Extremely soft matrices do not allow the necessary balance between cell tractional forces and ECM counter-resistance (33). The stiffness of a substrate also affects phenotypic destiny of cells during differentiation. Soft gels mimicking the mechanical properties of brain tissue prompted MSCs to differentiate towards a neuronal phenotype (suggested by upregulation of neuronal markers nestin and β-3 tubulin, and the development of dendritic extensions from cells). On harder gels MSCs developed a myogenic phenotype, whilst even stiffer surfaces promoted differentiation into an osteogenic cell type (34). This behaviour is likely mediated by focal adhesions which transduce the tensile characteristics of the microenvironment by influencing actin-myosin contractions. Related, is the finding that nanoscale

mechanotransductive stimuli (10-14 nm displacements at a frequency of 10 kHz, termed 'nanokicking') can be used to induce osteoblastogenesis in MSCs (35).

1.3 Neurons, networks and nervous systems

Cell theory dictates that the specialized function of cells and how they interact determines the function of a tissue. By consilience, aspects of brain function can be inferred by reductionist analysis of its component cellular units.

> *"'You', your joys and your sorrows, your memories and your ambitions, your sense of personal identity and free will, are in fact no more than the behaviour of a vast assembly of nerve cells and their associated molecules."*
>
> Francis Crick (36)

The 'Neuron Doctrine' posits the neuron as the key structural, developmental, and functionally independent unit of the nervous system, with a phenotype specialized for information processing and transfer. Consisting of soma, dendrites, and axon, neurons are electrically excitable and maintain ion concentration gradients across their membranes using metabolically driven ion pumps. Neurons communicate with one another by chemical and electrical signalling at synapses, and in this way form interconnected networks. The law of dynamic polarization describes the cell body and dendrites as receptor components, whilst the axon functions to communicate the cell's output. These fundamental principles were articulated over a century ago. Whilst core aspects of this dogma persist, the modern view of information processing in the nervous system involves far more extensive and intricate mechanisms (37).

1.3.1 Functional components

Neurons

Cajal developed the view of neurons as *individual*, polarized, functional units receiving signals via root-like dendrites and delivering outputs via the axon (38). Early electrophysiological studies suggested conductance of electrical activity along axons in an 'all or nothing' manner, with the self-propagating changes in cell membrane potential termed action potentials. This finding encouraged the idea that neuronal activity itself was similarly binary, with neurons either 'on' or 'off'. It later

became apparent that information processing is far more subtle and in fact involves graded electrical events (both in terms of amplitude and frequency) and also that these electrical responses occur in the context of additional spontaneous background activity (39).

Another layer of complexity comes from a plethora of neuromodulatory substances termed neuropeptides. These are capable of external reconfiguration of neuronal circuits, enabling different patterns of functional connections (40). Compared with the millisecond temporal scale of chemical synapses, neuropeptides remodel and tune circuit behaviour over minutes, hours, or even days. In addition, the intricacies of nervous system histo-architecture are becoming steadily better appreciated. It is now apparent that regions of conserved and consistent anatomical structure exist alongside areas determined by activity-related plasticity (41). Furthermore, the roles of a diverse mosaic of voltage-gated ion channels (varying by type, density, and property) are also being explored. Regulation of such channels (from transcription through to post-translational changes) informs how a neuron ultimately responds to its various inputs (for examples, see (42,43)).

Glia

Glia are non-neuronal cells found in nervous systems that have well described neuronal support roles (including structural, maintenance of homeostasis, myelin formation, and an immunological function). For some time, they were considered to have no place in neurotransmission and information processing. However, it is now apparent that some glial cells *do* modulate neurotransmission. Chemical synapses between neurons and oligodendrocyte precursor cells have been demonstrated (44) whilst astrocyes also communicate via glial transmitters and gap junctions. This represents a parallel and inter-related system of information processing, operating alongside and informing neuron-to-neuron interactions.

Together, these findings illustrate the naivety of the original simple and static models of nervous system connectivity. Neuronal properties are hugely variable, extensive, and sophisticated. Non-neuronal cells participate actively and cannot be considered merely supportive.

1.3.2 Information transfer

The transfer of information from one neuron to another occurs at synapses (45,46). The vast majority of synaptic transmission is chemically mediated. Pre-synaptic and post-synaptic membranes are separated by a synaptic cleft into which neurotransmitter is secreted. Neurotransmitter release (by exocytosis from the pre-synaptic membrane) is triggered by the arrival of an action potential. Depolarisation causes voltage-gated Ca^{2+} channels to open, consequent influx of Ca^{2+} ions, fusion of neurotransmitter-filled vesicles with the pre-synaptic cell membrane, and release of neurotransmitter into the synaptic cleft. Neurotransmitters then bind to specific receptors on transmitter-gated ion channels in the post-synaptic membrane. This results in a conformational change that opens the ion channel pore. The outcome is either a transient excitatory post-synaptic depolarization or inhibitory hyperpolarization (depending upon ion channel and neurotransmitter type). Most neurons in the CNS receive thousands of synaptic inputs, each activating various combinations of transmitter-gated ion channels. The post-synaptic neuron transforms these complex chemical and ionic signals into a simple output: the action potential. The process of converting many inputs into a single output constitutes a neural computation, of which a human brain performs billions per second in parallel. This computational process is fundamental to all neural information processing.

The ‘connectome’ and the ‘synaptome’ are terms relating to different scales of connectivity in nervous systems. Beyond the microscopic scale, we remain largely ignorant of the highly complex histoarchitecture of neuronal connections in the brain. The connectome includes macroscopic (major tracts, visible with human eye) and intermediate sized structures (visible with light microscopy). The synaptome refers to the smaller ultrastructural level (visible by electron microscopy). Despite extensive efforts, we do not currently possess complete connectome data for the nervous system of any species, with the exception of the nematode worm *C elegans* (47).

Work is underway to catalogue the human connectome with the overarching goal of building a realistic statistical model of the human brain (48) (www.humanconnectome.org/consortia/). Although tempting to embrace a wiring

diagram analogy, this is insufficient. The connectome and synaptome evolve dynamically during development, life, ageing, and in response to disease. The strength or weight of synaptic connections can be up or down-regulated, new synapses can be created and others eliminated, neurite architecture can be modified, and even neurons themselves can be created or destroyed.

The brain as a complex system

The human brain contains ~86 billion neurons (49) equipped with an average of ~7000 synapses per neuron (50), collectively performing $\sim 12 \times 10^{16}$ calculations or computations per second[§]. This is further complicated by multiple different neurotransmitters, the variable influence of glia, and a dynamic ultrastructure influenced by network activity. Given such complexity, a reductionist experimental approach is attractive (and has proved effective) in identifying most of the components and many of the interactions in nervous systems. However, there remains a paucity of convincing hypotheses regarding *system* properties. As the connectome and synaptome become better defined, it becomes critical to understand how information flows and is represented within neuronal networks, and how autonomous neurons operate collectively to generate behaviour.

1.4 Rationales for engineering neuronal networks

1.4.1 System level data from a controlled environment

Complex systems in which many interactions occur rapidly and simultaneously (e.g. financial markets, swarms of birds, nervous systems) are hard to explain. Whilst such systems can appear overwhelmingly complex from the outside, a few simple rules or laws of interaction may actually explain key aspects of their behaviour.

Considering the complex motions of a flock of birds (or a school of fish), individual and collective behaviour can be modelled closely by instigating just three simple

[§] This approximation is based on assumptions of 86 billion neurons, connected via 7000 synapses/neuron, firing at an average frequency of 20 Hz, resulting in 1.204×10^{16} firing events per second. In fact, synaptic density and neuronal number vary across individuals and by age. Moreover, this approximation fails to appreciate other 'calculations' attributable to glia:neuron interactions or neuropeptides, for example.

steering rules in a computer simulation: 'alignment', 'separation', and 'cohesion'. 'Alignment' dictates that a bird will turn so that it is moving in the same direction as nearby birds. 'Separation' means a bird will turn to avoid another bird in close proximity. 'Cohesion' means a bird will move towards other nearby birds. Using these rules, computer simulation can successfully reproduce what is superficially a highly complex behaviour (51). This is an example of emergence, whereby complex systems and patterns arise as a result of several relatively simple interactions. Extrapolated, biology can be considered an emergent property of the laws of chemistry, itself an emergent property of particle physics.

Determining the equivalent emergent 'rules of engagement' for cells of the nervous system is fundamental. Ideally this would be achieved by observing all component parts in action, whilst simultaneously quantitatively measuring different variables of electrical and chemical activity. However, the anatomically small scale and consequent inaccessibility restricts our ability to record and stimulate multiple neurons at the ideal spatio-temporal scale. Whilst single cell recordings *in vivo* have enhanced understanding of sensory responses in *single* neurons, they do not generate data regarding broader network activity, nor do they specify the spatial distribution and sub-threshold activity at synapses. Newer techniques are improving resolution. For example, combining whole cell patch-clamp recordings with two-photon microscopy to allow the *in vivo* measurement of calcium signals from dendritic spines of cortical neurons (52). Other techniques utilising optogenetics are also beginning to provide better *in vivo* system-level data (53), but have their own specific limitations (being highly invasive and requiring light to penetrate through tissues). Traditional dissociation procedures used for *in vitro* cell or organotypic cultures are undermined in this sense by the loss of resolution and connectivity that results from their preparation.

An alternative methodological approach is to study the behaviour of *in vitro* neuronal networks with *imposed* topographies. To be able to design, engineer and then interrogate simplified neuronal networks in this way promises to enhance understanding of how individual neurons cooperate as part of larger, more complex, networks.

Imposing a given topography upon cells requires the use of bio-patterning technologies. Collecting cellular activity data requires that the patterning platform be compatible with non-invasive recording techniques, such as multi-electrode arrays (MEAs). Stimulation and recording from sites within such controlled networks (at cellular or subcellular resolution) promises to provide important insights into emergent network behaviours. This approach is a core motivation for many researchers in the field of neuronal network engineering.

It is acknowledged that such networks have limitations. Most are two-dimensional and do not realistically reproduce several facets of the *in vivo* nervous system environment (e.g. inter-relationship with glia, blood supply dynamics). However, the ability to control or rationalise (or even remove) these factors is also the core strength; simplifying the system into one from which dynamic activity may be recorded and emergent properties extrapolated.

Reflexes proposed as a key CNS functional unit

Reflex arcs may underpin phylogenetically early neuronal networks that have since evolved to become the more complex nervous systems of higher animals. Even *Paramecium*, an eukaryotic single cell organism with no true nervous system, is equipped with an inherent 'object avoidance' reflex. The entire organism operates in a manner analogous to a single polarizable neuron. *Paramecium* moves through liquid by coordinated motion of cilia on the cell membrane. Ion exchange channels maintain a graded electrical potential across the plasma membrane. Mechanical stimulation caused by encountering an obstruction results in activation of membrane calcium channels (54). As a result, external calcium ions enter, with simultaneous efflux of potassium ions. This causes a reversal of cilia beating direction and the entire organism is consequently propelled away from the obstruction. This represents an elegant, simple, and efficient pro-survival reflex.

In larger organisms equipped with a nervous system, the reflex arc exists as a basic neuronal pathway mediating a useful action reflex (see Figure 1-2). Requiring a minimum of just two neurons, the reflex arc can be considered the simplest neuronal network.

Figure 1-2 The archetypal somatic reflex arc

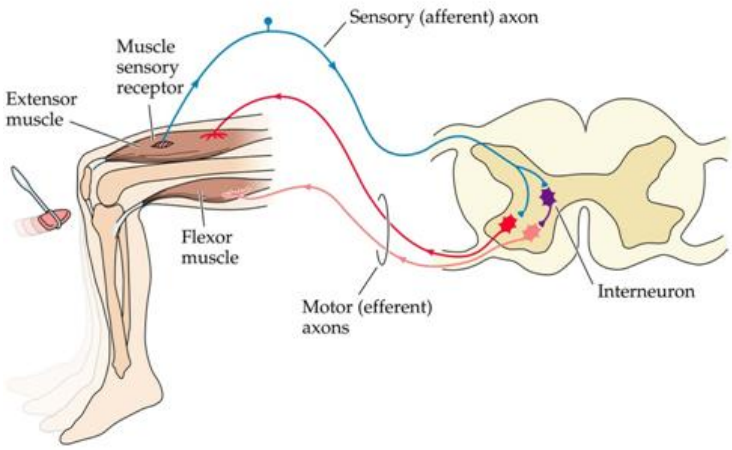

A reflex arc controls an action reflex. In their simplest form, one sensory and one motor neuron combine to mediate a response to an external stimulus. Image reproduced courtesy of Wikipedia commons.

Interestingly, primitive human reflexes seen transiently during normal neurodevelopment can re-emerge with the onset of neurodegenerative disease. For example, the palmar grasp reflex that disappears in children at five or six months can re-emerge in Alzheimer's disease and other fronto-temporal dementias (55). Similarly, central nervous system lesions tend to cause peripheral reflexes to be enhanced due to attenuated basal CNS inhibition. This implies a possible hierarchy of computation, with reflexes occupying the lower tiers. In complex, evolved nervous systems these basic stereotyped responses are normally obscured by higher centres, only to re-emerge in states of CNS damage.

Two conflicting selective pressures impact upon nervous systems: a need to minimise energy consumption and a need to generate adaptive behaviour in fluctuating environmental conditions. Neurons have a high-energy budget. A heavily energy-dependent computational mechanism would therefore be selected out, unless it conferred a *significant* survival advantage. Simple reflex arcs permit useful survival-enabling behaviours and rely on the activity of very few neurons. For example, the withdrawal reflex enables pro-survival behaviour using a network

consisting merely of a sensory neuron, interneuron, and motor neuron. This represents a highly energy efficient computational and behavioural mechanism. For these reasons, re-creating simple reflex arcs represents an interesting initial neuro-engineering goal, en route to creating more complex networks.

1.4.2 Disease modelling and pharmacological testing

Engineered neuronal networks can offer insights into neuropathological processes otherwise difficult to define. Changes in network connectivity have been described in neurological diseases including Alzheimer's disease (56) and epilepsy (57). Arguably, however, engineered networks may offer greatest utility in efforts to understand neuropsychiatric disorders. There has been no significant progress in the management of either depression or schizophrenia during the last twenty years, in stark contrast to other areas of medicine. One reason is a profound ignorance of the underlying pathophysiology or even the anatomical regions of disease. There is a growing consensus that diseases including mood disorders, schizophrenia, and autism may represent 'connectopathies' (58) which manifest as a result of aberrant connectivity at a scale that has, to date, eluded detection.

As such, neuronal network engineering offers an interesting disease modelling opportunity. *In vitro* networks that model such diseases also present an opportunity to utilise novel experimental interventions that might not be practical *in vivo*. For example, targeted exposure to a pharmacological agent via microfluidics (see 1.5.2).

1.4.3 Brain-computer interfaces

Engineering and interacting with *in vitro* neuronal networks has specific translational relevance in the field of brain-computer interfaces (BCI). A BCI is an artificial link between an organism's nervous system and the external world within which it behaves, augmenting the *status quo* where interaction with the outside world is enabled by motor, sensory, and special sensory systems. BCIs offer (and in select clinical contexts have already delivered, see Table 1) a method of overcoming disability caused by neurological or musculoskeletal pathology.

Pathology that interrupts any downstream component of behaviour is theoretically amenable to therapy with an output BCI. By recording from viable CNS domains, the region(s) of pathology are circumvented and a meaningful functional interaction with the outside world can be re-established. Proof-of-concept experimental motor BCIs are already in use in humans. By recording neuronal ensemble activity via a 96-channel micro-electrode array implanted in primary motor cortex, neuronal activity has been decoded to enable volitional movement of an on-screen computer cursor (59). This allowed a tetraplegic patient to interact with a computer operating system and to open his email, amongst other activities. The fidelity of this system has recently been improved, now enabling a robotic limb to perform three-dimensional reach and grasp movements (60).

Fundamentally, electricity governs the function of both computers and nervous systems. Whilst electrons move in solid-state lattices of microelectronic semiconductors, ions move in polar fluids to depolarize neuronal membranes. Joining these two systems together, so as to create an iono-electric interface, is a significant challenge. Table 1 details some key discoveries to date, afforded directly by exploring the interface between nervous and electrical systems.

A BCI requires real-time measurement of the electrophysiological state of the brain. Both invasive and non-invasive systems are in use, capable of recording different electrophysiological variables with varying fidelity. Cortically embedded intra-parenchymal electrode arrays are capable of recording electrical activity from individual neurons (and potentially even resolving sub-cellular components) and have been used effectively in humans and monkeys. Small (~20μm in diameter) electrodes are capable of detecting relatively large extracellular action potentials. Intra-cortically recorded signals have high fidelity but the stability of such recordings can be variable and may decay over time (61).

Intra-cortical electrode placement is inherently invasive. As well as causing local parenchymal damage, there is a risk of CNS infection. Placement of electrodes often results in activation and migration of microglia and astrocytes (62). Reactive gliosis around electrodes causes local neuronal cell death and impedes electrical conduction.

This is one reason why some human BCI devices suffer from gradual recording quality degradation over time, making long-term use (decades) unfeasible. Improved understanding of the abiotic:biotic / electrode:parenchyma interface will inform novel electrode probe architectures.

As such, developments in neuronal patterning and engineering work are particularly relevant to the advancement of BCIs. One approach that promises to ameliorate some issues (notably the need for long-term recording), utilises 'neurotrophic' electrodes. Here, the implantation dogma is reversed. Rather than positioning an electrode adjacent to cortical tissue, the neurotrophic electrode promotes neurite growth into a specialised glass recording chamber. These 'annexed' neurites become myelinated axons within months and in this context unwanted gliosis has not been encountered (63).

Advanced microelectrode arrays are also needed to improve the spatial resolution of recording from a given brain region of interest. Currently, vast amounts of electrical activity pass unnoticed. New technologies, such as micro-fabricated electrode arrays combined with neuronal patterning techniques, open the door to high channel, sub-cellular resolution recording. Such advances will ultimately improve the practicality, fidelity, and lifespan of human BCIs.

Table 1 A timeline of discoveries achieved by interfacing electricity with nervous systems. Adapted from (64).

40AD	Scribonius Largus, physician to Emperor Claudius, advocates the use electricity to treat headache by applying an electric fish (*Torpedo mamorata*) across the brow of sufferers.
1771	Italian physician Galvani publishes his discovery of bioelectricity, demonstrating that nerves and muscles of frogs are electrically excitable.
1790	Volta (developer of the electric battery, or voltaic pile) demonstrates that electrical stimulation of the auditory system can create the perception of sound.
1809	Using a voltaic pile and crude electrodes, Rolando pioneers direct electrical stimulation of the nervous system as a means of studying localization of brain function.
1874	Bortholow, an American physician, stimulates living human brain via a pathological skull defect to induce limb movements (ultimately resulting in seizure and death).
1884	Horsley, a British neurosurgeon, uses intra-operative cortical stimulation to localize epileptic foci in humans. Aided by Clarke, they pioneer the stereotactic technique; enabling use of a Cartesian coordinate system to target brain regions.
1924	Berger, a German physician scientist, records electrical activity from the human brain using a prototypic electro-encephalogram (EEG).
1929	Foerster, a German neurosurgeon, creates phosphenes (the sensation of seeing light without light entering the eye) by electrical stimulation of occipital cortex.
1930s	Penfield, a Canadian neurosurgeon, uses cortical stimulation in awake patients (during procedures to treat epilepsy) to map the motor and sensory homunculus.
1968	Brindley & Lewin, British physiologists, develop the first implantable cortical stimulator for restoration of visual inputs.
1969	House, an American otologist, develops the first wearable cochlear implant.
1970s	Vidal, a Belgian electrical engineer, coins the term brain-computer interface, in work part-funded by Defence Advanced Research Projects Agency (DARPA).
1978	Schmidt *et al.* demonstrate that monkeys can learn to voluntarily control the firing rates of neurons in primary motor cortex through conditioning.
1978	Dobelle, an American neuroscientist-entrepreneur, implants a single array input BCI into visual cortex, enabling a blind person to detect light again.
1989	Georgopoulos derives a mathematical relationship between electrical activity of single cortical motor neurons in monkeys and the direction in which they move their arms, paving the way for translational computer algorithms.
1980s	Kennedy and colleagues pioneer the development of the neurotrophic electrode
1998	Kennedy & Bakay implant neurotrophic electrodes in a human (with severe amyotrophic lateral sclerosis) that elicits signals of sufficient quality to re-establish some control over their environment.
1999	Dan *et al.* reconstruct moving images observed by cats, by recording from an electrode array embedded in the lateral geniculate body of the thalamus.
2000	Nicolelis *et al.* use multiple multi-channel cortical arrays to produce accurate real-time predictions of hand trajectory in primates.
2005	Work by Donoghue & Hochberg enables a tetraplegic patient to be the first to control, in near real-time and informed by visual feedback, a prosthetic robotic hand using a 96-electrode BCI implanted in primary motor cortex.
2012	Refinements in invasive motor BCIs enable human control of a robotic arm, allowing three-dimensional reach and grasp movements. One quadriplegic study participant is able to use the system to drink coffee from a flask.

1.4.4 Biomimetic brain-inspired computation

Turing's prediction of massive advances in computing power (dating back to the 1940s) has failed to materialise to the extent envisaged. This is explained in part by fundamental rate-limiting steps in computational architectures. Most computers work in a rigid, sequential, step-by-step, fault intolerant mode. By contrast, nervous systems operate with parallel, fluid, dynamic, interconnected neurons, and an inherent degree of fault tolerance. The brain has a computational robustness due to this distribution of processing. A computer's lack of parallelism is compensated in part by executing instructions exceedingly fast. However, there is a high tariff in terms of energy and time in shuttling data repeatedly through a central processing unit (CPU). The Blue Gene supercomputer (capable of performing 10^{16} computations/s) requires 1.5 MW to operate. The human brain which, by comparative models of analysis, also functions at a comparable 12×10^{15} bits/s, requires just 20-25 W[**]. The ability to build computational systems that are similarly energy efficient is unsurprisingly of great interest to industry.

For example, Boahen *et al.* try to reverse engineer computational strategies observed in living nervous systems in an effort to enhance computer power and efficiency, and move away from sequential von Neumann architectures (65). This neuromorphic approach is fundamentally restrained by our appreciation of computational mechanisms in real nervous systems. The construction and interrogation of engineered *in vitro* nervous systems is therefore key to informing and advancing these projects.

1.5 Cell patterning technologies

Cell patterning technologies are manifold and diverse. Several key performance measures require appraisal. Some are generic whilst others are context and goal-dependent.

[**] The average human male requirement of 2500 kilocalories/day equates to 0.0289 kilocalories per second. This translates to 121 joules per second or 121 W. The brain demands ~20% of cardiac output. As such, its power requirement can be grossly estimated as approximately 24.2 W.

Resolution: The resolution at which individual cells and subcellular components can be controlled is key. Importantly, this control may attenuate over time depending on the platform and cell type. This is particularly important for cells requiring time to mature into their final functional phenotype.

Cell behaviour: As discussed above, cell behaviour and phenotype can be influenced significantly by the interaction with an adjacent synthetic substrate. Undifferentiated cells are particularly susceptible to influence.

Dimensionality: Most cell patterning platforms are two-dimensional. In certain contexts, this is very restrictive (e.g. tissue engineering). The growing availability of technologies such as 3D printing, and the use of porous scaffolds (66), is enabling more three dimensional approaches.

Interface compatibility: Depending on the rationale for cell patterning, it is often important to *interact* with patterned cells (e.g. local exposure to pharmacological agents/specific growth media or, for electrically excitable cells, to record or stimulate action potentials). Certain platforms facilitate this whilst others are inherently restrictive. To be able to prospectively or retrospectively incorporate relevant interface technologies into a patterning platform may be key, depending upon its intended use.

For example, micro-electromechanical systems (MEMS) are extremely small mechanical devices driven by electricity; overlapping with the nano-scale equivalent, nanoelectromechanical systems (NEMS). Microfabrication techniques developed for semiconductor electronics have found utility for creating electrodes for electrophysiological measurements of cells. For example, adapted MEMs constructs combined with cell-communication via multi-electrode arrays (MEAs) allow multi-site cell stimulation and recording.

Practicality of fabrication process: This includes factors such as cost, potential for repeat use, potential for mass manufacturing, and turnaround time. The theoretical ideal is a low cost, reusable platform with rapid turnaround from design phase to readiness.

Biocompatibility: Certain cell patterning/interface projects are undertaken with the explicit aim of downstream *in vivo* use. These platforms must be mindful of broader biocompatibility issues from the outset, as certain components may be unsuitable or even toxic *in vivo*. For example, whilst platinum has several appealing characteristics for creating novel MEMs constructs (67), its overt toxicity *in vivo* (68) precludes its use in implants.

1.5.1 Neuron-specific considerations for patterning

Guidance of axons and neurites:

In vivo, orchestrated genetic programs (operating in concert with experience-based changes) enable neuronal cell bodies to locate correctly, form appropriate pathways, and reach precise targets. During development, neural stem cells generate daughter cells whose fate is regulated by developmental gene expression. Radial glial cells, for instance, provide a radiating fibre scaffold for cortex-bound daughter cells to migrate. Initially neurites grow out from the soma. One neurite becomes the dominant axon whilst others become dendrites. Fine structure depends upon environmental factors with neurons in different locations developing characteristic cyto-architecture and cell-to-cell connections.

Axons reach appropriate targets through a combination of cell-to-cell communication and cell-to-ECM communication. The growth cone of the neurite consists of flat sheets of cell membrane called lamellipodia from which extend filopodia. Integrins and other CAMs in neuronal growth cones dictate migration, adhesion, guidance, and outgrowth (69). Filopodia probe the environment seeking a suitable substrate upon which to take hold and advance the growth cone. Growth and adhesion occurs in the context of appropriate ECM proteins, along a haptotactic or chemotactic gradient (see Figure 1-3).

The laminar cytoarchitecture of cerebral cortex manifests due to appropriate neuronal migration. Radial migration occurs via somal translocation or locomotion (70) whilst interneurons migrate tangentially into neocortex (71). Distinct integrin receptor expression, combined with changing availability of ligands, allow cortical cells to manifest varying adhesive properties and to activate different intracellular signal

transduction pathways. As a result, different neuronal layers emerge. Other guidance mechanisms include chemotaxis (movement of a cell in response to a chemical concentration gradient) and galvanotaxis (where an electric charge is the orienting stimulus). Netrins[††] are an example of a chemotactic protein involved in axonal guidance. Netrins, mediated by UNC-40/DCC cell surface receptors, induce a growing axon to either move towards or away from a region of higher concentration (72).

These finely tuned *in vivo* mechanisms may inspire or inform techniques that can be used to gain control of neuronal behaviour *in vitro*, enhancing the topographic control and resolution of an engineered neuronal network.

Neuronal polarity:

Cell polarity broadly relates to spatial differences in structure, shape, and function and is seen almost universally across cell types. During neuronal differentiation, symmetry is broken and morphology alters dramatically to create two functionally and structurally distinct compartments (dendrites and axons) (73) (74).

From an electrophysiological perspective, neurons are polarised such that information flows in one direction (dendritic synapse → cell body → axon initial segment → axon → pre-synaptic terminal, see Figure 1-4). This unidirectional flow of information through an integrated network of neurons and glia is fundamental to nervous system function. Achieving appropriate polarity for an *in vitro* neuronal network is similarly critical. Functional polarity is dependent upon anatomical polarity, as manifest by the distinction between axonal and somato-dendritic domains. Experimental findings suggest that, during development, axon-dendrite differentiation is established through both extracellular cues and intracellular signalling pathways. Polarity is also seen at a sub-cellular level, with protein complexes, organelles, and ion channels found in distinct membrane regions or cellular compartments (75).

[††] Named after the Sanskrit word '*netr'*, meaning 'one who guides'.

Achieving appropriate polarity in patterned *in vitro* neuronal networks is a significant challenge. Differentiating neurons may possess the capacity to self-organise to establish appropriate polarity. Terminally differentiated cells, however, may require specific topographic (or other) guidance cues, or may in fact be incapable of retrospectively assuming appropriate polarity.

Figure 1-3 Schematics illustrating haptotaxis and chemotaxis.

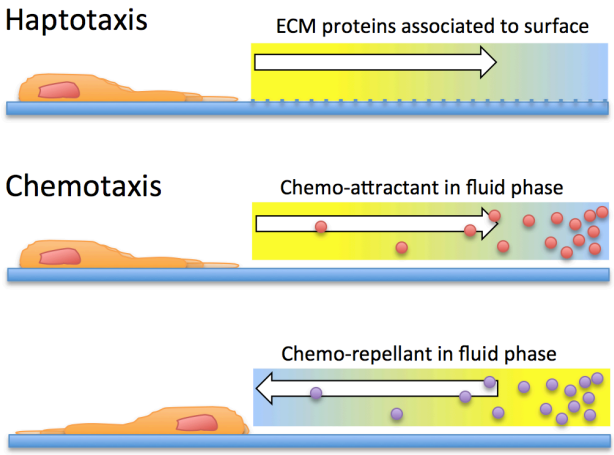

In haptotaxis, the direction of movement or growth of a cell occurs along a gradient of substrate-bound chemo-attractants. Such gradients occur naturally in the extracellular matrix or can be generated artificially on biomaterials. In contrast, chemotaxis involves a soluble chemo-attractant or chemo-repellent. ECM, extracellular matrix.

Figure 1-4 Neurons as anatomically and functionally polarised cells.

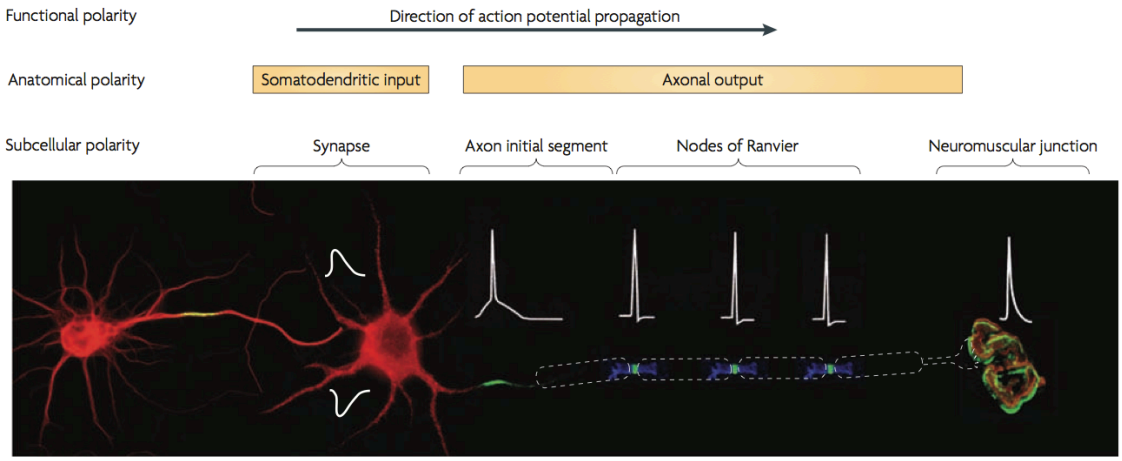

Functional polarity means that action potentials propagate in a single direction. At the axon initial segment, excitatory and inhibitory inputs are integrated. The action potential propagates along the axon with ultimate neurotransmitter release at the nerve terminal. Anatomic polarity manifests with the presence of a somatodendritic input domain and an axonal output domain. Various subcellular domains manifest further anatomic and functional polarity. Adapted from Rasband et al. (74).

1.5.2 Existing neuronal patterning platforms & technologies

The concept of building topographically defined neuronal networks *in vitro* is not new, with pioneering work first occurring over 40 years ago (76-78). Several diverse approaches have been employed to date.

Inkjet printing

Conventional inkjet printers pattern pigments by depositing 10-100 μm droplets under robotic control. The same principle can be used to pattern pro-adhesive cytophilic substances (e.g. collagen or poly-D-lysine) onto a cytophobic background (see Figure 1-5). Roth *et al.* used this technique to pattern smooth muscle cells (79). Collagen was printed using a commercially available inkjet printer with shapes including lines, dot arrays, and gradients. A cell line of smooth muscle cells, derived from rat aorta, was cultured on the patterned surface. This allowed the creation of viable cellular patterns with a resolution of 350 μm. More broadly, inkjet printing-based processes have also been used for biosensor development, DNA arrays, and free-form fabrication techniques to create polymeric scaffolds. Inkjet printing has also been used to pattern hippocampal rat neurons and glia (80). This approach is relatively inexpensive, repeatable, flexible, and high throughput. However, resolution is significantly restricted (to tens of μm at best) and only certain materials can be printed upon.

Micro-contact printing

Microcontact printing requires fabrication of an elastomeric[‡‡] stamp. First, silicon is coated with a pre-designed pattern of photoresist termed the 'master'. A liquid phase pre-polymer (often poly(dimethyl)-siloxane, PDMS) is applied to the master to form the stamp. After curing, the stamp is 'inked' with cytophilic proteins (e.g. fibronectin) and applied to a given surface. This approach has been used with various 'inking' molecules and a variety of different cell types including fibroblasts and keratocytes (81). Belkaid *et al.* used this approach to pattern neuronal cells (82),

[‡‡] An elastomer is a viscoelastic polymer.

using PDMS stamps 'inked' with poly-L-lysine and printed onto untreated coverslips. In this way, primary murine hippocampal and cortical cells were successfully patterned on linear and octagonal patterns (see Figure 1-6).

Microcontact printing is conceptually simple and reasonably flexible. However, after stamping, pattern degradation occurs rapidly due to protein denaturation. This demands rapid use of the printed substrates. Considering downstream integration of MEAs or other MEMs components, microcontact stamping is also problematic. Specifically, it is difficult to accurately align the stamp with pre-fabricated components on a separate substrate.

Physical immobilisation

Physical immobilisation techniques range from fabrication of three-dimensional structures (such as pillars or compounds) to trap cell bodies, to modification of surface topography or roughness to alter adhesion characteristics. Individual neurons from snail (*Lymnaea stagnalis*) have been immobilized using a microscopic 'picket fence' of polyimide on a semiconductor chip (see Figure 1-7). These physically restrained cells formed a network with post-synaptic excitation modulating the current of an on-chip transistor (83).

A similar approach utilised 'nanopillar' arrays (84). Here, in an effort to reduce neuronal migration on patterned substrates, arrays of vertical nanopillars (dimensions 150 nm × 1 μm) were created by ion beam platinum deposition. Movement of neurons in contact with nanopillars was significantly restricted (see Figure 1-8).

Such immobilization methods tend not to rely on biological agents or activation of potentially short-lived chemical cues. However, fabrication processes for these bespoke micron scale surfaces are complex and expensive. Moreover, whilst physical immobilisation may serve to define the location of a cell body, there is limited control of *neurite* behaviour.

Figure 1-5 Cell patterning using inkjet printing

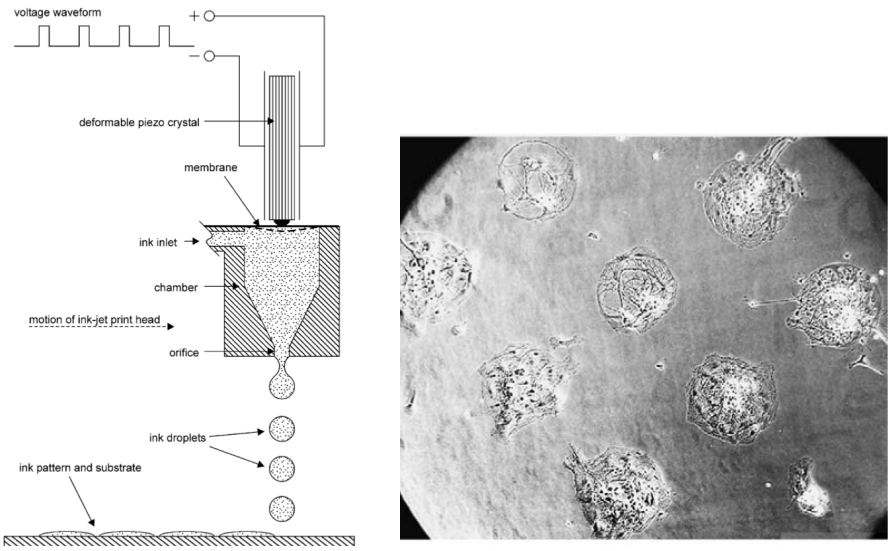

Left: Schematic illustrating the operation of an ink-jet print head. Microscopic droplets (10-100 μm in diameter) take a ballistic trajectory onto the underlying substrate. The print head moves robotically as droplets are ejected. Right: rat hippocampal cells adhering to 350 μm diameter printed islands of collagen/poly-D-lysine after 8DIV. Adapted from Sanjana et al. (80).

Figure 1-6 Microcontact printing for cell patterning

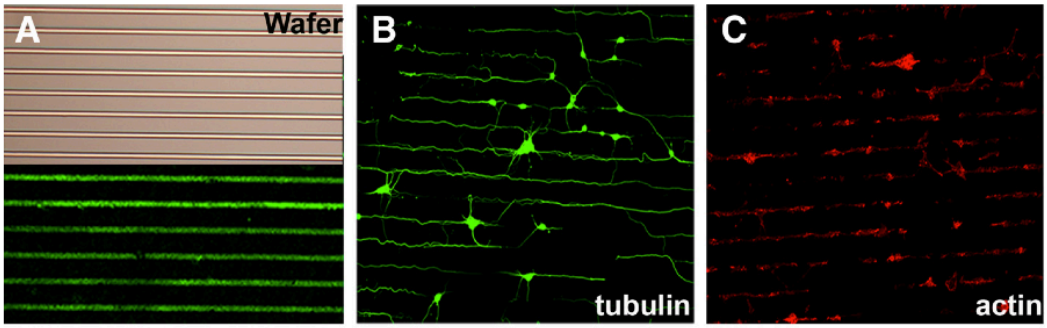

Example of microcontact printing to guide neuronal morphogenesis. A: (top) silicon master with 10 μm thick lines separated by a pitch of 60 μm, (bottom) uFITC-conjugated poly-L-lysine (PLL) lines printed onto coverglass. B:Primary hippocampal neurons plated on micropatterned PLL and immuno-stained for neuron-specific β-3 tubulin. C: Primary cortical neurons plated on micro-patterned PLL and stained for F-actin. From Belkaid et al. (82).

Figure 1-7 Physical immobilisation using a 'picket fence'

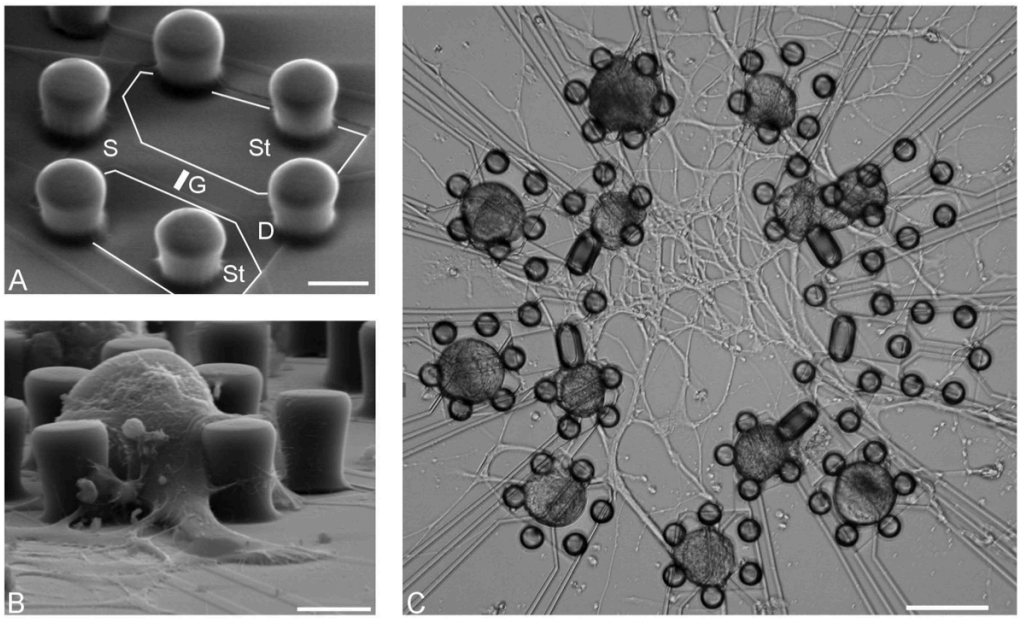

A: Electron micrograph of two-way contact with a 'picket fence' made of polyimide. Stimulator wings (St) and transistor (S, source; D, drain; G, gate) are marked (scale bar 20 μm). B: Post fixation electron micrograph of neuron in the picket fence after 3 days in vitro (scale bar 20 μm). C: Micrograph showing neuronal cell bodies in picket fences on a circle of two-way contacts connected by neurites after 2 days in vitro (scale bar 100 μm). From Zeck & Fromherz (83).

Figure 1-8 Physical immobilisation using a nanopillar array

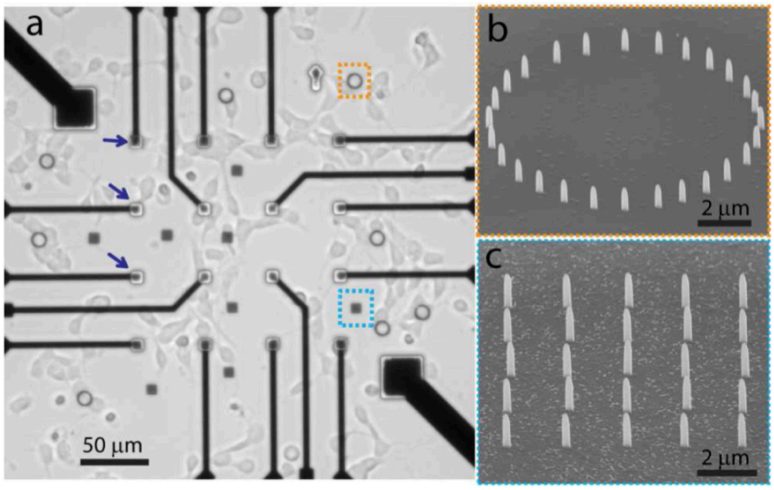

Cultured neurons on a nanopillar substrate, from Xie et al. (84). *A: Bright field image of neurons on MEA substrate with nanopillar arrays located both on the microelectrodes (blue arrows) and in open areas (orange and cyan squares). B: SEM image of ring-shaped nanopillar array. C: SEM image of 5×5 square nanopillar array.*

Topographic 'inducement'

In a similar vein, topographic variation of the substrate surface can be used to alter adhesive behaviour more subtly. Dowell-Mesfin *et al.* explored the impact of specific topographical cues on murine hippocampal neurons (85). Neurons were grown on poly-L-lysine coated silicon surfaces containing regions of pillars created using photolithographic processes. 1 μm high pillars with different width and inter-pillar spacing were assessed. Neurite growth on smooth surfaces was random, whilst growth on regions with pillars of width of 2.0 μm and inter-pillar distance 1.5 μm demonstrated more orthogonal growth (see Figure 1-9).

Carbon nanotubes also show potential as a means of harnessing control of aspects of neuronal adhesion. CNTs have unique mechanical, chemical, electrical and surface properties. They are electrically conducting, allowing excellent interfacial electrical impedance (86). Sorkin *et al.* cultured neurons on 20 μm CNT islands on a background of quartz (87). Their findings suggest that entanglement, a mechanical effect, may constitute an additional mechanism by which neurons (and possibly other cell types) anchor themselves to nano-roughened surfaces. Neurons bound preferentially to the rough-textured CNT islands, with processes curled and entangled amongst the nanotubes (see Figure 1-10).

Figure 1-9 Altering surface topography to inform neurite growth direction

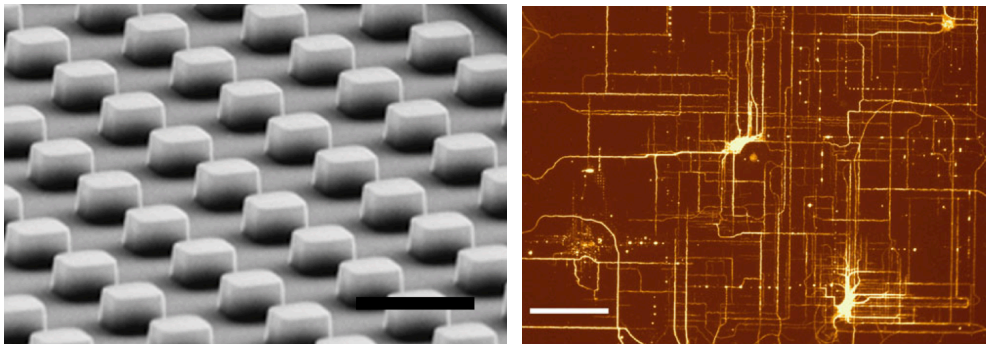

Left: High magnification SEM image illustrating an array of pillars with height 1 μm. Scale bar 4 μm. Right: Automated tracing of β-3 tubulin-labelled rat hippocampal neurons grown on the pillar array. Note the orthogonal growth pattern of neurites. Scale bar 100 μm. Adapted from Dowell-Mesfin et al. (85).

Figure 1-10 Entangling neurons with carbon nanotubes (CNTs)

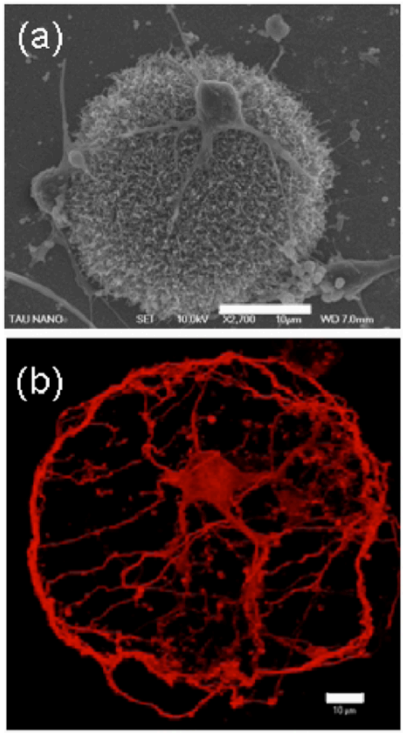

Rat neurons entangled on carbon nanotube (CNT) islands. A: High resolution scanning electron micrograph (HRSEM) image of 20 μm CNT island with 3 adherent, entangled neurons. B: Three-dimensional rendering of immunofluorescent confocal laser scanning microscope image of neurons atop a CNT island (immuno-labelled with β-3 tubulin). Scale bar 10 μm in both images. Adapted from Sorkin et al. (87).

Photolithographic methods

Photolithography involves transfer of geometric features from mask to substrate via illumination (usually ultraviolet light). A mask is designed using an appropriate computer-aided design (CAD) platform and fabricated on a quartz plate coated with a thin layer of non-transparent chromium that represents the desired geometric pattern. Standard feature resolution is 1 μm with some mask fabrication processes allowing sub-micron resolution. The substrate to be patterned is then coated with a thin layer of photoresist, a UV-sensitive polymer. The coated polymer is aligned and brought into close contact with the mask. An UV source is applied such that unprotected areas are irradiated and therefore become soluble and removable in a subsequent development step; leaving a representation of the mask pattern behind. This process has a long history of use in the fabrication of semiconductor devices, where silicon dioxide wafers are frequently used as a substrate.

Use of this technology in cell patterning has taken several different forms. For example, micro-patterns of different metal oxides can be created. Cells recognize the difference between aluminium, niobium, titanium, or vanadium-patterned regions and showed differential surface adhesion and migration behaviours (88). Interestingly, the preference of cells for surfaces composed of TiO_2, Nb_2O_5 and V_2O_5 correlated with an increased concentration of bound fibronectin.

Microfluidics

Microfluidics deals with behaviour, control, and manipulation of fluids at sub-millimetre scale. For cell patterning, a substance such as PDMS is used to create a network of three-dimensional channels that are flooded with a cell suspension or irrigated with cell adhesive molecules. Morin *et al.* (89) combined a 3D PDMS construct with a commercially available planar MEA. After flooding with either poly-L-lysine or laminin, neurons (derived from mouse or chick embryos) were successfully seeded into the microsystem.

This approach suffers from the same *post hoc* alignment issues as microcontact stamping. Moreover, the low flow in some microfluidic constructs can result in

insufficient diffusion of nutrients in growth media. Conversely, a clear benefit of such constructs is the ability to locally manage the fluid microenvironment, opening the way to targeted pharmacological therapy, for example.

Real-time manipulation

This technique involves dynamically altering the position and growth of cells in culture in real-time. Application of extracellular direct current across a culture is an example. In this way, Kim *et al.* utilised galvanotaxis to modulate the behaviour of *Tetrahymena pyriformis*, a eukaryotic ciliate (90). Taking advantage of a behavioural response called cathodal galvanotaxis, they were able to steer a cell in a given direction at a microchannel intersection by altering a two-dimensional electric field created using four electrodes.

As shown in Figure 1-11 and Figure 1-12, sophisticated additional apparatus is required, real-time cues need to be applied continuously to the culture, and specificity is undermined by the global nature of the manipulation.

Figure 1-11 Real-time manipulation of cells using galvanotaxis

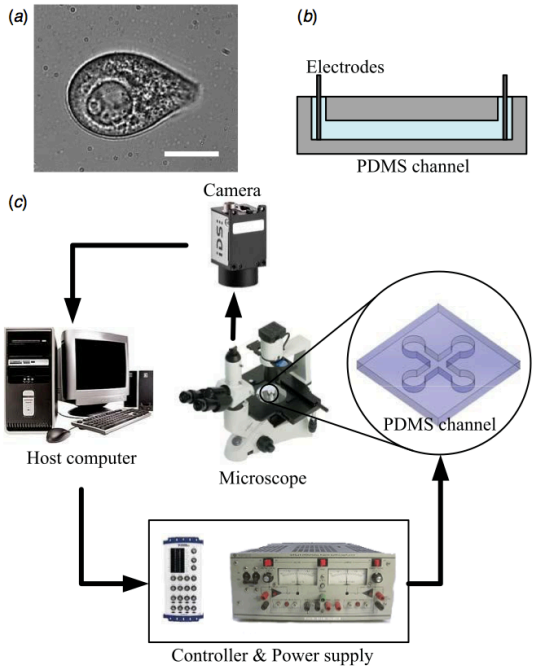

A: Photomicrograph of Tetrahymena pyriformis, scale bar 10 μm. B: Schematic of the PDMS micro-channel for galvanotaxis. Platinum wires at the ends of the microchannel are used as electrodes. C: The overall system for galvanotaxis, including microscope and PDMS channel as a galvanotactic chamber. From Kim et al. (90).

Figure 1-12 *Tetrahymena pyriformis* guided by polarity changes

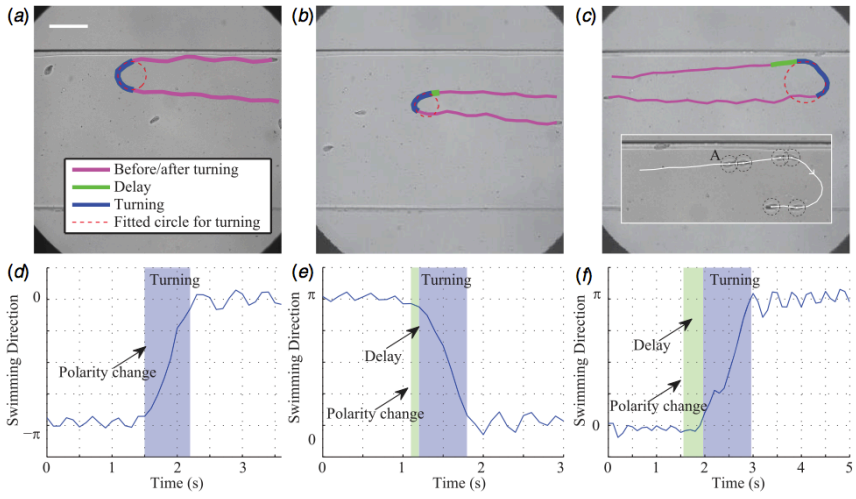

Swimming trajectory of Tetrahymena pyriformis can be influenced by polarity changes. Magenta, green and blue lines represent trajectory before/after turning, during delay, and during turning, respectively. Red dashed line represents the fitted circle for a cell's turning trajectory. Scale bar is 200 μm. From Kim et al. (90).

1.6 The parylene-C:SiO_2 platform

1.6.1 Motivation, inception and development

The parylene-C:SiO_2 platform at the centre of this project was originally born out of a desire to incorporate on-chip neuronal patch-clamps[§§] into a neuronal patterning platform (91). Equipped with an in-built array of patch-clamps recording from a patterned neuronal network, the goal was to record multiple whole-cell recordings simultaneously. Given that putative patch-clamp devices (or alternative MEA-type electrodes) were to be made using microelectronic cleanroom techniques, it was considered important that the cell-patterning platform itself be similarly compatible with cleanroom protocols and MEMS fabrication processes. Importantly, this combined approach also removes the alignment difficulties inherent to two-stage processes such as micro-contact stamping.

As photolithographic techniques are at the core of many microelectronic fabrication processes, the aim was to use similar processes to create a high fidelity neuronal patterning platform. Photolithographic patterning onto SiO_2 is a good candidate for this coalition: the fabrication processes mirror those for integrated circuit construction and the background SiO_2 facilitates incorporation of microelectronic recording or stimulation devices. Moreover, photolithography offers patterning at potentially very high resolution (sub-micron with high specification masks) and relatively low cost.

Delivopoulos *et al.* initially pursued this goal, aiming to photolithographically define cell attractant regions upon a cyto-repulsive background substrate. Early efforts using boron-doped SiO_2 patterned with photoresist were unsuccessful, with no reproducible cell patterning (92). Similarly, plain SiO_2 patterned with boron-doped SiO_2 also failed as a cell-patterning platform. Given the well-described relationship between hydrophobicity and cell repulsion, the next substrate tested (with a view to

[§§] Patch clamp recording is an electrophysiological technique allowing the study of excitable cell types. An electrode, typically in the form of a fluid filled glass micropipette with tip diameter of ~1 μm, is pressed against the cell membrane and suction applied. This forms a high resistance seal, enabling recording of currents measured across the membrane patch.

increasing the contrast between adhesion and repulsion), was the hydrophobic polymer parylene-C.

Parylene-C

Parylene is a trade name for a range of polyxylylene polymers. A number of different isomers and derivatives exist, with parylene-N, parylene-C, and parylene-D used most frequently. Parylene-C differs from parylene-N in the substitution of one of the aromatic hydrogen atoms with a chlorine atom (see Figure 1-13).

Parylene can be deposited by chemical vapour deposition (CVD), during which the monomer absorbs to a surface and then polymerises spontaneously to form high molecular weight linear parylene films (see Figure 1-14). Importantly, this process can take place at room temperature, making the coating process compatible with pre-fabricated *in situ* heat-sensitive components (93).

Due to low water and gas permeability, parylene has long been used to protect printed circuit boards. Being amenable to photolithographic etching processes, it has been deposited and patterned for use as dielectric layers in the semiconductor industry and as coatings for MEMs. Low water absorption, the highly homogenous nature of the parylene film, its thermal stability and high corrosion resistance, has also promoted use in vascular stents, cardiac pacemakers, and for insulating neural electrodes.

Parylene-C has also found utility in the context of cell patterning, sometimes incorporating the techniques described above. For example, parylene has been used as a peel-off stencil (94). Combined with inkjet printing to increase resolution, different proteins can be printed over different parylene fenestrations prior to peel-off (so called ‘print-and-peel’, see Figure 1-16). Furthermore, parylene can be deployed for use in microfluidic constructs. Ilic *et al.* (95) created high aspect ratio trenches by etching into silicon. Deposition of parylene over these trenches resulted in the uppermost aspect of the trench ‘pinching off’ to create a sealed microfluidic tube (see Figure 1-17).

Figure 1-13 Parylene subtypes and chemical structures

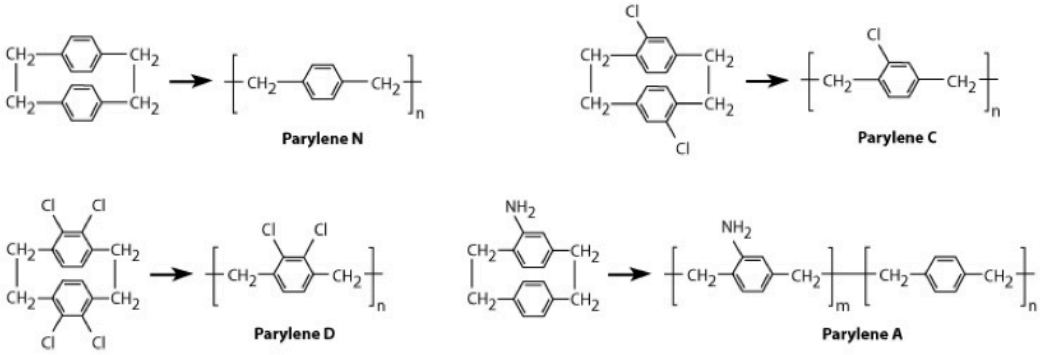

Figure 1-14 The parylene chemical vapour deposition process

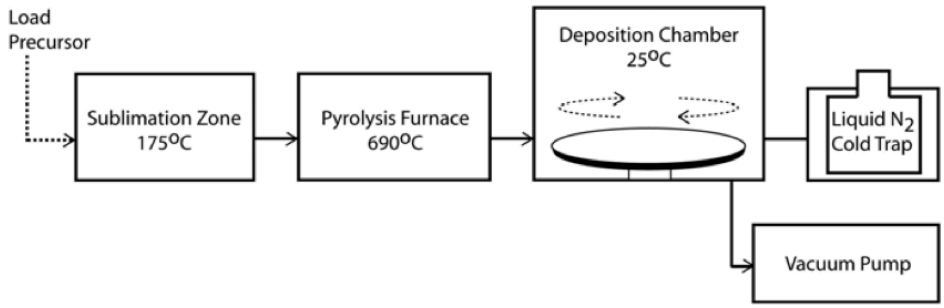

Chemical vapour deposition (CVD) of parylene-C. Precursor is loaded into a sublimation zone. Pyrolysis (of the sublimed form of the precursor into the reactive monomer) occurs in the furnace. The monomer polymerises spontaneously into parylene as it cools in the deposition chamber.

Figure 1-15 Fabrication of parylene-C stencils

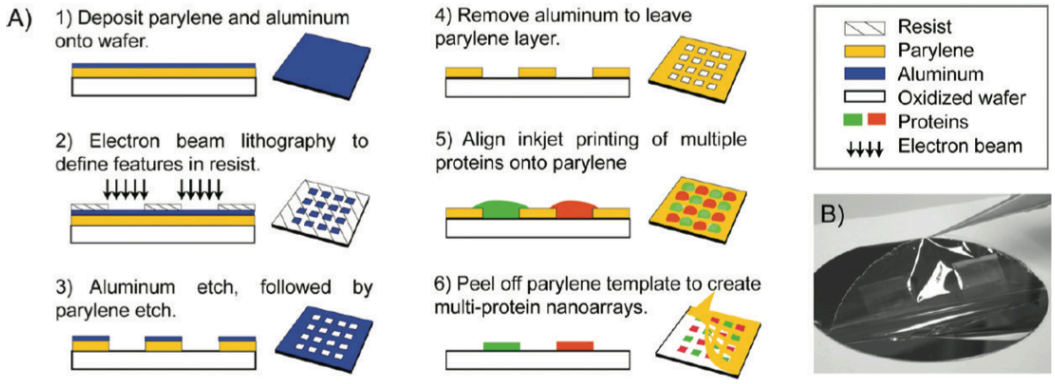

Parylene-C stencils can be used in a 'print-and-peel' process to create protein nano-arrays. A: Schematics illustrating the electron beam lithography process. B: Peeling off the parylene template from a 4" oxidised silicon wafer. From Tan et al. (94).

Figure 1-16 Combining 'print-and-peel' with inkjet printing

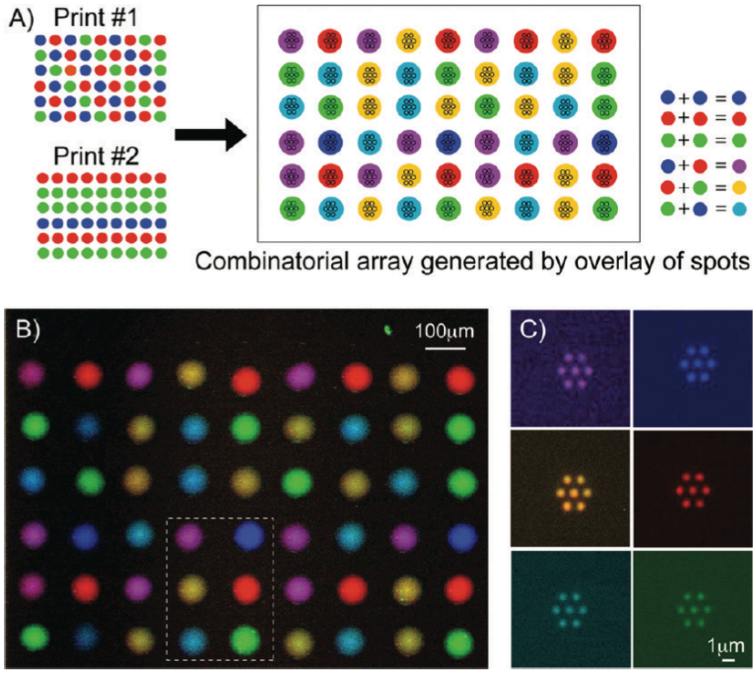

Using the 'print-and-peel' process to generate combinatorial biomolecular nanoarrays. A: Schematic showing superimposition of second inkjet print-run immediately over the first to generate six different combinations of antibodies. B: Pseudocolour merged fluorescence image showing the combinatorial array. C: Antibody nanoarrays of six different biomolecular combinations generated after parylene peel-off, corresponding to the demarcated region in B. From Tan et al. (94).

Figure 1-17 Using parylene for micro-fluidic constructs.

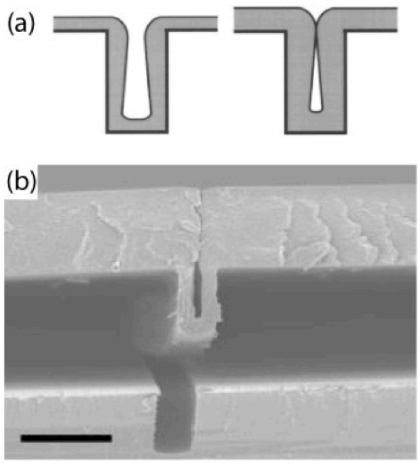

A: Non-conformal step coverage of the high aspect ratio deep trench. B: Cross-sectional scanning electron micrograph of a partially delaminated fluidic channel from a high aspect ratio silicon template. Scale bar: 5 µm. Adapted from Ilic et al. (95).

Parylene-C as utilised in the current platform

Parylene-C is hydrophobic with a baseline water contact angle of 87° (see appendix 6.1 for parylene properties). This contrasts with a baseline water contact angle of 43° for SiO_2 (96). On this basis, Delivopoulos *et al.* hypothesized that parylene-C would serve as a cell repellent surface, contrasting with cell adhesion on SiO_2. In fact, the *reverse* was noted. Murine hippocampal cells (a combination of neurons and glia) adhered to parylene-C but were repulsed from SiO_2. Figure 1-18 shows cultured cells (with the glial component stained with glial fibrillary acidic protein, GFAP). Here, background SiO_2 has been patterned with vertically aligned strips of parylene-C, both with and without a serum activation step. Importantly, the platform only served to pattern cells if the chips were incubated in foetal calf serum prior to cell culture. The use of serum in this way was motivated by its prior observed use for promoting cell adhesion to synthetic materials, but without a specific mechanistic hypothesis in mind.

In addition, the impact and importance of a number of other steps in the protocol (shown fully in Figure 1-19) remained undefined and unexplained. Several steps were included because they represented normal practice in photolithography and microelectronics clean room processes, not because of a hypothesis relating to cell patterning.

Figure 1-18 Murine hippocampal cells on parylene-C:SiO_2 substrates

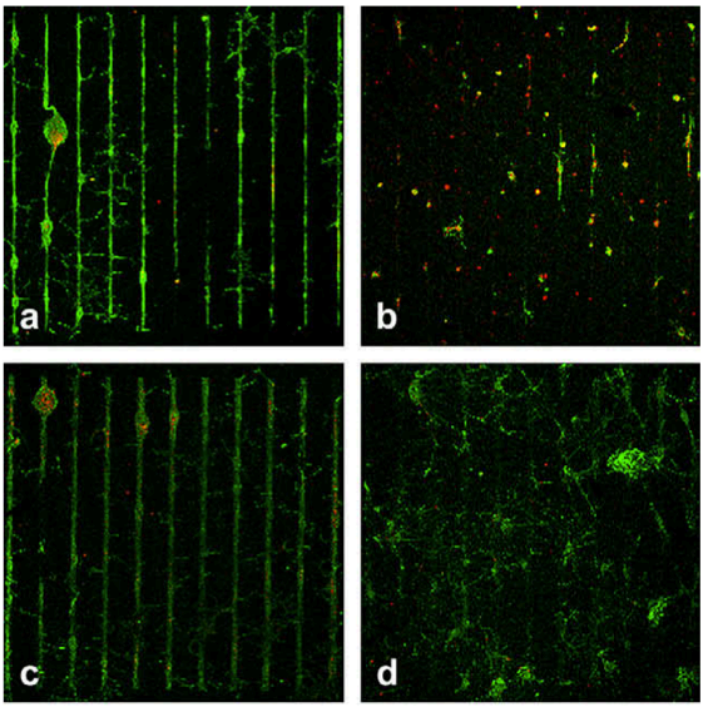

Early work using the parylene-C:SiO_2 platform. Culture examples of serum treated (A & C) and control (B & D) chips. Square area is 2000 μm × 2000 μm. In A and B, vertically orientated parylene strips (of width 20 μm) are separated horizontally by 180 μm of bare SiO_2. In C and D, parylene strips are 40 μm wide with 160 μm horizontal separation. Mouse hippocampal cells are stained with GFAP to label the glial component of the culture. From Delivopoulos et al. (91).

Figure 1-19 Fabrication and preparation of parylene-C:SiO_2 substrates

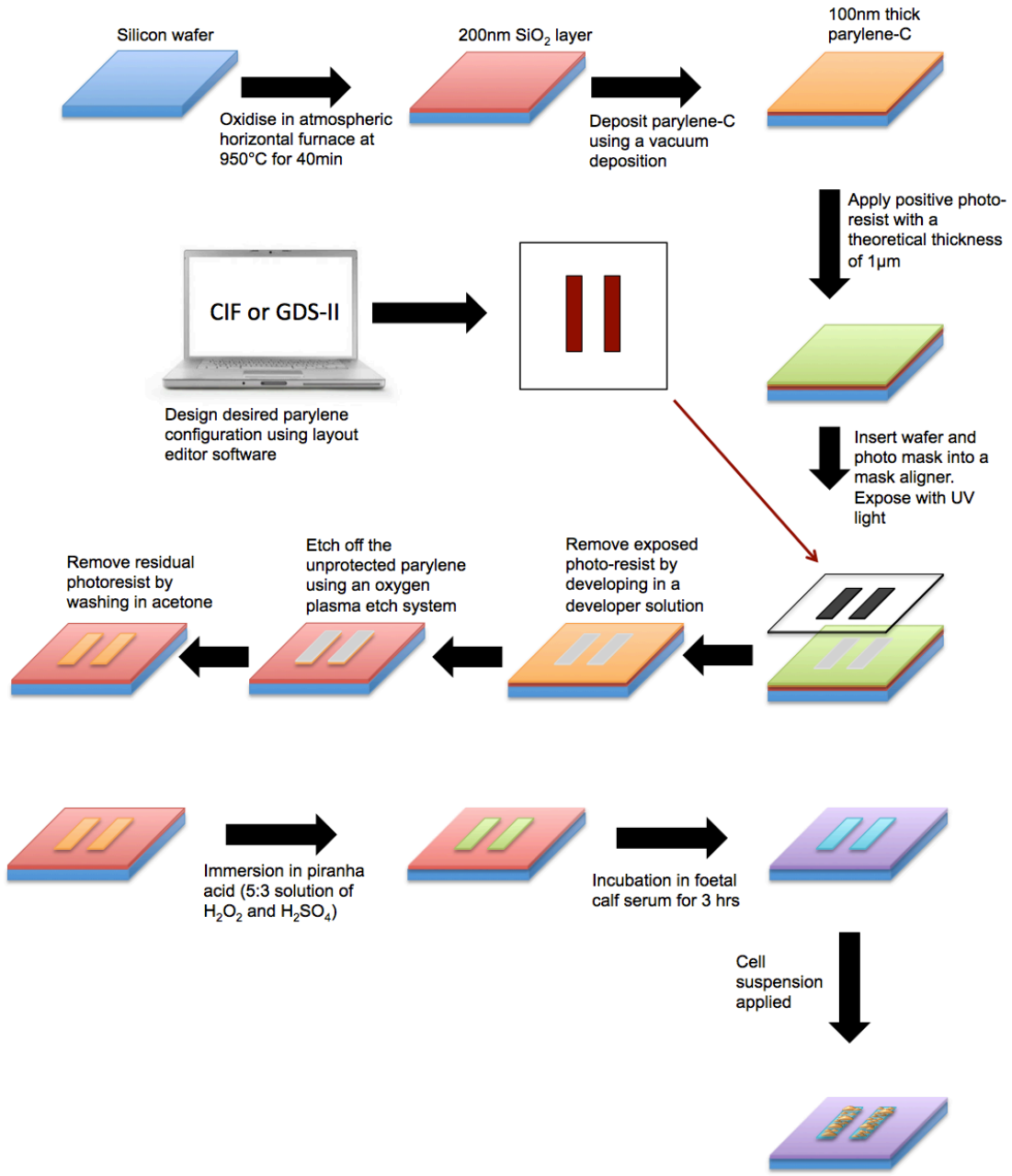

Schematic illustrating the entire process flow for design, manufacture, and activation of parylene-C:SiO_2 chips. Uppermost: Stages that occur in predominantly in a microelectronics clean room context. Lower figure: Stages performed in a biomedical sciences context. CIF, Caltech Intermediate Form; GDS-II, Graphic Database System-II. Both refer to file formats used for wafer design.

1.6.2 Unanswered mechanistic questions and hypotheses

Serum activation constitutes the key *biological* step in chip preparation. Prior efforts to dissect the mechanisms underpinning cell patterning on the parylene-C:SiO_2 platform focused primarily on the impact of this step, hypothesising that specific serum proteins bind to the two substrates in different quantities and/or conformations. As a consequence, 'serum-activated' SiO_2 and parylene-C surfaces present a repulsive or adhesive environment, respectively, for a cell coming into contact with the chip surface. Although protein elution of serum-incubated parylene-C and SiO_2 surfaces illustrated that parylene-bound vitronectin may (at least in part) be responsible for imbuing parylene with its adhesive character (91), this hypothesis remains undeveloped.

As described above, physico-chemical factors also impact significantly upon cell adhesion. The chip fabrication processes deployed prior to serum incubation may affect both wettability and surface roughness. To date this area has received limited consideration. For example, piranha acid is used routinely in semiconductor manufacturing processes to clean chips following photolithographic manufacture (ensuring removal of all organic material). This step was therefore incorporated into the current protocol with a motivation solely to clean, as opposed to any overt or suspected contribution to the cell patterning mechanism (Delivopoulos, personal communication). In fact, piranha acid is likely to have a significant impact on the surface properties of parylene-C and SiO_2; potentially altering surface roughness, surface chemistry, or contact angle, and therefore impacting downstream cell adhesion.

Contact angle

A polymer surface can be rendered more hydrophilic by treatment with acid or hydroxide. This process increases the presence of oxygen-containing groups on the surface, increasing surface free energy and thereby enhancing the *functional* absorption of adhesion-promoting ECM proteins. Given the pre-existing hypothesis that bound serum proteins enable adhesion and enforce repulsion to parylene-C and SiO_2 regions respectively, measuring the change in contact angle of the two different

surfaces during chip fabrication, cleaning, and activation may provide insights into downstream serum protein interactions.

Importantly, parylene-C has a baseline hydrophobic character. Therefore, chip fabrication and post-fabrication processes would need to induce a particularly large decrease in contact angle of parylene-patterned domains, if contact angle does indeed play a dominant role in cell patterning. Regarding the piranha acid stage, it is hypothesized that rather than simply cleaning the chip of unwanted organic matter, piranha acid in fact etches and oxidizes the two substrates so as to effect a marked contrast in serum protein binding characteristics, and hence produce cyto-phobic and cyto-philic domains.

Another relevant process is the oxygen plasma etching stage inherent to photolithography. Oxygen plasma removes unprotected parylene-C from the chip surface, creating the desired parylene pattern. An etch time of 120 s is considered sufficient to reliably remove 100 nm thick parylene-C right down to underlying SiO_2 (etch rate is ~100 nm/min). An important additional question, therefore, is whether this etch phase also impacts the underlying SiO_2, altering its surface chemistry and contact angle.

Surface roughness

Given that nanoscale roughness (<100 nm) is considered to have a positive effect on cell adhesion (because cell-adhesion promoting molecules absorb in a sympathetic geometric orientation on nano-roughened surfaces), it may be that contrasts in surface roughness also contribute to the effectiveness of the parylene-C:SiO_2 platform. If roughness does play a role, cyto-adhesive parylene might be expected to exhibit greater nano-scale roughness, whereas cyto-repulsive SiO_2 might have surface features that are less conducive to functional binding of adhesion-mediating molecules. Again, the processes utilised in chip fabrication may impact surface roughness at different stages. As with changes in surface wettability, it is worth appreciating that other adhesion mechanisms may dominate ahead of surface roughness, potentially leading to counter-intuitive findings.

Biological hypotheses

The behaviour of serum components during incubation with the chip surface is influenced by the aggregate effect of all upstream pre-serum processes, as discussed above. However, patterning may ultimately rely upon differential absorption of a key serum protein (or proteins) to parylene-C or SiO_2, which may in fact be de-coupled from the physico-chemical factors explored above.

Serum is a complex solution derived from blood. Whole blood is refrigerated and allowed to clot. After removing all cells by centrifugation, all clotting factors, and the clot itself, serum remains. Serum is a key component in the classical basal media used extensively for *in vitro* cell culture (usually foetal bovine serum (FBS) at a concentration of 5-20%). However, it remains poorly characterized, containing over 1000 different components including many proteins, electrolytes, lipids, carbohydrates, enzymes, hormones and other unidentified constituents (see Table 2). Producing FBS is costly and inefficient, with composition also varying somewhat from batch to batch. Identifying the protein(s) from this milieu that enable cell patterning would illuminate a key aspect of the cell patterning mechanism and would also supplant the need for serum, with its inherent heterogeneity between batches.

Table 2 Concentration of select components of foetal bovine serum. Adapted from *Price & Gregory* (97).

Description	Concentration
Inorganic salts	
Calcium	13.6 mg/100 ml
Chloride	103 meq/L
Inorganic phosphorous	9.8 mg/100 ml
Potassium	11.2 meq/L
Selenium	0.026 μg/ml
Sodium	137 meq/L
Other components	
Alkaline phosphatase	255 mU/ml
Blood urea nitrogen	16 mg/100 ml
Creatine	3.1 mg/100 ml
Total bilirubin	0.4 mg/100 ml
Glucose	125 mg/100 ml
Haemoglobin	11.3 mg/100 ml
Lactate dehydrogenase	864 mU/ml
Uric acid	2.9 mg/100 ml
Steroids and hormones	
Cholesterol	31 mg/100 ml
Cortisol	0.5 μg/ml
Follicle stimulating hormone	9.5 ng/ml
Growth hormone	39 ng/ml
Leutinizing hormone	0.79 ng/ml
Parathyroid hormone	1.718 pg/ml
Progesterone	8 ng/ml
Prolactin	17.6 ng/ml
Prostaglandin E	5.91 ng/ml
Prostaglandin F	12.33 ng/ml
T3	119 ng/ml
T4	12.1 ng/ml
Testosterone	40 ng/ml
Thyroid stimulating hormone	1.22 ng/ml
Selected proteins	
Total protein	3.8 g/100 ml
Albumin	2.3 g/100 ml
Insulin	10 mU/ml

Prior work by Delivopoulos, using X-ray photoelectron spectroscopy (XPS), showed that the chlorine and silicon peaks (which would be expected on untreated parylene and SiO_2, respectively) are attenuated after serum incubation (91). In parallel, a spectral peak at ~400 eV (characteristic of nitrogen) emerges on both parylene and SiO_2 surfaces following serum activation. The carbon specific C1s spectra of serum-treated parylene-C and SiO_2 reveal characteristic contributions attributable to the peptide bonds of adsorbed protein. In summary, these findings show that a layer of proteins is coating *both* surfaces.

Elution of these bound proteins, followed by polyacrylamide gel electrophoresis (PAGE), found both albumin and vitronectin bound to both parylene-C and SiO_2 regions. Parylene-C substrates displayed a slightly higher intensity band for vitronectin than did SiO_2, and no fibronectin was eluted from either substrate. The observed dominance of vitronectin ahead of other serum proteins is consistent with its recognised ability to bind competitively to polymer biomaterials according to a Vroman effect[***] hierarchy (98). These findings suggest a potential pro-adhesive role for the ECM protein vitronectin. However, its presence on both parylene and SiO_2 suggests that a functionally important conformational difference in protein structure may be important, as opposed to a simple difference in quantity. Specifically, vitronectin bound to SiO_2 may be denatured and therefore unable to engage with reciprocal cell membrane-bound integrins. This reinforces the potential utility of assessing surface characteristics that impact upon protein folding and conformation.

The binding of albumin (found at high concentrations in serum) tends to fall as surface hydrophobicity decreases, as albumin molecules bind preferentially to less oxygenated hydrophobic surfaces. Although found, after elution, to be present on both surfaces, albumin is a candidate for contributing to repulsion from SiO_2,

[***] The Vroman effect describes absorption behaviours of different proteins in solution onto a given surface. Different proteins diffuse to the surface at different rates. Highest mobility and more highly concentrated proteins arrive and absorb first, but may later be replaced by less mobile proteins that have higher overall surface affinity.

potentially via an unopposed repulsive effect when bound to SiO_2, versus repulsion *countered* by pro-adhesive vitronectin in the context of parylene-C.

It was initially hypothesised, therefore, that parylene-C manifests a cell-adhesive phenotype through absorption of vitronectin (which maintains a functional conformation) whilst background SiO_2 enables 'contrast' repulsion by exerting a dominant cytophobic effect mediated by bound albumin, with any co-bound vitronectin denatured and unable to promote adhesion. Furthermore, it is suggested that this protein binding arrangement is facilitated by differences in the surface roughness and contact angle of the two surfaces that follow chip fabrication processes.

If vitronectin indeed binds to parylene-C ahead of other serum proteins due to its hierarchical binding status, and the hypotheses above are correct, a solution devoid of vitronectin but containing another pro-adhesive protein may conceivably attain the ability to bind to parylene-C. This is important as it would afford the opportunity to define the patterned integrin-ligand, allowing the parylene-C:SiO_2 platform to be tailored to a specific cell type (with a known CAM profile).

Temporal considerations in substrate preparation

From both a practical and mechanistic standpoint, it is interesting to consider the time frame of effectiveness of different stages of chip fabrication and activation. Prior work with the parylene-C:SiO_2 platform illustrated that fabricated chips can be stored for years (prior to piranha treatment and serum activation stages) without detriment to their subsequent patterning ability. However, whether the effect of piranha acid is time-limited, and whether serum incubation needs to occur immediately after piranha treatment, remains unexplored. The duration of action of serum is less pertinent from a practical perspective as, from this point on, sterility is key and any delay would likely compromise this.

Generalizability of patterning

If cell adhesion to parylene-C relies, as hypothesised, on cells binding to a specific surface-bound protein or proteins, cell patterning will require the presence of

complimentary CAM receptors on the cell membrane. Given the heterogeneity of cell surface receptors across cell types, it is hypothesised that cell adhesion behaviours will therefore not be constant across cell types. Certain cells will lack the necessary CAM(s) and therefore be unable to engage with parylene-C-bound proteins.

Furthermore, some cell types possess the capacity to self-generate and exocytose ECM proteins (such as collagen or fibronectin) in significant volumes. This could obliterate patterning, as a cell-generated adhesion-promoting protein would coat both substrates indiscriminately.

1.6.3 Neuron-specific patterning questions

Neurons in isolation

Previous neuronal patterning was achieved in the context of primary murine hippocampal cells (i.e. a combination of both neurons *and* glia, see Figure 1-20) (91). It remains unknown whether neurons *in isolation* are capable of patterning on this platform, or whether it is glia that adhere to parylene-C and (by close association) enable neurons to similarly respect the underlying parylene geometry.

The presence of glia amongst patterned neurons, though better reflecting the *in vivo* environment, complicates downstream efforts to resolve, record, and stimulate individual neurons. It is therefore important to ascertain whether neurons are capable of patterning on-chip in isolation, or whether they are dependent on the presence of glia.

Directionality and polarity

Beyond dictating the location of adhesion for a neuronal cell body, the next challenge is to control the directionality of axonal and dendritic projections. Given the potential to alter the shape of patterned parylene-C, one interesting idea is whether projections from a differentiating cell might be guided haptotactically towards a given target, along a suitable parylene-C 'path'.

If this were found to be feasible, the issue remains of how to ensure that adjacent patterned neurons connect with appropriate axo-dendritic polarity. Differentiating neurons (whose cell bodies are anchored to specific locations) may possess the capacity to self organise their axo-dendritic projections and connections, though this needs to be explored. Identifying rules governing neurite organisation might open the way to manipulation, potentially enabling a greater degree of control over connectivity and polarity.

1.6.4 Rationale for choice of neuronal cell type

Primary murine neurons were used in previous parylene-C:SiO_2 patterning work (91,99,100). Similarly, this project will ultimately require a suitable model neuronal cell type for network engineering experiments. However, the initial priority is to better understand the cell patterning platform itself. This task does not justify the use of primary animal cells, given the anticipated requirement for multiple (potentially high throughput) trials. Specifically, given the National Centre for the Replacement, Refinement, and Reduction of Animals in Research guidelines (www.nc3rs.org.uk) such non-specific use of primary animal cells is unjustifiable. Furthermore, their use might even complicate the interpretation of certain cell patterning findings.

Similarly, anticipated downstream network engineering experiments are conceptually so reductionist, and so early-stage, that utilising primary animal cells here does not lend sufficient additional power as to justify their use. Instead, the American Type Culture Collection (ATCC, www.lgcstandards-atcc.org/) database of cell lines and hybridomas was interrogated for a suitable neuronal cell line. Important neuronal phenotypic characteristics were assessed, including electrophysiological behaviour, the capacity to form functional synaptic connections, and the protocol and time frame for neuronal differentiation.

The Lund Human Mesencephalic (LUHMES) cell line was identified as fulfilling requirements (101). This cell line was created by transforming committed neural precursor cells with *myc* oncogenes, thus ensuring immortalization and continuous proliferation. LUHMES are a sub-clone of the tetracycline-controlled, *v-myc* overexpressing, human mesencephalic-derived cell line MESC2.10 (originally from

Lund University, Sweden). A differentiation process, triggered by shut down of the *myc* transgene, results in the formation of post-mitotic neurons within 5 days (see Figure 1-21).

Differentiated cells develop one or two long projections (often >500 μm). Time-lapse imaging illustrates dynamic growth cone behaviour. Whole cell patch clamping illustrates the presence of functioning voltage-gated K^+ and Na^+ channels in differentiated cells. After 10 days of induced differentiation, cells generate spontaneous action potentials. As such, LUHMES have an appealing combination of characteristics, making them a viable choice for *in vitro* neuronal network engineering work. That said, little is known regarding their CAM profile.

Figure 1-20 High magnification examples of murine hippocampal cells cultured on serum-treated, parylene-C patterned SiO_2.

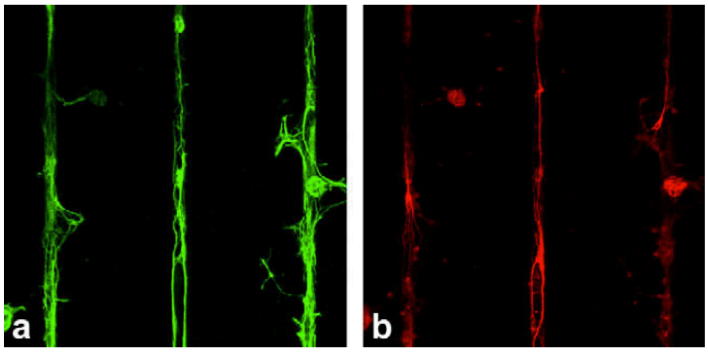

Square area represents 500 μm × 500 μm area with underlying parylene-C patterned as vertically orientated strips of width 20 μm. (a) Immuno-stained with GFAP to label glial component. (b) Immuno-stained with β-3 tubulin to label neuronal component. From Delivopoulos et al. (91).

Figure 1-21 The LUHMES neuronal cell line

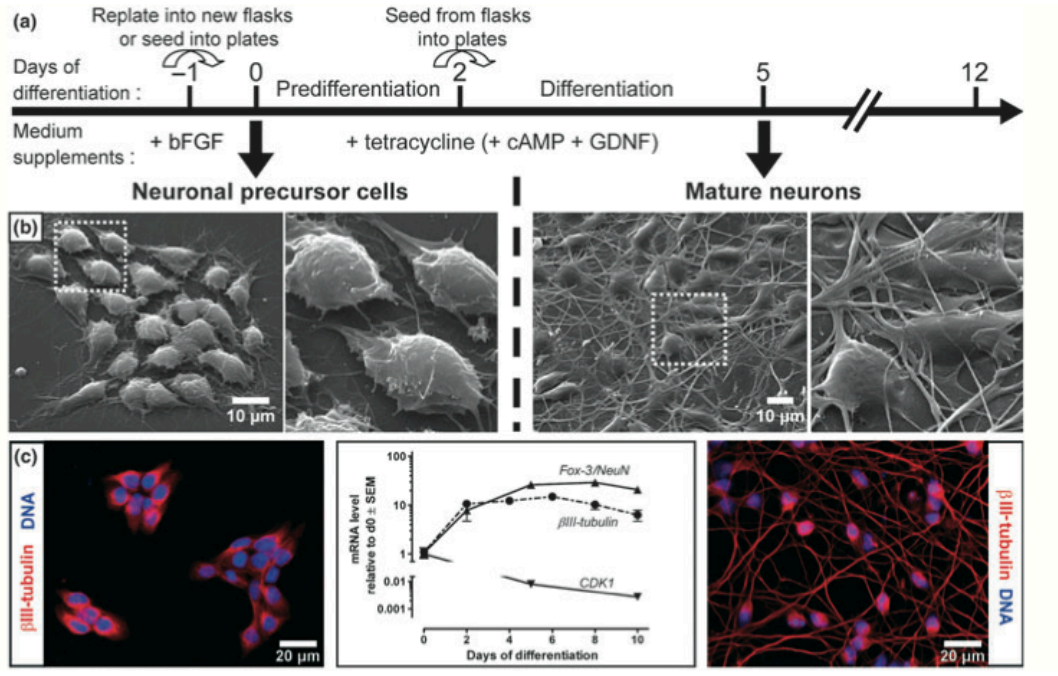

The conversion of proliferating undifferentiated LUHMES into post-mitotic neurons. (a) Schematic of differentiation procedure; (b) Scanning electron microscopy (SEM) images of undifferentiated (day 0) and differentiated (day 5) LUHMES; (c) LUHMES immuno-stained for β-3 tubulin and H-33341 (nuclear) dye and mRNA expression levels of β-3 tubulin, Fox-3/NeuN and CDK-1. From Scholz et al. (101).

1.7 Core project aims

The core hypothesis of this project is that parylene-C-patterned SiO_2 substrates can be utilized to construct, refine, and interact with simple, functional neuronal networks. The following stepwise goals were set:

- Investigate the currently elusive mechanisms of cell patterning on parylene-C:SiO_2, using both a cell and substrate centric approach.
- Achieve reliable patterning of neuronal cells on parylene-C:SiO_2.
- Establish control over neuronal morphology, with respect to axo-dendritic processes, in order to create topographically defined networks.
- Explore techniques to stimulate and record from patterned networks, to ensure that patterned neurons retain a viable and functional phenotype.
- Construct and stimulate simple, appropriately polarised poly-neuronal reflex arcs.

Chapter 2 Exploring cell patterning on parylene-C:SiO_2

This chapter describes the exploration of substrate-centric and cell-centric hypotheses regarding the cell patterning mechanisms in action on parylene-C:SiO_2.

2.1 Substrate-centric approaches

2.2 Introduction

An initial aim was to systematically assess the contribution of different chip fabrication and activation processes to the downstream effectiveness of the cell patterning platform. In order to measure changes in cell patterning, a model cell line was sought. The primary requirement was that this cell type reliably and accurately patterns on-chip using the pre-existing protocol. Secondary considerations were ease of use and availability.

2.2.1 HEK 293 as a candidate model cell line

The immortalized human embryonal kidney (HEK 293, see Figure 2-1) cell line was first described in 1977 (102); having been derived from primary human embryonal kidney by transformation with fragments of adenovirus 5 DNA. HEK 293 cells are straightforward to culture, have a short doubling time, are practical to work with, and consequently are used extensively in transfection studies. Importantly, they also have a well-described transmembrane CAM profile. HEK 293 cells express at least five β1-integrin containing subunits (αVβ1, α2β1, α3β1, α5β1, α6β1) (103). This diversity of integrin expression allows adherence to a wide variety of ECM proteins that includes vitronectin, laminin, fibronectin, and collagen. This profile therefore represents an obedient phenotype for protein-dependent cell adhesion research.

Prior opinion considered HEK 293 cells a derivative of embryonic fibroblastic or endothelial renal cells. However, contemporary research instead points towards a potential early neuronal lineage, suggested by the presence of mRNA and gene products typically found in neurons (neurofilament-M, neurofilament-L, α-internexin) and endogenous expression of voltage-gated ion currents (104,105).

Previous work involving protein elution from serum-incubated plain parylene-C or plain SiO_2 surfaces, followed by PAGE, illustrated that parylene-bound vitronectin may be responsible (to some degree) for imbuing parylene with its cell adhesive character (91). On this basis, it was hypothesized that the HEK 293 integrin profile (which includes vitronectin receptors) would enable cell adherence to parylene-C domains. Regarding contrasting repulsion from background SiO_2, early thinking was that repulsion was a more generalized, non-specific phenomenon. The recognition that HEK 293 cells are not known for an innate capacity to generate large quantities of adhesion-promoting ECM proteins is also in their favour in this regard.

If HEK 293 cells pattern successfully, this additionally provides an opportunity to assess the impact of parylene-C feature geometry upon the morphology of this cell, as well as allowing the assessment of how cell adhesion behaviour varies with the passage of time.

Figure 2-1 The HEK 293 cell line

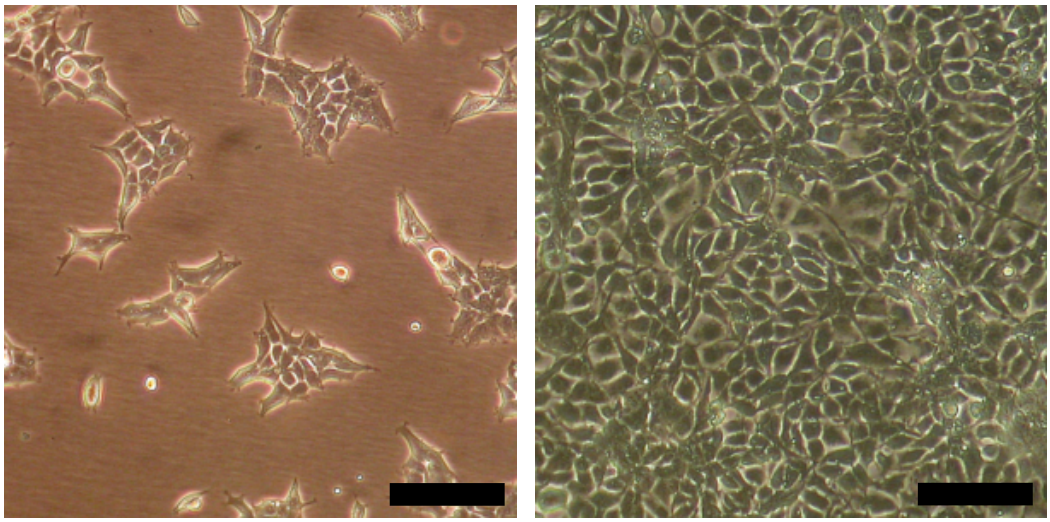

Photomicrographs of HEK 293 cells in culture. Left image shows a low density culture, right is high density confluent culture. Scale bar 200 μm.

2.2.2 Physico-chemical hypotheses

Given the impact that surface roughness and contact angle have upon serum protein adhesion and configuration, and therefore cell adhesion, an early goal was to assess how these two variables change during chip fabrication and activation processes. The aim was to ascertain the relevance (or not) of such factors to the ultimate effectiveness of the patterning platform.

Substrate hydrophobicity, as assessed by contact angle goniometry

The accepted dogma is that hydrophobic synthetic substrates are cell repulsive whilst hydrophilic substrates are cell adhesive (see section 1.2.2). Given that parylene-C is known for its high baseline water contact angle (~87°, reflecting significant hydrophobicity) and that SiO_2 has a lower contact angle, one would anticipate cell adhesion to occur on SiO_2 and for cells to be repulsed from parylene-C. However, as described, the reverse was observed in prior work (see Figure 1-20). Therefore, if contact angle *is* of relevance, the fabrication and activation steps would be expected to cause significant changes to the baseline contact angle of the two substrates.

Specifically, it was hypothesized that beyond merely cleaning the chip of unwanted organic matter (as previously reported), piranha acid in fact differentially etches the two substrates so as to alter contact angle and subsequent serum protein-binding characteristics; ultimately resulting in parylene-C becoming cell adhesive and SiO_2 becoming cell repulsive.

Surface roughness, as assessed by atomic force microscopy (AFM)

Atomic force microscopy (AFM) is a very high-resolution form of scanning probe microscopy capable of assessing surface roughness at the nano-scale. A sharp tip at the end of a cantilever is scanned over a surface. The tip is deflected according to surface features. By consolidating cantilever deflections, a topographic image of the surface can be generated.

Assessing alterations in surface roughness at different stages of chip fabrication and activation may similarly reveal changes that, downstream, alter the binding characteristics of serum proteins. If roughness plays an important role, cyto-adhesive

parylene might be expected to exhibit greater nano-scale roughness whereas cyto-repulsive SiO_2 might be expected to have larger surface features that are theoretically less conducive to functional binding of adhesion-mediating molecules. The caveat here is that the influence of surface roughness upon cell adhesion remains variable, controversial, and is cell- and context-dependent.

Temporal considerations in substrate preparation

Whether the effect of piranha acid is time-limited, and whether serum incubation needs to occur immediately after treatment, remains unexplored. If the effect of piranha acid treatment is transient, this would suggest a *reversible* process occurring on one or both of the substrates, which in turn might help to illuminate the underlying mechanism. As such, experiments were designed to assess changes in contact angle, and HEK 293 cell patterning, in the context of time delays between piranha acid treatment and serum incubation.

2.2.3 Biological hypotheses

Identifying the key proteins in serum that ultimately enable patterning would remove the need for serum, with its inherent heterogeneity between batches, as well as illuminate a key mechanistic aspect of cell patterning. One potential explanation, based on prior protein elution and PAGE experiments, is that serum-activated parylene manifests a cell-adhesive phenotype through competitive absorption of the ECM protein vitronectin (which maintains a functional conformation) whilst background SiO_2 enables 'contrast' by exerting a cytophobic effect mediated by the repulsive effect of bound albumin (with any SiO_2-bound vitronectin denatured and therefore unable to promote adhesion).

On this basis, if vitronectin does indeed bind to parylene-C ahead of other serum proteins, a solution devoid of vitronectin but containing another pro-adhesive protein ought then attain the ability to bind to parylene-C. This is important as it would represent an opportunity to define the patterned integrin-ligand, allowing the platform to be tailored towards a given cell type (with a specific, identified CAM in mind). To explore these ideas, rationalised solutions of vitronectin in combination

with albumin (and other ECM protein combinations) were tested in place of serum, in an attempt to replicate and modulate serum-mediated chip activation.

Raman spectroscopy of serum activated surfaces

Raman spectroscopy is opportune as a more direct approach to interrogate serum-activated chip surfaces. This spectroscopic technique relies on Raman scattering of monochromatic light delivered from a laser. The sample is illuminated and light interacts with molecular vibrations of the interrogated substance. Light returning from the illuminated spot is collected and sent through a monochromator. The shift in energy of laser photons gives information about the vibrational modes in the system.

This technique is used frequently in chemistry, as vibrational activity relates specifically to chemical bonds and symmetry of a molecule. As a result, different molecules have different Raman 'fingerprints', enabling identification. As such, Raman spectroscopic examination of parylene-C and SiO_2 surfaces, both before and after serum-incubation, offers a potentially powerful method to identify important chip-bound serum proteins.

2.2.4 Fabricating a transparent chip

Oxidised silicon wafers are opaque. This is suboptimal as it precludes use of certain potentially useful imaging platforms to assess cultured cells (specifically, any requiring inverted microscopes). A transparent chip would allow easier assessment of cell adhesion behaviour and also facilitate patch-clamping, useful for assessing the electrophysiological behaviour of patterned cells. The pool of potential materials used to make wafers for microelectronics includes borosilicate glass[†††], which is optically transparent. There is a high percentage of SiO_2 in borosilicate glass (81%) but it also contains boric oxide (12%), sodium carbonate (4.5%), and aluminium oxide (2.0%). A prototype chip using a borosilicate wafer as the background

[†††] Borosilicate glass is made by adding boric oxide to the usual glass-making combination of silica sand, soda, and ground lime.

substrate was fabricated in an effort to create a transparent chip. All subsequent photolithographic processes and activation protocols were kept the same as those used for SiO_2 wafers.

Key questions:

1. Will HEK 293 cells pattern effectively on parylene-C:SiO_2 substrates prepared according to the established protocol?
    1. How does HEK 293 cell patterning behaviour change over time?
    2. Is HEK 293 cell morphology influenced by the underlying parylene-C geometry?
2. Effect of serum
    1. What impact does the serum incubation step have upon subsequent HEK 293 cell patterning behaviour on the two substrates?
    2. How does the contact angle of the two substrates change as a result of serum incubation?
    3. Can important serum components be identified by using Raman spectroscopy to interrogate chip surfaces pre- and post- serum incubation?
    4. Can a simplified solution of vitronectin and albumin (or other recognised ECM molecules) be used in place of serum to similarly activate parylene-C:SiO_2 surfaces for cell patterning?
3. Effect of piranha acid
    1. What impact does the piranha acid treatment step have upon HEK 293 cell patterning behaviour on parylene-C and SiO_2?
    2. What impact does piranha acid have on the contact angle of parylene-C and SiO_2?
    3. Is the effect of piranha time-limited? Does serum incubation need to occur immediately after piranha treatment?
    4. What impact does piranha acid have on the surface roughness of parylene-C and SiO_2, as measured by AFM?
4. What is the impact upon HEK 293 adhesion for a chip fabricated from a borosilicate glass wafer, in place of SiO_2?

2.3 Methods

2.3.1 Photomask design

For all chips, the desired parylene-C configuration was initially mapped out using a layout editor software package, capable of reading/writing CIF (Caltech Intermediate Form) or GDS-II (Graphic Database System-II) files. CIF and GDS-II are industry standard file formats for integrated circuit artwork layout. Two different photomask designs were used for this initial sequence of experiments:

Chip 1:

This design consisted of three iterations of circular parylene-C nodes with a centred 'cross-hair' (node diameters 250 μm, 100 μm, and 50 μm, orthogonally-orientated cross hairs measuring 450 μm in length for the largest node size and 300 μm for smaller nodes) on chips 7.7 mm × 5.9 mm in dimension (see Figure 2-2). The rationale for this particular layout was informed by questions relating to downstream neuronal network organisation and is described in detail in section 4.1.

Chip 2: extensive geometric variation

This design was far more diverse, with elements designed to test chip resolution and also the impact of parylene geometry on cell morphology. Chip dimensions were 10 mm × 10 mm, whilst specific regions of parylene geometry can be seen in results Figure 2-7.

2.3.2 Chip fabrication process

Silicon wafers (Siltronix, Archamps, France) were oxidised in an atmospheric horizontal furnace (H2 1.88 SLM and O2 1.25 SLM) at 1100 °C for 40 min to produce a 500 nm SiO_2 layer (measured with a Nanometrics NanoSpec 3000 reflectometer). Oxidised wafers were primed with Merck Silane A174 adhesion promoter, followed by deposition of 100 nm coating of parylene-C (at 22 °C at a rate of 1.3 nm/mg of dimer using a SCS Labcoter 2 deposition Unit, Model PDS2010).

Next, hexamethyldisilazane (HMDS) adhesion promoter was deposited on parylene-coated wafers in an SVG 3 inch photo-resist track followed by application of a 1 μm

thick film of Rohm & Hass SPR350-1.2 positive photoresist, by spinning at a speed of 4000 rpm for 30 s. The wafer was then soft baked for 60 s at 90 °C. Both the wafer and pre-manufactured photo mask (Compugraphics International Ltd, Glenrothes, UK) were placed in a Suss Microtech MA/BA8 mask aligner. Exposure results in UV negative representation of the desired parylene-C configuration on the photoresist-coated wafer. After baking for 60 s at 110 °C, exposed photo-resist was removed by developing in Microchem MF-26A developer.

The wafer was inserted into a JLS RIE80 etch system for 120 s (at a 50 mTorr chamber pressure, 49 sccm O_2, 100 W RF power at 13.56 MHz) to etch off unprotected parylene (at an etch rate of 100 nm/min) to reveal underlying SiO_2. The wafer was cut with a DISCO DAD 680 Dicing Saw (spindle speed 30 000 rpm, feed speed 7 mm/s), rinsed in water, blown dry with nitrogen, and stored in dust-free boxes.

Figure 2-2 Design for chip 1

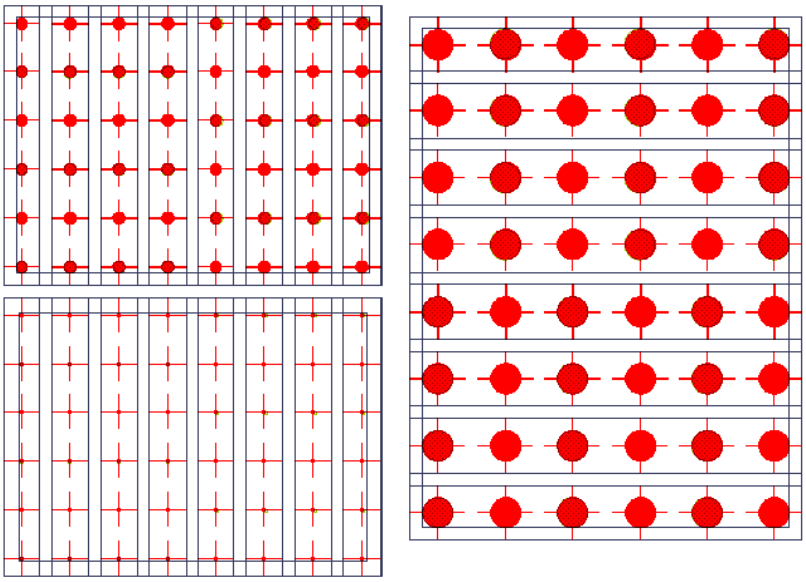

Schematic illustration of the parylene-C design on chip 1. Overall chip dimension 7.7 mm × 5.9 mm. Node diameters 250 µm, 100 µm, and 50 µm, orthogonally orientated cross hairs measuring 450 µm in length for the largest node size and 300 µm for smaller nodes. A distance of 100 µm separates the end of one cross hair from the beginning of the next, in all cases.

2.3.3 Standard chip activation protocol

Any residual photoresist was removed by washing chips in acetone for 10 s, followed by rinsing in de-ionised distilled H_2O three times. Piranha acid is a 5:3 ratio of 30% hydrogen peroxide and 98% sulphuric acid that must be prepared with great care. It is an extremely powerful oxidiser, is strongly acidic, and mixing hydrogen peroxide with sulphuric acid is a significantly exothermic reaction. This stage was performed in an acid fume hood, allowing 2 mins to pass after mixing piranha acid, but using within 10 mins.

Chips were immersed in piranha acid for 10 mins, followed by rinsing three times in de-ionised distilled H_2O, followed next by transfer to sterile culture dishes. Two chips were placed per well in a 6-well plate, followed immediately by the addition of 2 ml of FBS (FBS, Gibco Invitrogen) so as to fully immerse chips. Chips were then incubated at 37 °C overnight. These, and all subsequent cell culture stages, are performed under sterile conditions in a laminar flow tissue culture hood.

2.3.4 HEK 293 maintenance, plating, and imaging protocols

HEK 293 cells (human embryonic kidney cells; American Type Culture Collection, Virginia) were maintained at 37 °C and 5% CO_2 in Dulbecco's modified Eagle's medium (DMEM, Gibco Invitrogen) supplemented with 10% FBS. HEK 293 cells were applied to chips as a 2 mL/well suspension (at 5×10^4 cells/mL concentration) in normal growth media.

First, the capacity to pattern HEK 293 cells using prior established protocols was tested using chip 1. Temporal aspects of cell patterning behaviour were evaluated by interval (daily) imaging, acknowledging the continued mitotic proliferation of cultured HEK 293 cells. The impact of parylene-C geometry upon HEK 293 cell morphology was further explored by plating cells on chip 2 (at the same density), with its greater geometric variation.

Cells were imaged alive on sequential days *in vitro* using a dissecting light microscope (Wild Heerbrugg, Switzerland) adapted for use with a Nikon Coolpix 4500 digital camera (Tokyo, Japan) using an MDC2 relay lens. Image J (version

1.44o, National Institute for Health, USA) was used for image analysis and measurement of cell surface areas.

2.3.5 Quantification of patterning and assessment of cell behaviour

Two indices were derived to assess contrasting aspects of cell patterning on-chip and are described in Figure 2-3:

Parylene-C Adhesion Index (PAI)

A square region of interest (ROI), consisting of one iteration of the parylene node pattern surrounded by SiO_2, was defined. The PAI was calculated by dividing the surface area of cell material adherent to parylene-C by the total surface area of available parylene-C in the ROI.

SiO_2 Repulsion Index (SRI)

Similarly, SRI was calculated by dividing the surface area of cell material adherent to SiO_2 by the total available surface area of SiO_2; and subtracting the result from 1.

Hence, perfect patterning on parylene would result in a PAI of 1 (reflecting complete cell coverage of all parylene-patterned areas) and a SRI of 1 (reflecting complete absence of cell material from SiO_2). The theoretical range of patterning behaviours can be illustrated by plotting PAI against SRI (see Figure 2-4).

Figure 2-3 Schematic illustrating the method for calculating SRI and PAI.

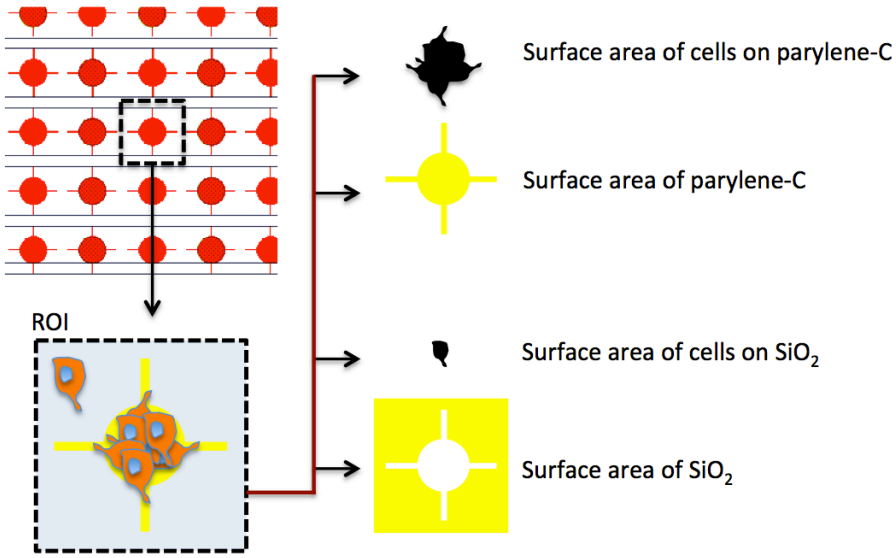

A square region of interest (ROI), consisting of one iteration of the parylene node pattern surrounded by SiO_2, is defined. PAI is calculated by dividing the surface area of cell material adherent to parylene-C by the total surface area of available parylene-C in the ROI.

SRI is calculated by dividing the surface area of cell material adherent to SiO_2 by the total available surface area of SiO_2; and subtracting the result from 1. ROI, region of interest; PAI, parylene adhesion index; SRI, silicon dioxide repulsion index.

Figure 2-4 The range of possible cell adhesion behaviours

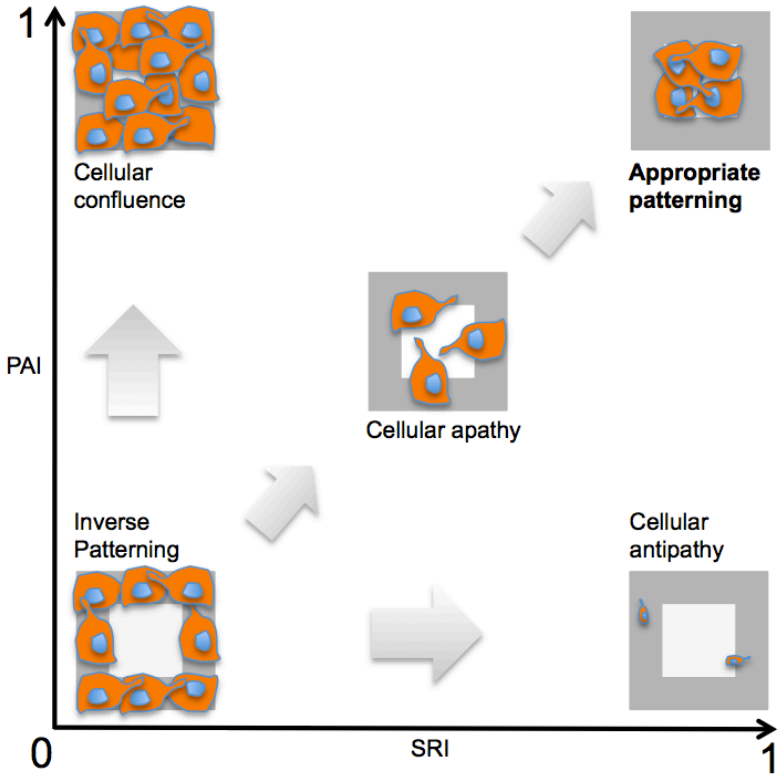

Parylene-C adhesion index (PAI) plotted against silicon repulsion index (SRI), with representative cartoon illustrations of the range of potential patterning behaviours on a theoretical chip consisting of a central square of parylene-C (white) on a background of SiO_2 (grey).

2.3.6 Experimental fabrication and activation protocols

Rationalised protein solutions

Following standard piranha acid treatment, chips (chip design 1) were incubated overnight at 37 °C in the following alternative activation solutions:

- Bovine serum albumin (BSA) alone (0.3 mg/ml, 3 mg/ml, 30 mg/ ml dissolved in Hanks Balanced Salt Solution (HBSS, Gibco Invitrogen).
- BSA with vitronectin (0.3 mg/ml, 3 mg/ml, 30 mg/ml BSA with 1 µg/ml vitronectin).
- BSA and fibronectin (0.3 mg/ml, 3 mg/ml, 30 mg/ml BSA with 1 µg/ ml fibronectin).
- Vitronectin alone (1 µg/ml)
- Fibronectin alone (1 µg/ml),
- Laminin alone (1 µg/ml)
- Collagen alone (1 µg/ml)
- Poly-L-ornithine alone (50 µg/ml)
- De-ionised distilled H_2O (control)

For experiments using simplified protein solutions in place of serum, cells were passaged and transferred to Freestyle™ 293 expression medium (Gibco Invitrogen) prior to plating. This is a serum-free and protein-free growth medium chosen specifically to avoid confounding the contribution of rationalized protein activation solutions.

For each patterning trial, a minimum of 27 ROIs were interrogated (nine for each of the three node diameters present on the chip, pooled). Charted data is illustrated as means ±SEM. Kruskal-Wallis tests[‡‡‡] were used to compare patterning indices

[‡‡‡] The Kruskal-Wallis one-way analysis of variance by ranks was chosen (a) because patterning data is non-parametric and (b) because of the need to compare more than two different samples. Kruskal & Wallis. 1952. Use of ranks in once-criterion variance analysis. Journal of the American Statistical Association. 47:260; 583-621.

between different chip treatment and activation protocols. The method involves ranking all data from all groups together from 1 to *N*. The test statistic is given by:

$$K = (N-1)\frac{\sum_{i=1}^{g} n_i(\bar{r}_{i\cdot} - \bar{r})^2}{\sum_{i=1}^{g}\sum_{j=1}^{n_i}(r_{ij} - \bar{r})^2},$$

Where:

- n_i is the number of observations in group *i*
- r_{ij} is the rank (amongst all observations) of observation *j* from group *i*
- *N* is the total number of observations across all groups

Prism 5 for Mac OS X (GraphPad Prism Software Inc., California, USA) was used for statistical analyses.

Assessing the impact of piranha

To assess the impact of piranha treatment on patterning, HEK 293 cells were plated on both piranha-activated and non piranha-activated (water-control) chips, both of which went on to standard serum incubation.

To assess the effect of delayed serum activation following piranha treatment, chips were piranha-treated, left for an interval of between one and 50 days (at room temperature, in the dark, in non-airtight 6-well plates), then serum-activated, and then plated with HEK 293 cells as described previously.

2.3.7 Goniometry to assess contact angle

Surfaces were prepared to represent the chip in different stages of fabrication and activation:

- Plain SiO_2 wafer, no treatment.
- SiO_2 wafer coated with parylene-C.
- SiO_2 wafer coated with parylene-C, followed by 120 s oxygen plasma etch to remove all parylene-C and reveal underlying SiO_2.

- SiO_2 coated with parylene-C, followed by the complete photolithographic etch process (photoresist, baking, UV exposure, etching), performed so as to leave all parylene (i.e. entire surface protected by photoresist).
- SiO_2 wafer coated with parylene-C, followed by 120 s oxygen plasma etch to remove all parylene-C and reveal underlying SiO_2, then followed by piranha treatment.
- SiO_2 wafer coated with parylene-C, followed by 120 s oxygen plasma etch to remove all parylene-C and reveal underlying SiO_2, and followed by piranha treatment, then serum incubation, then brief HBSS wash.
- SiO_2 wafer coated with parylene-C, followed by the complete photolithographic etch process (photoresist, baking, UV exposure, etching), performed so as to leave all parylene (i.e. entire surface protected by photoresist). Followed by acetone to remove photoresist layer.
- SiO_2 coated with parylene-C, followed by the complete photolithographic etch process, performed so as to leave all parylene-C *in situ*. Then followed by acetone treatment to remove photoresist layer and piranha acid treatment.
- SiO_2 coated with parylene-C, followed by the complete photolithographic etch process, performed so as to leave all parylene-C *in situ*. Then followed by acetone treatment to remove photoresist layer, piranha acid treatment, serum incubation, and a final brief HBSS wash.

At room temperature, an Optem micro video zoom lens (Qioptiq, Luxembourg) with a digital interface was used to image a 5 μL droplet of de-ionised distilled H_2O on each of the surfaces described. 3 measurements were taken per surface. IC Capture 2.0 (NCH Software, CO, USA) was used to acquire droplet images and FTA 32 (First Ten Angstroms, VA, USA) was used to measure the contact angle.

2.3.8 Atomic force microscopy to assess surface roughness

A Veeco Explorer AFM (Veeco, Plainview, NY, USA), with a Bruker probe (Bruker, Camarillo, CA, USA) in tapping mode, was used to assess chip surfaces representing the following:

- Parylene-C domains before piranha acid treatment

- Parylene-C domains immediately after piranha acid treatment
- SiO_2 domains before piranha acid treatment
- SiO_2 domains immediately after piranha acid treatment

Chips were prepared by MH. AFM measurements were performed by Andy Downes (School of Engineering, University of Edinburgh).

2.3.9 Raman spectroscopy

A Renishaw InVia (Renishaw, Wooton-under-Edge, UK) Raman spectroscope (785 nM illumination, 50 mW laser power, in an upright microscope) was used to assess the following wafer surfaces:

- Plain, untreated SiO_2 wafer
- Plain SiO_2 wafer treated with piranha acid but no serum
- Plain SiO_2 wafer treated with piranha acid and then serum-activated
- Plain SiO_2 wafer untreated with piranha acid but then serum activated
- SiO_2 wafer coated with parylene-C, no piranha acid nor serum treatment
- SiO_2 wafer coated with parylene-C, treated with piranha acid but no serum
- SiO_2 wafer coated with parylene-C, treated with piranha and then serum incubated
- SiO_2 wafer coated with parylene-C, untreated with piranha and then serum activated.

Surfaces were prepared by MH and transferred immediately for Raman spectroscopic measurements (performed by Andy Downes, School of Engineering, University of Edinburgh).

2.3.10 Fabrication of borosilicate glass chips

A borosilicate glass wafer (Borofloat 33 [reference V015.04-0003], Plan Optik, Germany) underwent the same oxidation and photolithographic process as described in 2.3.2. After standard activation with piranha acid and serum incubation, HEK 293 cells were plated as a suspension of 5×10^4 cells/ml in growth media. Chips were imaged daily as previously described, in order to assess PAI and SRI.

2.4 Results

2.4.1 HEK 293 cell patterning

HEK 293 cells patterned effectively on parylene-C:SiO_2 substrates that had been prepared using the pre-established protocol (of piranha acid treatment followed by serum incubation). Cells adhered specifically to parylene-C regions and were repulsed from SiO_2 (see Figure 2-5).

Figure 2-6 illustrates PAI and SRI from day 1 to day 7 *in vitro* for each of the three different node diameters on chip 1, with representative images of patterned HEK 293 cultures (all were piranha-treated, serum-incubated chips). PAI starts low (due to the relatively low cell plating density) and increases to approach 1 by day 7 (reflecting almost total coverage of parylene with cell matter). SRI starts and remains high for all node geometries, with a gradual decline manifesting at day 6 or 7. This growth pattern is similar for all three parylene node sizes.

Figure 2-7 illustrates high resolution patterning of HEK 293 cells on chip 1 and chip 2, compared with random growth on an un-patterned polystyrene cell culture flask. Underlying parylene geometry influences HEK 293 cell morphology. A lower density culture (2×10^4 cells/mL) on the 100 μm diameter node pattern demonstrates the ability to capture single cell bodies on parylene 'cross hairs' (solid arrow, Figure 2-7B) and the potential to dictate the direction of an extending cell process (dashed arrow). Figure 2-7C-G illustrates persisting high fidelity patterning achieved using chip 2, with its more extensive variations in parylene geometry.

Figure 2-5 HEK 293 on chip 1

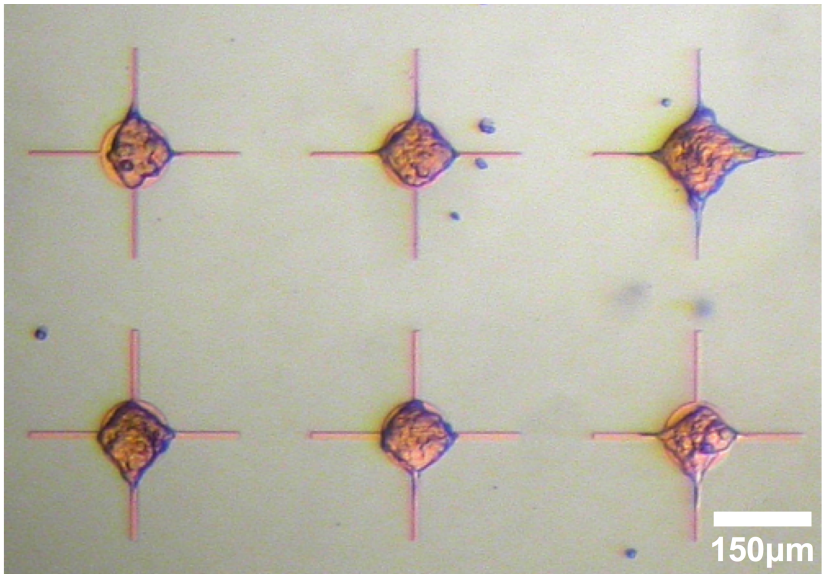

Photomicrograph of live HEK 293 cells cultured on chip 1 after 3DIV. HEK 293 cells grow to confluence on parylene-C nodes but not on SiO_2. Only occasional, spherical cell fragments are seen on surrounding SiO_2 domains. Imaged region depicts parylene nodes of diameter 100 µm with 300 µm long 'cross-hairs'.

Figure 2-6 Changes in HEK 293 cell patterning indices over time

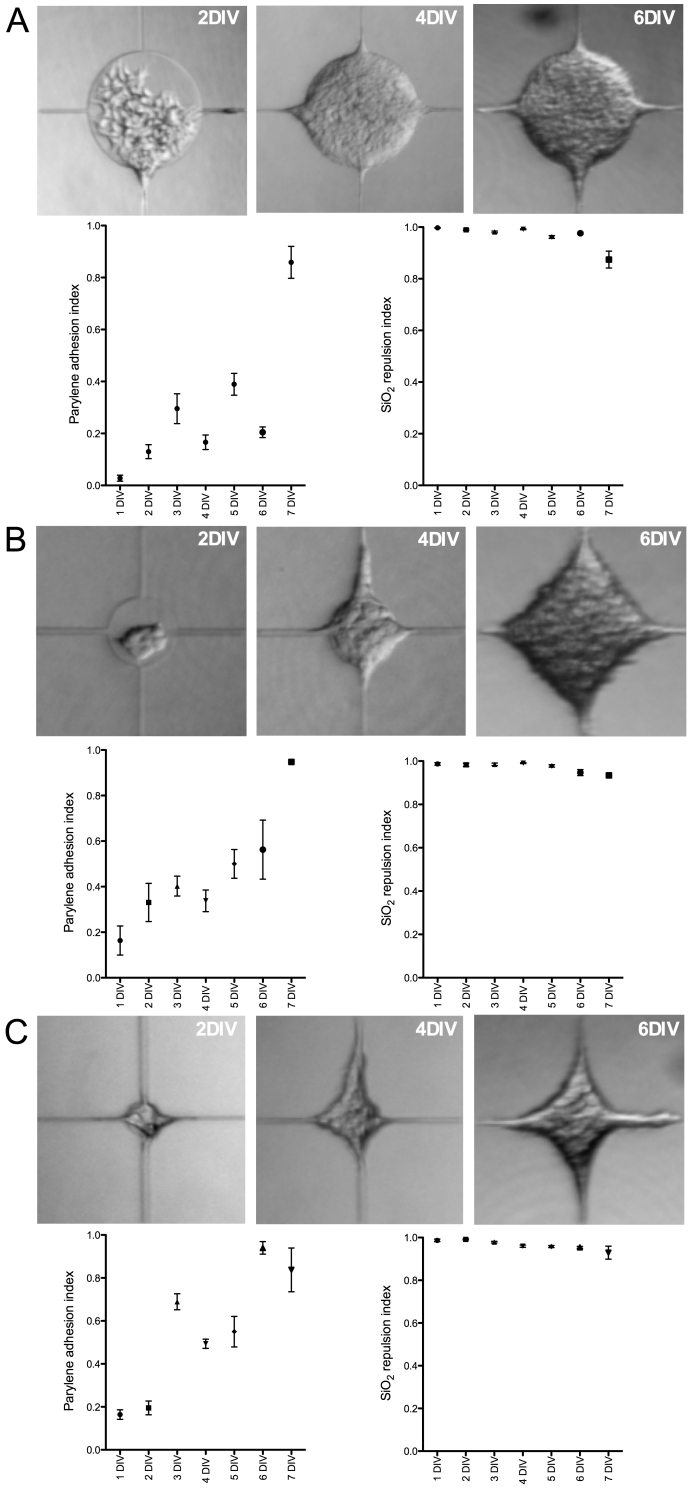

Temporal changes in PAI and SRI for HEK 293 cells cultured on the three different node diameters on-chip. A: 250 μm diameter node, region shown measures 450 μm × 450 μm, B: 100 μm diameter node, region shown measures 300 μm × 300 μm, C: 50 μm diameter node, region shown measures 300 μm × 300 μm, DIV, days in vitro. Data presented as mean±SEM. For each of the three different node sizes, 18 ROIs from 3 independent chips were assessed.

Figure 2-7 Impact of parylene-C geometry upon morphology of patterned HEK 293 cells.

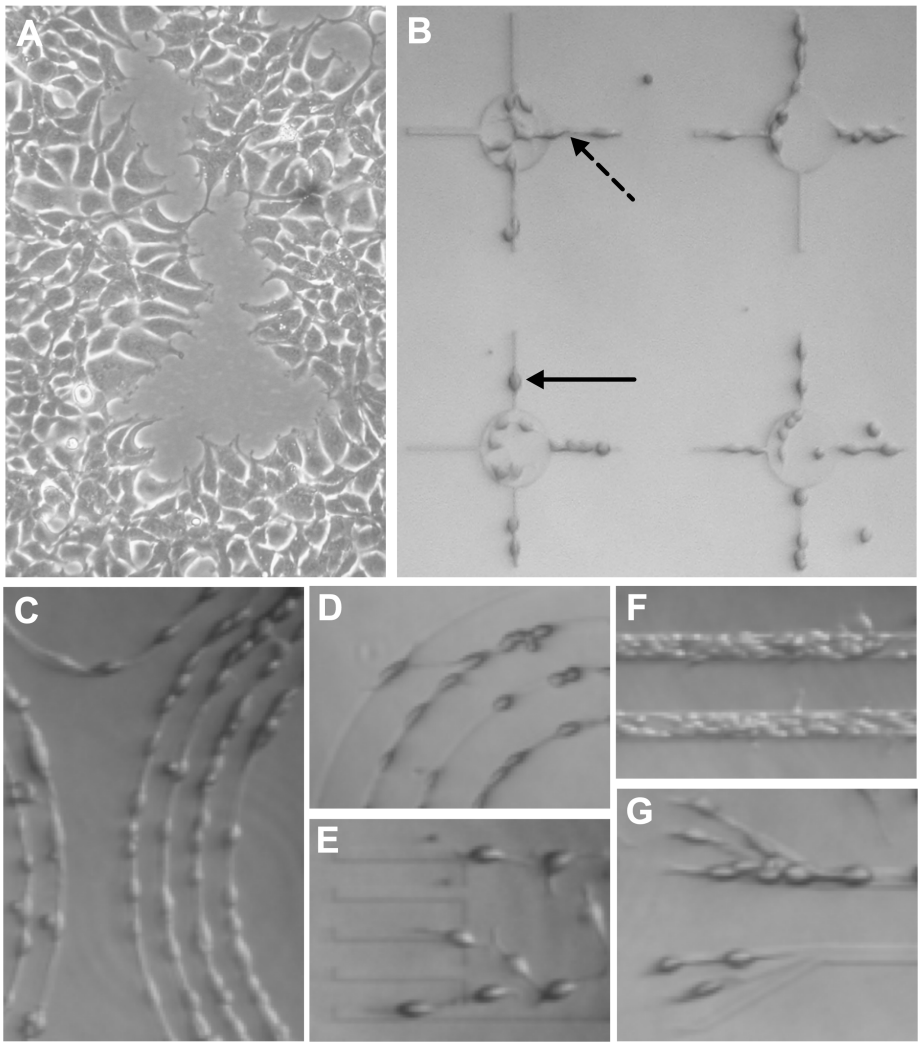

A: HEK 293 cells approaching confluence in a standard polystyrene cell culture flask, region shown measures 360 μm × 240 μm, B: Low density HEK 293 culture on chip pattern 1, illustrating single cell capture (filled arrow) and guided process extension (dashed arrow). Parylene node diameter 100 μm, region shown measures 720 μm × 720 μm C - G: Consistent high resolution patterning on diverse parylene geometric patterns using chip 2. All images taken at 4DIV. C measures 600 μm × 380 μm, D measures 200 μm × 380 μm, E measures 150 μm × 220 μm, F measures 150 μm × 220 μm, G measures μm × 250 μm,

2.4.2 Experimental fabrication and activation protocols:

Piranha treatment and serum activation impact HEK 293 behaviour

Figure 2-8 illustrates the effect of serum activation and piranha treatment (both in isolation and in sequence) upon HEK 293 patterning, as measured by PAI and SRI. Effective cell patterning only occurs when piranha acid treatment is followed by serum incubation. Piranha-treated chips incubated with H_2O instead of serum do not manifest a patterning capability. SiO_2 domains revert to being relatively cell tolerant whereas parylene-C domains became less cell-adhesive. Non piranha-treated chips incubated with serum also lacked discriminative adhesion behaviour between the two substrates; both parylene-C and SiO_2 became relatively cell-tolerant. Notably, cell morphology on non piranha-treated, water-activated chips is profoundly abnormal (Figure 2-8C).

Only in the context of piranha-treated, serum-incubated chips is a situation established where both PAI is high and SRI is close to the requisite maximum of 1. The overall result of this is effective, discriminative patterning.

Effect of delaying serum activation after piranha treatment

Figure 2-9 illustrates changes in PAI and SRI that occur when a time delay is incorporated between piranha acid treatment and serum incubation. Regardless of a delay ranging from 1 to 50 days, parylene-C domains retain their downstream adhesive character with no significant change in PAI. However, SRI shows a significant drop off following (and beyond) a 24 hour delay. The effect is to undermine patterning, as illustrated in Figure 2-9C.

To assess whether the attenuation in SRI is salvageable by repeat piranha-treatment, chips were piranha-treated, left for 7 days, re-piranha treated, underwent serum incubation without delay, and were then plated with HEK 293 cells. The result was to successfully re-establish effective cell repulsion from SiO_2 domains. However, parylene-C patterns were damaged by the second piranha treatment, as shown in Figure 2-10.

Figure 2-8 Impact of piranha treatment and serum incubation upon HEK 293 cell patterning

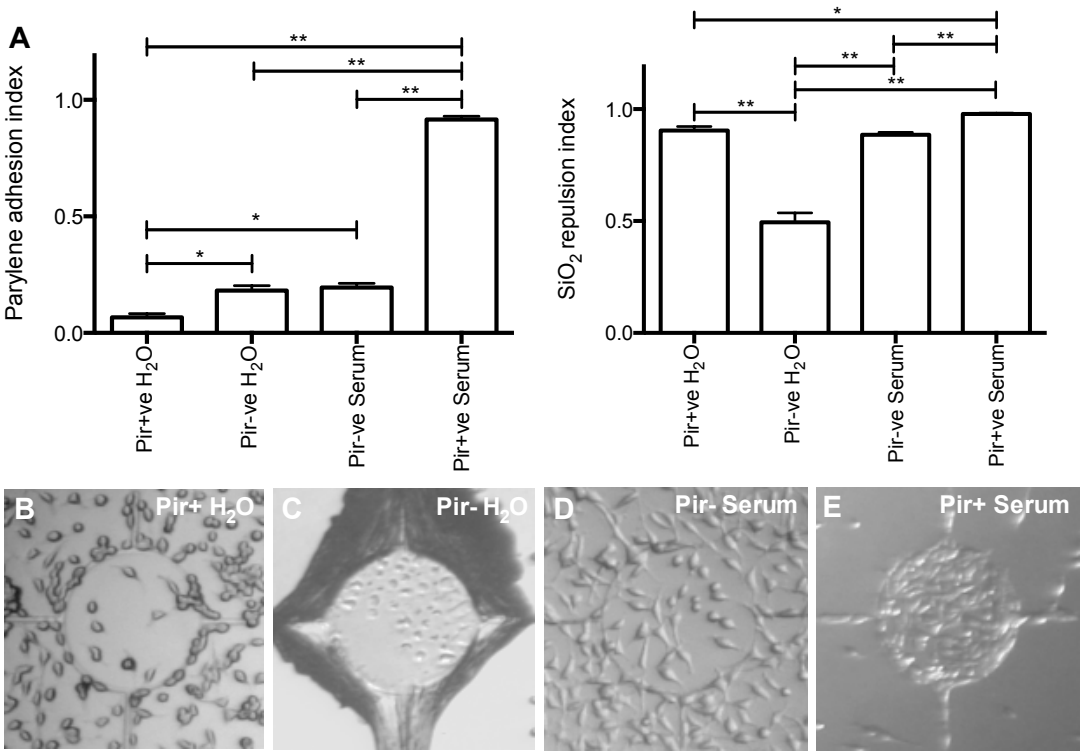

*A: Cell patterning indices illustrating the impact of piranha treatment, with and without subsequent activation with FBS or water, upon HEK293 cell adhesion and patterning. B-E: Representative images of each protocol showing the 250 μm diameter node pattern, each region shown measures 450 μm × 450 μm. Pir+ve/Pir-ve denotes treatment with/without piranha solution respectively. Data is illustrated as mean ±SEM. Kruskal-Wallis test used to compare groups, * denotes P<0.05, ** P<0.001. For each activation protocol, 27 ROIs from 3 independent chips were assessed.*

Figure 2-9 Impact of introducing a delay between piranha treatment and serum incubation upon HEK 293 cell patterning behaviour.

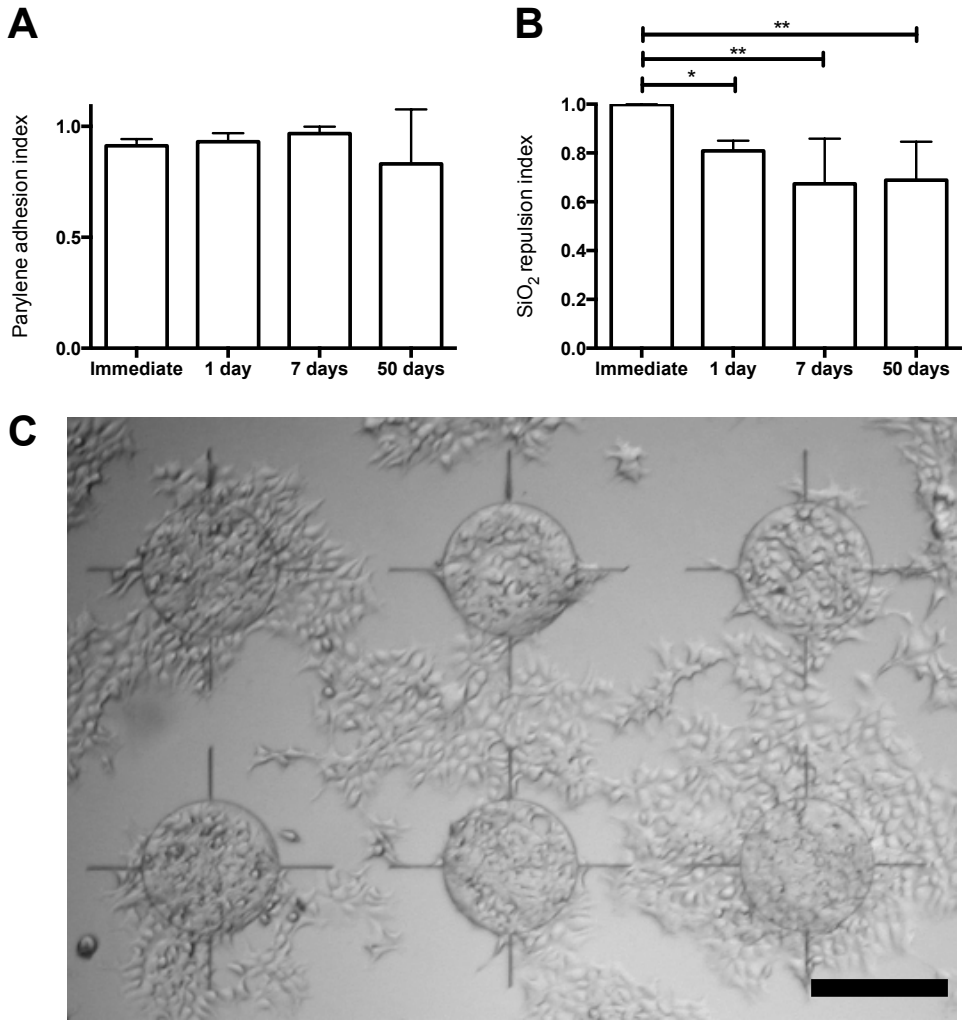

*A: Changes in parylene adhesion index. B: Changes in SiO_2 repulsion index. C: Illustrative photomicrograph showing failed HEK 293 cell patterning due to HEK 293 cell adhesion to SiO_2, when a 7-day delay post-piranha treatment was introduced. Scale bar 250 μm. PAI is relatively unaffected by a delay between piranha acid treatment and serum incubation. However, SRI is significantly reduced after a 1 day delay or more. Data presented as mean±SEM. Kruskal-Wallis test used to compare groups. * denotes P<0.05, ** P<0.001. For each time delay protocol, 18 ROIs from 3 independent chips were assessed.*

Figure 2-10 Attempting to salvage cell patterning by repeat piranha treatment.

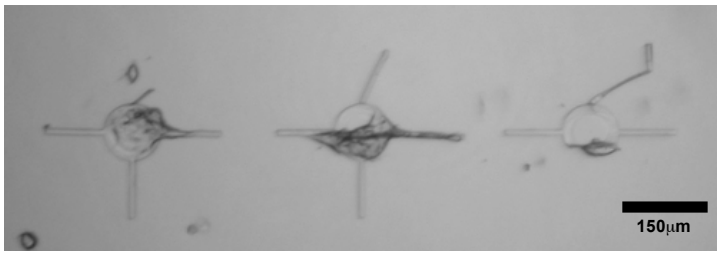

Cell repulsion from SiO_2 can be re-asserted by repeat piranha acid treatment. Imaged chip underwent piranha acid treatment, a 7-day delay, a second piranha treatment, followed by immediate serum incubation. Imaged after 3DIV. Note disruption of parylene-C design, particularly with respect to the 'cross-hair' components that have been damaged or deformed.

Rationalized protein activation solutions

Patterning indices derived from chips activated with rationalized protein activation solutions are shown in Figure 2-11. With solutions of BSA alone, parylene becomes notably cytophobic (particularly at a concentration of 30 mg/mL) while SiO_2 becomes relatively cell-tolerant. This inverts the prior-observed patterning effect to produce a 'negative' cell-patterning image. A similar result is seen with BSA co-dissolved with vitronectin or fibronectin, though solutions with fibronectin manifest a further significant reduction in PAI. Adhesion indices also differ according to the concentration of BSA in which vitronectin or fibronectin is co-dissolved.

The four purified solutions of vitronectin, fibronectin, laminin, or collagen alone resulted in a PAI significantly greater than that for either water control, pure BSA solutions, or combinations of BSA with vitronectin or fibronectin. However, the concomitant attenuation of the SiO_2 repulsion index resulted in a substrate that no longer manifests contrasting adhesive or repulsive qualities and therefore ceases to pattern cells. Poly-L-ornithine enabled excellent cell adhesion to parylene (PAI approaching one), comparable to that seen with serum-activated chips (see Figure 2-11B). However, its effect too was indiscriminate with similarly confluent adhesion on SiO_2 (SRI almost zero).

Figure 2-11 Rationalized protein activation solutions

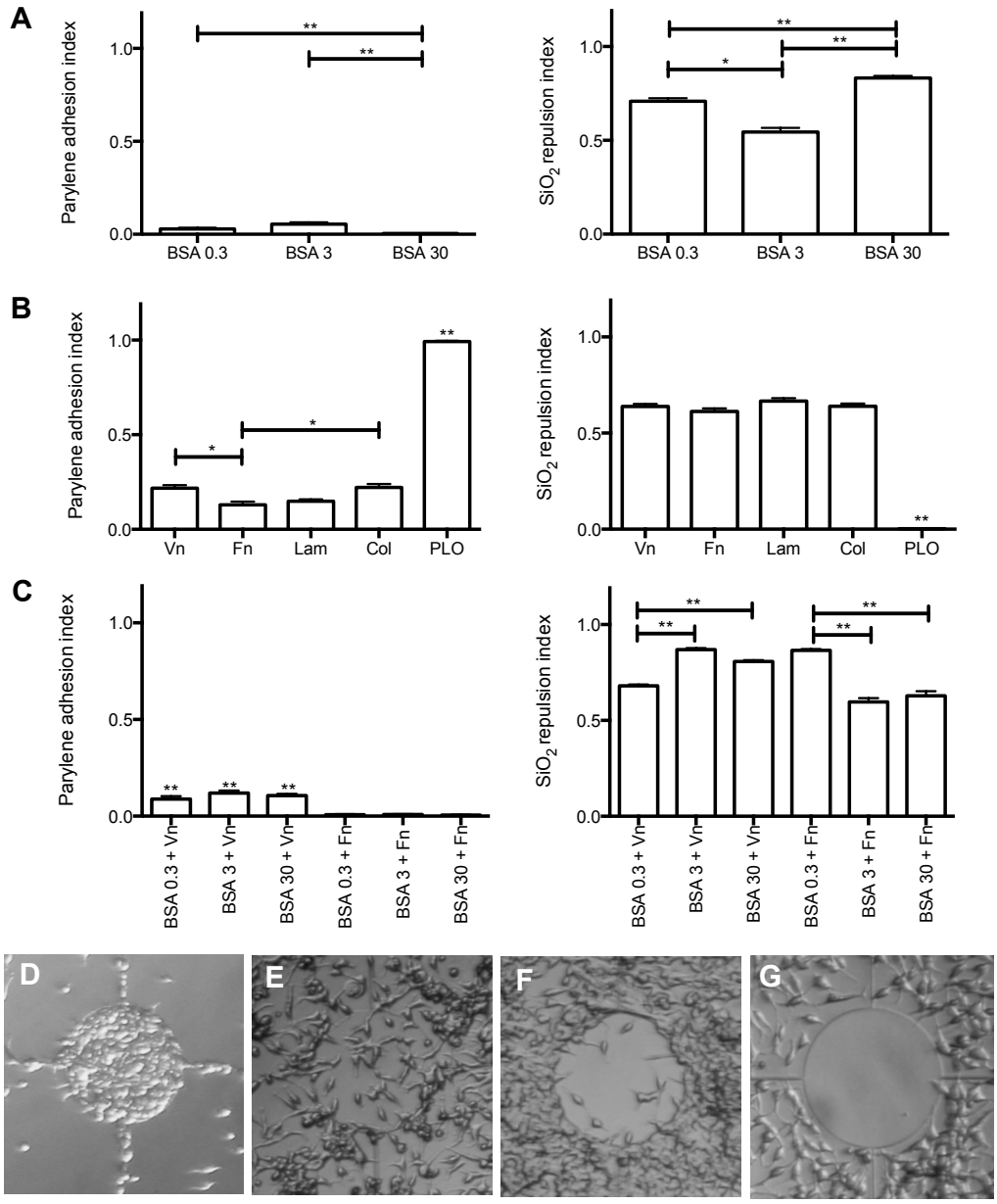

*A-C: Parylene adhesion and SiO_2 repulsion indices for HEK 293 cells cultured in Freestyle™ media on substrates activated with rationalised protein solutions. All indices measured at 4DIV. For PLO-treated chips, SRI was significantly lower and PAI significantly higher than for vitronectin, fibronectin, laminin, or collagen treated chips. For vitronectin co-dissolved in any of the different concentrations of BSA, PAI was significantly greater than that of fibronectin co-dissolved with BSA. D-G: representative images of the 250 μm diameter node pattern for specific activation solutions. Each region shown measures 450 μm × 450 μm D: serum, E: Vn alone, F: BSA 3mg/ml + Vn, G: BSA 3mg/ml + Fn. BSA, bovine serum albumin; Vn, vitronectin; Fn, fibronectin; Lam, laminin; Col, collagen; PLO, poly-L-ornithine. Data presented as mean±SEM. Kruskal-Wallis test used to compare groups. * denotes P<0.05, ** P<0.001. For each protein activation protocol, 27 ROIs from 3 independent chips were assessed.*

2.4.3 Contact angles during fabrication and activation

Table 3 illustrates the contact angles measured for wafer surfaces representing the different stages of chip fabrication and activation. Prior to piranha treatment, surfaces representative of on-chip background SiO_2 are relatively hydrophilic with a contact angle of 27°. Piranha treatment further reduces this to just 6°. In contrast, surfaces representative of on-chip parylene-C prior to piranha treatment are hydrophobic with a contact angle of 75°. Piranha treatment reduces this somewhat to 60°. Following serum incubation, however, both surfaces have a similar contact angle of 14°.

Table 4 illustrates changes in contact angle of SiO_2 regions that occur with the passage of time after piranha acid treatment. Following an interval of 31 hours, contact angle increased spontaneously from 6° to 18°, trending back towards the pre-piranha value of 27°.

Table 3 Contact angles of chip substrates during various stages of fabrication and activation.

Start substrate	Treatment; *indicative of*	Contact°
Plain SiO_2	No treatment**;** *SiO_2 baseline*	**47.8±0.2°**
SiO_2 coated with parylene-C	No treatment**;** *parylene-C baseline*	**86.1±0.4°**
SiO_2 coated with parylene-C	120 s O_2 plasma etch to reveal underlying SiO_2**;** *exposed regions of SiO_2 on fabricated chips prior to piranha or serum*	**17.4±0.6°**
SiO_2 coated with parylene-C	Complete photolithography and O_2 plasma etch process, leaving all parylene protected with photoresist; *parylene-C domains on fabricated chips, with a residual coat of photoresist remaining*	**74.8±0.3°**
SiO_2:		
SiO_2 coated with parylene-C	120 s O_2 plasma etch to reveal SiO_2, then acetone wash; *SiO_2 regions on fabricated chips after acetone wash (i.e. residual photoresist removed) but prior to piranha treatment*	**27.3±0.8°**
SiO_2 coated with parylene-C	120 s O_2 plasma etch to reveal SiO_2, then acetone wash, then piranha etch; *SiO_2 regions on fabricated chips after acetone wash & piranha etch, but prior to serum incubation*	**5.6±0.3°**
SiO_2 coated with parylene-C	120 s O_2 plasma etch to reveal SiO_2, then acetone wash, piranha etch, incubation with serum, and brief HBSS wash, dry; *exposed SiO_2 regions on activated chips immediately prior to cell plating*	**14.1±0.8°**
Parylene-C:		
SiO_2 coated with parylene-C	Complete photolithography and O_2 plasma etch process (leaving parylene *in situ*), then acetone wash**;** *fully exposed parylene-C domains on fabricated chips*	**74.6±0.7°**
SiO_2 coated with parylene-C	Complete photolithography and O_2 plasma etch process, acetone wash, piranha etch**;** *Parylene-C domains on fabricated chips after acetone wash & piranha etch but pre-serum incubation*	**60.4±0.7°**
SiO_2 coated with parylene-C	Complete photolithography and O_2 plasma etch process, acetone wash, piranha etch, incubation with serum, brief HBSS wash, dry**;** *parylene-C domains on fabricated chips immediately prior to cell plating*	**14.2±0.3°**

(Mean of 3 measurements taken per surface. Data presented is mean±SEM).

Table 4 Contact angles of SiO_2 domains following piranha treatment and time delays ranging from 90 mins to 31 hrs.

Start substrate	**Treatment; *indicative of***	**Contact°**
SiO_2 coated with parylene-C	O_2 plasma etch to reveal SiO_2, acetone wash, piranha etch; *SiO_2 regions on fabricated chips after acetone wash & piranha etch (immediate baseline measure)*	**5.6±0.3°**
	- 90 mins delay	**10.3±0.4°**
	- 6 hr delay	**11.6±0.6°**
	- 31 hr delay	**18.0±0.4°**

(Mean of 3 measurements taken per surface. Data presented is mean±SEM).

2.4.4 Atomic force microscopy (AFM) findings

AFM surface roughness measurements were restricted to on-chip parylene-C and SiO_2 regions pre, and 30 minutes post, piranha treatment (with preceding steps occurring as per the established fabrication protocol).

The surface deflections on parylene-C changed minimally after piranha-treatment, with feature sizes of 5-25 nm both before and after piranha exposure. However, SiO_2 regions showed a pronounced change with feature sizes changing from just 1-2 nm to 20-40 nm following piranha treatment (see Figure 2-12).

2.4.5 Raman spectroscopy findings

Raman spectroscopy was able to detect a signal change denoting the presence of parylene on parylene-C coated wafers, compared with bare SiO_2 wafers. However, it was unable to resolve any further, potentially due to SiO_2 fluorescence obliterating smaller signals. Due to its limited utility, results are reserved for appendix 6.2.

2.4.6 Borosilicate glass as an alternative background substrate

Figure 2-13 illustrates HEK 293 cells cultured on a chip with borosilicate glass (in place of SiO_2) as the background substrate. Patterning fails due to an absence of cell repulsion from glass. Adhesion to parylene-C continues to occur. Overall, adhesion behaviour is not substrate-specific and reflects the random, spreading, confluent growth of established cell clusters. Data for PAI and SRI are shown in Figure 2-14, comparing chips fabricated from SiO_2 wafers with those from borosilicate glass.

Figure 2-12 Atomic force microscopy findings

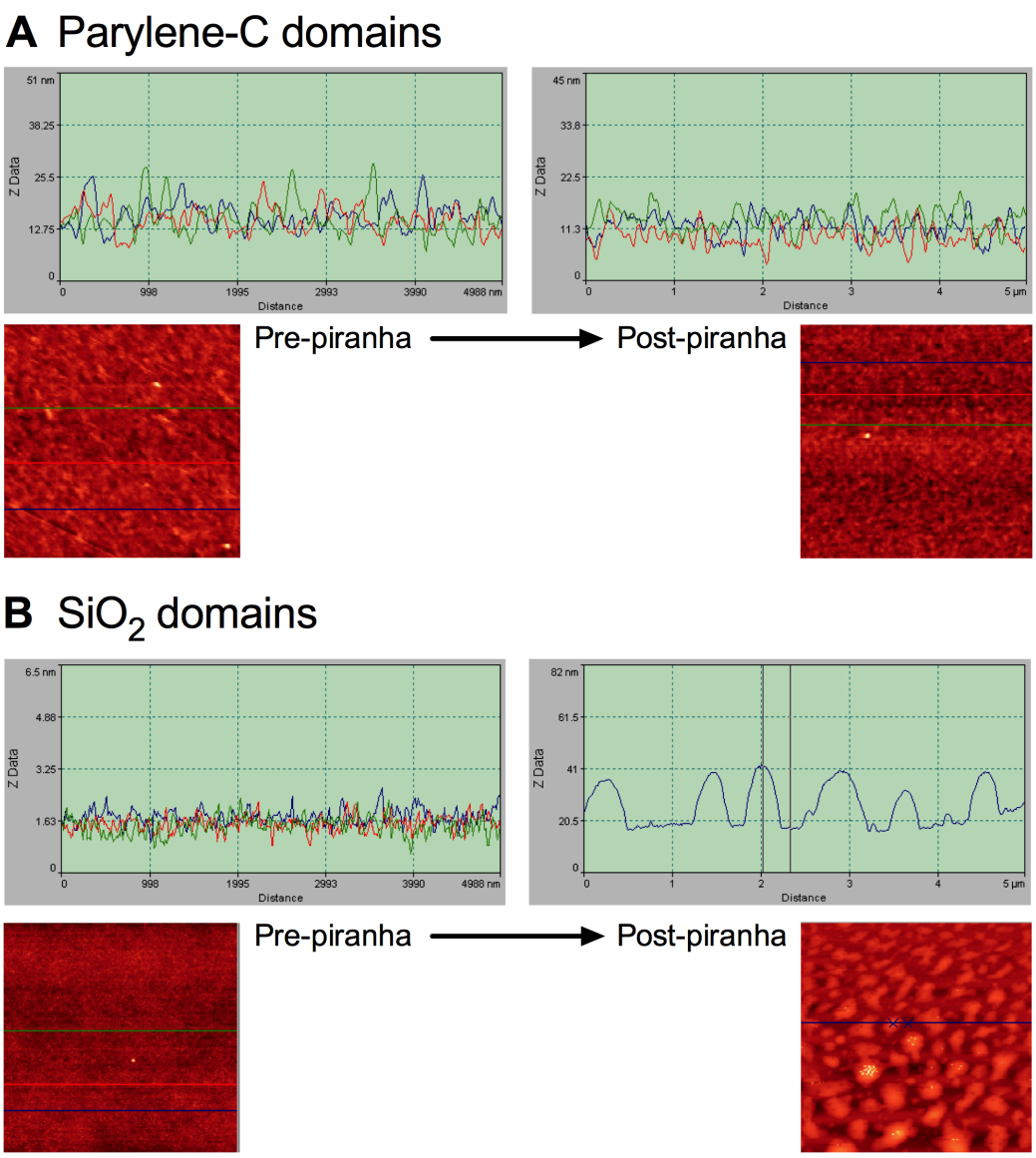

AFM deflections for parylene-C (A) and SiO_2 (B) regions on-chip, pre- and post-piranha treatment. Z data tracings reflect the corresponding colour-coded lines of scanning in the image beneath. NB The scale of the y axes of the deflection data, labelled 'Z Data', are not constant across the figure. The surface roughness of SiO_2 changes significantly following piranha acid treatment, with feature sizes changing from just 1-2 nm to 20-40 nm.

Figure 2-13 Borosilicate glass in place of SiO_2

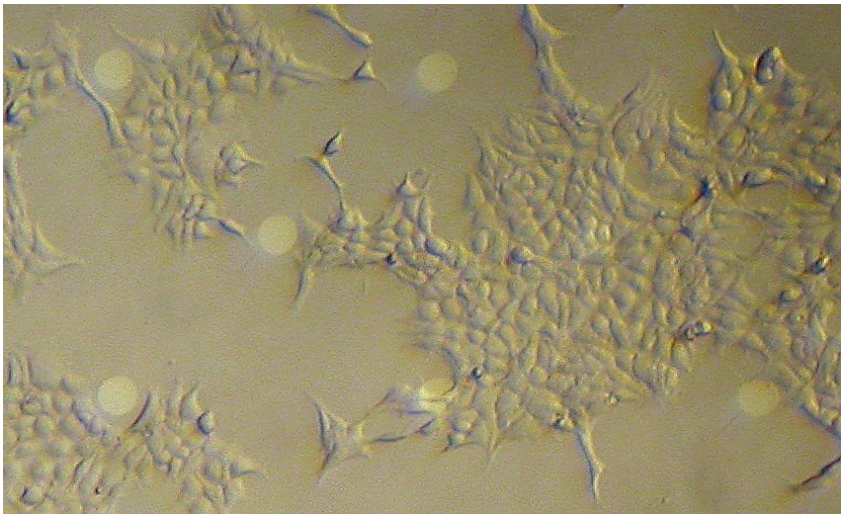

HEK 293 cells cultured on a version of chip 3 (for parylene design details see 4.1.1) fabricated on borosilicate glass wafer, in place of SiO_2. Note failed repulsion from the borosilicate background surface. Imaged after 3DIV. Parylene nodes are 50 μm diameter, region shown measures 700 μm ×1200 μm.

Figure 2-14 Patterning indices for HEK 293 cells cultured on borosilicate glass chips compared with SiO_2 chips

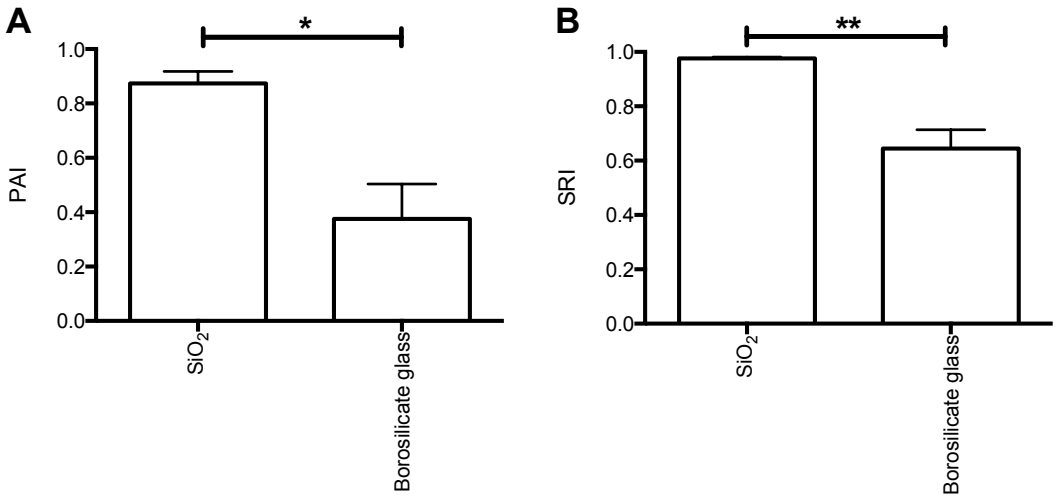

*Comparison of PAI (A) and comparison of SRI (B) for HEK 293 cells cultured on SiO_2 chips and borosilicate glass chips. Cultures assessed at 3DIV. Patterning fails on borosilicate glass wafers due to the absence of repulsion from background glass regions. Data is illustrated as mean±SEM. Mann Whitney U test used to compare groups, * denotes $P<0.05$, ** $P<0.001$. For each wafer type, 15 ROIs from 3 independent chips were assessed.*

2.5 Discussion

2.5.1 HEK 293 derived insights into patterning

HEK 293 cells patterned accurately using the pre-established protocol and therefore fulfilled their intended role as a model cell line. However, this finding does not in itself add credence to any particular patterning hypothesis. Although the HEK 293 integrin profile may be important in enabling adhesion to parylene-C, the broad range of potential ECM adhesion molecule ligands for which they possess receptors does not narrow the search for the key adhesion molecule(s). Indeed, arguably the core realisation from this sequence of experiments relates to repulsion from SiO_2. Absolute repulsion from SiO_2 domains is *fundamental* to effective cell patterning. The importance of repulsion from surrounding SiO_2 was not adequately considered when HEK 293 cells were initially selected.

The effect of time on HEK 293 patterning

SRI is high from the outset and attenuates only towards the end of the 7-day assessment window. Therefore cells evidently do not migrate from SiO_2 towards cytophilic parylene over time: SiO_2 appears to be hostile to cells from the *outset*. The late drop in SRI can be attributed to overgrowth of parylene-C-adherent cell clusters, with resultant impingement onto adjacent SiO_2. PAI increases towards a value of one from day one to day 7 in vitro, reflecting continued proliferation of cells adherent to parylene. Both initial cell plating density, cell proliferation rate, and the relative size of the patterned cell type evidently influences the PAI metric.

For downstream applications using functional neurons, it will be important to exert fine control over placement of both the cell soma and any extending axonal or dendritic components. As such, it is interesting to assess the impact of the parylene-C pattern upon cell morphology. HEK 293 cells patterned reliably on a wide range of different geometric parylene-C patterns. Single cell bodies could be isolated with appropriately small parylene-C feature sizes and cell projections and cell elongation were, in some instances, influenced by the underlying parylene-C design (see Figure 2-7). A more detailed assessment of the impact upon HEK 293 cytoarchitecture

might be achieved by immuno-staining cytoskeletal components (for example by immune-labelling neurofilament-M (104)).

HEK 293 phenotypic uncertainties – neuronal origin?

Certain neuronal cellular machinery has been identified in HEK 293 cells (namely neurofilament-M, neurofilament-L, α-internexin, together with endogenous expression of voltage-gated ion currents (104,105)). However, whilst HEK 293 cells may therefore have some characteristics of an early neuronal lineage cell, they are some way from manifesting a *functional* neuronal phenotype capable of generating spontaneous electrical activity, forming synapses, or releasing neurotransmitters.

2.5.2 The contribution of fabrication phases to downstream cell patterning

Impact of piranha treatment

For water-activated, non piranha-treated chips, cell adhesion and morphology is highly abnormal. Cell bodies are hard to resolve and a confluent sheet of cells dominates, adherent predominantly to SiO_2 but also apparently influenced to some extent by topography (see Figure 2-8). Piranha treatment without serum activation results in re-establishment of more normal HEK 293 morphology, but cells adhere to both surfaces similarly thus obliterating patterning capability.

When the parylene-C:SiO_2 platform was first developed, piranha treatment was included as a cleaning step, specifically to remove any residual organic material. Use of piranha acid in this way is well established in the microelectronics industry. This step was explicitly *not* motivated by a purported role in facilitating discriminative cell patterning. However, it has been shown to be crucial. Failure to perform piranha treatment results in a parylene-C patterned surface that does not possess an adequate differential between cell adhesive and cell repulsive domains. The primary role of piranha treatment is in enabling background SiO_2 to exert total cell repulsion after serum treatment, reflected by an SRI of one.

Furthermore, the action of piranha acid is time limited. If piranha-treated chips are not serum-incubated immediately, SRI falls. A corresponding change in the contact

angle of piranha-treated SiO_2 regions is also observed if surfaces are left (at room temperature in non-airtight boxes) and then re-assessed. Interestingly, this degradation of piranha-effect can be salvaged by repeat piranha treatment. However, from a practical point of view, parylene-C patterns cannot tolerate the second treatment and are subject to erosion and lift-off. It is also interesting to note that the efficacy of patterning deteriorated (specifically, the SRI decreased) when using piranha acid made from aged H_2O_2 (data not shown). This was resolved when new H_2O_2 was sourced, resulting in re-establishment of dominant repulsion from SiO_2.

In summary, effective piranha acid treatment causes a crucial but transient alteration in SiO_2 regions on-chip. These changes manifests as:

1. A reduction in contact angle from 27.3° to 5.6°, but which drifts back upwards if surfaces are left in atmospheric conditions.
2. An alteration in surface roughness from features of just 1-2 nm size to features of 20-40 nm size.

This piranha acid effect is necessary in enabling subsequent serum incubation to imbue SiO_2 domains with their crucial cytophobic character. One potential explanation is that piranha acid treatment results in a SiO_2 surfaced dominated by free hydroxyl groups. These free hydroxyl groups result in impaired *functional* serum protein absorption. However, with the passage of time, hydroxyl groups become cross-linked. The result of cross-linking is that, following serum incubation, serum proteins adhere in a more sympathetic conformation, and cells are therefore able to engage via their CAMs. A gradual hydroxyl cross-linking process is consistent with the change seen in contact angle before and after piranha treatment, and by the gradual increase in contact angle over time following piranha treatment. Moreover, previous work using parylene-patterned SiO_2 noted that UV exposure to chips prior to serum incubation (as a means of sterilization) resulted in impaired downstream patterning due to increased cell adhesion to SiO_2 (100). UV light has a heating effect on SiO_2, which would be expected to promote more rapid cross linking of hydroxyl groups and therefore increase undesirable serum protein adhesion. This hypothesis could be explored further through use of infra-red spectroscopy, a technique which

has previously been deployed to determine the concentration of hydroxyl groups on SiO_2 surfaces (106).

Considering parylene-C domains, the impact of piranha acid exposure is less significant. Even without performing the piranha step, parylene-C domains facilitate cell adhesion following serum incubation. Surface roughness of parylene-C areas was also not altered to any significant degree by piranha acid treatment. Delayed serum incubation following piranha treatment did not significantly alter downstream PAI, in contrast to the situation observed for SiO_2. Contact angle was, however, reduced by a similar order of magnitude to that seen on SiO_2 (74.6° → 60.4°), though this did not parallel a change in cell adhesive behaviour.

Impact of serum incubation

Cell patterning is only achieved when piranha acid treatment is followed immediately by serum incubation. In this context, serum activation affords a dramatic downstream increase in PAI and pushes SRI close to the maximum of 1. The overall result is effective, discriminative cell patterning (see Figure 2-8E). Interestingly, the effect of serum incubation upon contact angle is such that both surfaces, immediately prior to cell plating, are similarly hydrophilic with the same contact angle of ~14° (parylene-C falls from 60.4° to 14.2° whilst SiO_2 increases from 5.6° to 14.1°). This finding most likely reflects that both surfaces are coated with a protein layer following serum incubation. Unfortunately Raman spectroscopy was unable to discern specific components of this protein layer. The likely cause for this failure in resolution is signal noise generated by fluorescence or heating of silicon, which obliterates the ability to detect small adherent protein molecules.

2.5.3 Effect of rationalised protein activation solutions

Cell patterning relies on contrasts. None of the rationalised protein solutions was able to induce the patterning behaviour observed with serum activation, where SiO_2 is profoundly cytophobic and parylene is cytophilic. However, under certain activation conditions, the patterning process could be inverted owing to a total reversal of adhesive characteristics of the two substrates.

Pure solutions of the ECM proteins vitronectin, fibronectin, laminin, or collagen enabled significantly enhanced adhesion to parylene-C compared with water controls (with vitronectin and collagen exerting the greatest effect). However, the extent of adhesion remained approximately 5× poorer than for serum-activated chips. Importantly, the concentration of single protein used (1 μg/ml) is of a similar order of magnitude to that found in serum (reported values range from 0.14-0.6 μg/ml in human serum (107)). In any event, patterning is undermined in these cases by attenuation of the SRI. The combination of cell tolerance to both substrates results in failure of cell patterning.

Solutions of BSA alone caused parylene to become notably cytophobic (especially at 30mg/ml concentration), while SiO_2 became relatively cell-tolerant. This is an unexpected finding in the context of an early hypothesis that albumin may be responsible for imbuing SiO_2 with a cyto-*repulsive* character. Combinations of BSA with vitronectin or BSA with fibronectin resulted in a similar patterning configuration. However, the presence of vitronectin in BSA solutions did somewhat mitigate the observed decrease in PAI. Nevertheless, in combination with a persisting cell tolerance on SiO_2, the net result is inverted, or negative, patterning.

The observed changes in PAI and SRI are modulated by the concentration of BSA in which a second protein is co-dissolved. The cause for this in unclear but it is, interestingly, a phenomenon that has been observed before in the context of fibronectin binding on hydrophobic surfaces (108). One explanation is that co-bound albumin alters the configuration or packing of the second protein such that its binding sites are more or less available.

Given these findings, a model of adhesion relying on pro-adhesive and pro-repulsive proteins in isolation is probably an oversimplification. More likely is a *combinatorial* effect of different proteins, in different functional states, giving the two regions of the chip their contrasting adhesive characteristics. Although we cannot as yet identify the key protein combinations in serum, we have (in the context of HEK 293 cells) developed the capacity to induce cell-tolerance to SiO_2 and cell repulsion from

parylene (a complete reversal of the serum-induced parylene patterning effects reported previously (91,99,100,109,110).

2.6 Conclusions and new hypotheses

Work in this chapter has demonstrated the ability to pattern, at high resolution, HEK 293 cells on parylene-C:SiO_2 substrates. Moreover, the geometry of underlying parylene-C can influence the morphology of the cell.

Chip fabrication processes have a significant impact upon the surface characteristics of the two patterned substrates. Piranha acid treatment is key to enabling SiO_2 domains to exert cell repulsion after serum incubation. Both a decrease in contact angle and a marked change in surface roughness reflect the impact of piranha acid upon SiO_2. However, its effect is transient meaning that serum incubation must occur immediately after piranha treatment.

No rationalised protein activation solutions were able to reproduce the effect of serum incubation. We have not identified the key components of serum that interact to imbue each substrate with its respective cyto-adhesive or cyto-repulsive character, though vitronectin appears to have a role in enabling adhesion to parylene-C. Although the overarching mechanism of action of the platform has not been determined, this sequence of experiments has illustrated key fabrication steps that, if deviated from, will undermine patterning. This is important for downstream cell patterning work.

2.7 Cell-centric approaches

To compliment insights derived by assessing chip surface characteristics, the patterning platform was next assessed from a *cell*-centric perspective.

2.8 Introduction

2.8.1 Patterning behaviour across different cell types

If adhesion to parylene-C relies on cell engagement with specific parylene-bound protein(s), adhesion will require the presence of appropriate complimentary CAMs in the cell membrane. Given the extensive heterogeneity of CAMs across cell types, it was hypothesised that cell adhesion behaviours will not be constant across different cell types. Certain cells will lack the necessary CAM(s), will therefore be unable to engage with parylene-bound proteins, and therefore will not adhere.

Similarly, repulsion may be a specific or non-specific phenomenon. If repulsion from SiO_2 manifests due to the generalized absence of any functional pro-adhesive proteins, the repulsive effect might be expected to impact broadly across all cell types. However, if repulsion depends on some form of specific interaction with the cell glycocalyx, then this aspect of patterning may too vary across different cell types.

Finally, some cell types have the capacity to self-generate ECM proteins in large volumes (e.g. myofibroblasts secrete copious quantities of ECM proteins) (111). This can enable adhesion to surfaces that might otherwise be repulsive, whereby a layer of secreted proteins becomes a pro-adhesive 'carpet'. Such a cell might fail to pattern on the parylene-C:SiO_2 platform, as it would adhere and spread indiscriminately on both surfaces.

To explore these ideas further, a broad range of different cell types was assessed on the parylene-C:SiO_2 platform (using the standard piranha acid and serum activation protocols). These included immortalised cell lines, primary cells, and embryonic stem cell-derived or stem-like cells. The core aim was to identify cell-specific features associated with given patterning behaviours; features that complimentarily might help to elucidate important chip substrate characteristics. Most cells tested

were of nervous system origin. Given the ultimate downstream goal of patterning neurons, LUHMES neurons (in both an undifferentiated and differentiated state) were included in the range of cell types tested. Bioinformatic analysis of micro-array mRNA expression data was also explored as a potential method of identifying expression of specific CAMs or other proteins associated with a given adhesion/repulsion phenotype.

Immortalised cell lines:

1. Human Embryonal Kidney (HEK 293). See 2.2.1 for details. Previously considered a derivative of mouse embryonic fibroblastic or endothelial renal cells (102) but now recognized to have some features of early neuronal lineage (104,105). As previously demonstrated, HEK 293 cells pattern accurately and therefore serve as a useful control.

2. Undifferentiated and differentiated Lund Human Mesencephalic (LUHMES) neurons. See 1.6.4 for full details. Sub-clone of the tetracycline-controlled, *v-myc* overexpressing, human mesencephalic-derived cell line MESC2.10 (originally from Lund University, Sweden). Differentiated cells represent a robust, functional dopaminergic neuronal model (101).

3. N9 microglia. A mouse-derived cell line with phenotypic characteristics similar to primary microglia (112). Microglia are the CNS equivalent of macrophages, release trophic factors and various cytokines, and have a role in tissue repair and neuro-protection.

4. Undifferentiated Neuro 2a (N2a). A mouse neural crest, neuroblastoma-derived cell line. N2a cells have been used to model neurite growth, neuronal differentiation, and signaling pathways (113).

5. Undifferentiated 3T3 L1 pre-adipocytes. Derived from 3T3 cells (themselves derived from primary mouse embryonic fibroblasts), these cells have fibroblast-like characteristics. They have been used for obesity and metabolism research due to their

ability to differentiate into adipocytes (114). Here, they were trialed in their undifferentiated pre-adipocyte state.

6. Human Brain Endothelial Cells (HBEC-5i). HBEC-5i were originally derived from post mortem fragments of human cerebral cortex by Dorovini-Zis and Bowman (115). These cells represent a useful model of aspects of the human blood-brain barrier (BBB) and consequently have been used extensively in malaria research (116).

7. mHypoE-N7. This is an immortalized murine hypothalamic cell line. This is one of a number of similar clonal neuronal cell lines which have been used, for example, to model neuropeptide regulation in feeding behaviour (117).

Primary cells:

1. Dispersed murine anterior pituitary cells – containing the following cell types:

- Somatotrophs (up to 50% of the cell population)
- Gonadotrophs (10-15%)
- Lactotrophs (10-25%)
- Corticotrophs (2-5%)
- Thyrotrophs (<10%)
- Non-endocrine folliculostellate cells (5-10%)

2. Murine hepatic pericytes (also known as hepatic stellate cells (HSC), perisinusoidal cells, or Ito cells). Pericytes are vascular cells found on small diameter blood vessels, but whose function is not yet well understood. They have some phenotypic similarities with smooth muscle cells and are broadly involved in the development and remodelling of blood vessels. In the CNS, they have a role in blood flow regulation and form a component of the BBB.

Embryonic stem (ES) cell-derived:

1. Wild type mouse ES cell-derived neurons and MeCP2 null neurons. ES-derived neurons represent an alternative model neuronal cell line, all be it one that is

more resource intensive and more complex to generate. MeCP2 null neurons are used to model Rett syndrome, an autism spectrum disorder.

In Rett syndrome, affected children lose previously learned motor and communication skills, and later develop cognitive impairment, motor dysfunction, and seizures. Rett syndrome can be caused by mutations in the gene that encodes MeCP2 (methyl-CpG binding protein). Some purport a role for MeCP2 in regulating synaptic function and propose that Rett syndrome is, ultimately, a neural network disorder (118). MeCP2 null neurons model, at a single cell scale, Rett syndrome. Given some of the ultimate motivations of this project, they were appealing with a view to potential disease modelling in the context of topographically defined neuronal networks.

2. Human Glioma Stem-like Cell (GSC) lines. GSCs are a subpopulation of cells within glial tumours. They have stem-like characteristics and are thought to be responsible for tumour recurrence and treatment resistance (119). The cell lines used for this work were newly derived during recent tumour debulking surgery. As such, they currently remain somewhat poorly defined.

However, high grade human glial tumours (similar to those from which these cell lines were derived) have previously been shown to express the αVβ3 integrin (120), which can bind vitronectin. Given prior work illustrating that adhesion to parylene may be mediated by vitronectin, this infers that GSC cell lines may too possess the capacity to bind to serum-activated parylene regions. Three different cell lines were extracted from patients undergoing tumour-debulking neurosurgery. Of the three cell lines used for patterning trials, one came from histologically confirmed glioblastoma (GSC-A) and two from oligodendroglioma (GSC-B and GSC-C).

Key questions:

1. Do cell patterning behaviours on the parylene-C:SiO_2 platform vary across different cell types?
2. Can cell-specific characteristics that are associated with the capacity to pattern effectively be identified?
3. Does the LUHMES neuronal cell line pattern effectively, either in an undifferentiated or differentiated state?

2.9 Methods

2.9.1 Cell maintenance and plating protocols

Chip fabrication and activation protocols were kept constant for all cell trials, using the standard piranha acid treatment and serum incubation phases detailed in section 2.3.3. Chip 1 (node and 'cross hair' design) was used for all experiments in this series.

Human embryonal kidney (HEK 293) cells.

See 2.3.4 for culture details. Cells were plated at a density of 5×10^4 cells/mL and imaged alive after 3DIV.

Lund Human Mesencephalic cell line (LUHMES)

LUHMES cells (American Type Culture Collection) were maintained at 37°C and 5% CO_2 in pre-coated plastic culture flasks (coated with 50 mg/mL poly-L-ornithine and 1 mg/mL fibronectin in H_2O for 3 h at 37 °C). Proliferation media consisted of Advanced DMEM/F12 (Gibco Invitrogen), 1×N2 supplement, 2 mM L-glutamine and 40 ng/mL recombinant basic fibroblast growth factor (FGF; Gibco Invitrogen). Differentiation media consisted of Advanced DMEM/F12 (Gibco Invitrogen), 1× N2 supplement, 2 mM L-glutamine and 1 mg/mL tetracycline.

To differentiate into post-mitotic neurons, proliferation media was changed to differentiation media 24 h after passaging cells. After 2 further days in differentiation media, cells were trypsinized and plated. Undifferentiated (UD) LUHMES were plated as a suspension of 5×10^4 cells/mL in proliferation media whilst pre-differentiated (DF) LUHMES were plated as a suspension of 30×10^4 cells/mL in differentiation media. Both were imaged alive after 3 days *in vitro*.

Undifferentiated 3T3 L1 pre-adipocyte cell line

3T3 L1 cells (a gift from Dr Luke Chamberlain, Strathclyde Institute of Pharmacy and Biomedical Sciences, University of Strathclyde) were maintained at 37 °C and 10% CO_2 in DMEM (Gibco Invitrogen) supplemented with 10% FBS and 1%

penicillin–streptomycin. Cells were applied to chips as a suspension of 5×10^4 cells/mL in growth media and imaged alive after 3 days *in vitro*.

N2a cell line

N2a cells (American Type Culture Collection) were maintained at 37 °C and 5% CO_2 in DMEM (Gibco Invitrogen) supplemented with 10% FBS. Cells were applied to chips as a suspension of 5×10^4 cells/mL and imaged alive after 3 days *in vitro*.

N9 microglial cell line

N9 cells (a gift from Prof Alun Williams and Dr Clive Bate; The Royal Veterinary College, University of London) were maintained at 37 °C and 5% CO_2 in Iscove's modified Dulbecco's medium (Gibco Invitrogen) with 5% FBS, 100 IU/mL penicillin, and 100 μg/mL streptomycin. Cells were applied to chips as a suspension of 15×10^4 cells/mL and imaged alive after 3 days *in vitro*.

mHypoE-N7

mHypoE-N7 (a gift from Javier Tello, Centre for Integrative Physiology, University of Edinburgh) were grown in DMEM (Gibco Invitrogen) supplemented with 5% FBS (Gibco Invitrogen), 20 mM glucose, 1% penicillin/streptomycin and maintained at 37 °C and 5% CO_2. Cells were applied to chips as a suspension of 6×10^4 cells/mL and imaged alive after 3 days *in vitro*.

Human brain endothelial cells (HBEC-5i)

HBEC-5i cells (a gift from Prof Rowe; Institute for Immunology and Infection Research, University of Edinburgh) were cultured in DMEM/F-12 medium (Sigma) with 2 mM L-glutamine supplement (Gibco Invitrogen), 1% penicillin–streptomycin, 10% FBS, and 30 μg/mL endothelial cell growth supplement. Cells were applied to chips as a 2 ml suspension of 5×10^4 cells/mL and imaged alive after 3 days *in vitro*.

2.9.2 Primary cells

Murine primary anterior pituitary cells

Anterior pituitary cell isolation was performed by Peter Duncan (Centre for Integrative Physiology, University of Edinburgh). Two mice were killed by cervical dislocation. Heads were removed, the pituitary glands were identified and carefully dissected free, and the posterior and intermediate lobes were removed and discarded. Remaining anterior lobes were broken down by hand using a single edged razor blade in two directions. This preparation was digested in a solution of DMEM (+4.5 g/L high-glucose, +L-Glutamine, +25 mM HEPES, -Pyruvate; Gibco) containing 0.25% Trypsin (Worthington, New Jersey, USA) and 10 μg/ml DNAse I and incubated at 37 ºC for 20 minutes.

Following digestion, cells were suspended in 5 ml of inhibition solution (DMEM [+4.5 g/L high-glucose, +L-Glutamine, +25 mM HEPES, -Pyruvate] containing 0.5 mg/ml Soybean Trypsin inhibitior, 100 kallikrein units aprotinin [200× dilution of Sigma stock], 10 μg/ml DNAse I). This cell suspension was passed through a pre-wetted 70 μm nylon mesh (BD Bioscience), diluted with an equal volume of culture medium (DMEM [4.5 g/L high-glucose, +L-Glutamine, +25 mM HEPES, -Pyruvate] with ITS [5 μg/ml insulin, 50 μg/ml transferrin, 30 nM sodium selenite], 0.3% BSA [w/v], 4.2 μg/ml fibronectin and antibiotic/antimycotic [100x dilution of sigma stock]) and spun in a centrifuge at 100 G for 10 minutes. After supernatant removal, cells were re-suspended in 4 ml of culture media. 200 μl of this cell suspension was pipetted onto the chip surface, left for 10 minutes to allow the cells to settle, and then a further 2 ml of culture media was gently added to the culture well. Cells were incubated at 37 ºC in 5% CO_2 and media was changed every two days with antibiotic/antimycotic-free media.

Murine liver-derived pericytes

Murine pericyte preparation was performed by Kylie Conroy (MRC Centre for Inflammation Research, Queen's Medical Research Institute, University of Edinburgh). Two mice were killed by cervical dislocation. Livers were perfused with HBSS+, dissected out, and digested using pronase/collagenase and the gradient

centrifugation method, as described in (121). Pericytes were seeded onto uncoated plastic tissue culture wells and cultured in a solution of DMEM (+4.5 g/L high-glucose, +L-Glutamine, +Pyruvate; Gibco), 16% FBS, and 1% penicillin–streptomycin. On day 6 post-isolation, cells were re-suspended in growth media and plated on chips as a 2 ml suspension of 5×10^4 cells/mL per well, and imaged alive after 3 days *in vitro*.

2.9.3 Embryonic stem cell-derived and 'stem-like' cells

Wild type and MeCP2 null ES-derived neurons

Preparation of all WT and MeCP2 null ES cell-derived neurons was performed by Kyla Brown (The Wellcome Trust Centre for Cell Biology, University of Edinburgh).

Wild type ES cell-derived neuronal differentiation:

4 x 10^6 mouse embryonic stem cells (E14 TG2a line from mouse substrain 129/Ola) were plated in 10 cm bacterial dishes (Greiner, Stonehouse, UK) in Embryoid Body (EB) medium (GMEM (Gibco); 10% fetal bovine serum (Hyclone); 1 mM sodium pyruvate; 1×MEM non-essential amino acids; 50 μM β-mercaptoethanol; 2 mM L-glutamine (Life Technologies)) on day 0. Medium was changed on day 2, day 4 (+5 μM retinoic acid) and day 6 (+5 μM retinoic acid). On day 8, cells were washed in PBS, trypsinised with 0.05% trypsin (Sigma) in 0.05% EDTA in PBS, neutralized with 10ml EB medium, spun down for 5 minutes at 1000 RPM, re-suspended in N2 medium (DMEM/F12, 1× N2 supplement, 1× penicillin streptomycin (all Invitrogen)) adjusted according to number of dishes and passed through a 40 μm cell strainer (BD Falcon). Cells were counted, spun for 5 mins at 1000 RPM, and then re-suspended in an appropriate volume of N2 medium. For patterning experiments, cells were plated on-chip as a 2 ml suspension of 5×10^4 cells/mL per well. After 1 day on-chip, medium was replaced with 1:1 N2:Neurobasal medium (+1× B27 supplement and 1× penicillin streptomycin (Invitrogen)). After 3 days on-chip, half the medium was removed and replaced with Neurobasal medium. Chips were imaged after 3 days *in vitro*.

MeCP2 null ES cell-derived neuronal differentiation:

A targeting vector (made by Dr Jacky Guy, The Wellcome Trust Centre for Cell Biology, University of Edinburgh) with exon 3 and exon 4 of MeCP2(R133C) (mutation made with Sigma QuikChange II XL Site-Directed Mutagenesis Kit; forward primer CCCAGGGAAAAGCTTTT**TGC**TCTAAAGTAGAATTG, reverse primer CAATTCTACTTTAGA**GCA**AAAAGCTTTTCCCTGGG), a GFP tag, a floxed NEO cassette, 2.8 kb 5' homology arm and 1.8 kb 3'. Gene targeting was performed on E14 TG2a ES cells, derived from the 129/Ola substrain mouse. Cells were grown in complete ES medium (Glasgow MEM (Invitrogen) supplemented with 15% fetal bovine serum (Hyclone), 1× MEM non-essential amino acids, 1 mM sodium pyruvate, 50 μM β-mercaptoethanol and 2 mM L-glutamine (all Life Technologies) with recombinant human LIF on gelatinized dishes). 2×10^7 ES cells were transfected with 30 μg linearized targeting vector in 0.6 ml HEPES buffered saline by electroporation (240 V, 500 μF, BioRad Gene Pulser) and plated in 10 cm dishes at 5×10^6 or 2.5×10^6 cells per dish on day 0. Cells were positively selected by growing in complete ES medium + 350 μg/ml G418 (Life Technologies) from day 1 and then 150 μg/ml G418 from day 3. On day 9 colonies were picked. For patterning experiments, cells were plated on-chip as a 2 ml suspension of 5×10^4 cells/mL per well. After 24 h on-chip, medium was replaced with 1:1 N2:Neurobasal medium (+1× B27 supplement and 1× penicillin/streptomycin (Invitrogen)). After 3 days on-chip, half the medium was removed and replaced with Neurobasal medium. Chips were imaged alive after 3 days *in vitro*.

Human primary glioma-derived cell cultures

The GSC cell lines were developed and maintained by Paul Brennan (Edinburgh Cancer Research Centre, Institute of Genetics and Molecular Medicine). MH was an assisting surgeon in two of the cases during which tumour tissue was isolated.

Human glioma-derived primary cell cultures were obtained from fresh human glioma tissue removed intra-operatively during surgery to diagnose and debulk tumours. All patients gave informed signed consent. The South East Scotland Research Ethics committee approved the process (LREC 2004/4/16). A single-cell suspension was

generated from the tumour and cells were allowed to form neurospheres in non-adherent conditions, similar to previous descriptions of glioma stem cell (GSC) primary culture (119). Briefly, cells were maintained at 37 °C and 5% CO_2 in Advanced DMEM F12 (1:1) (Gibco Invitrogen) supplemented with 1% B27 (10×), 0.5% N2 (100×), 1% Glutamax 100 mM, 1% penicillin–streptomycin, 1% fungizone, EGF 10 ng/mL (R&D Systems, Abingdon, UK), basic FGF 10 ng/mL (R&D Systems, Abingdon, UK), Heparin 5 mg/mL (Sigma Aldrich, Gillingham, UK). After neurospheres had formed in suspension culture, cells were expanded on plastic flasks coated with growth factor reduced Matrigel (BD Biosciences, Oxford, UK) diluted 1:80 in Advanced DMEM F12 for 30 min at 37 °C. In this way, GSC primary cultures were derived from three different tumours and named GSC-A, GSC-B, and GSC-C. A 50 μL droplet containing 10,000 GSC cells in suspension was pipetted onto each chip surface, incubated for 10 min, followed by addition of 2 mL maintenance media. Cells were imaged alive after 3 days *in vitro*.

2.9.4 Cell imaging and analysis

All cells were imaged live *in vitro* using a Wild Heerbrugg (Switzerland) light microscope adapted for use with a Nikon Coolpix 4500 digital camera using an MDC2 relay lens. Image J (version 1.44o, National Institute for Health, USA) was used for image analysis and measurement of cell surface areas. PAI and SRI (described previously) were measured to objectively assess patterning.

2.9.5 DNA micro-array data collection

The Gene Expression Omnibus (GEO, www.ncbi.nlm.nih.gov/geo/) and ArrayExpress (www.ebi.ac.uk/arrayexpress/) databases were searched for DNA micro-array data relating to all of the cell types trialled. When available, datasets were identified that represented normal or control experimental data. MH identified appropriate data sets. Raw data acquisition and data warehousing was performed by Donald Dunbar and Jonathan Manning (Bioinformatics Department, Queens Medical Research Institute, University of Edinburgh). As such, an online database allowing comparison of gene expression across different cell lines was created (URL: www.bioinf.mvm.ed.ac.uk/projects/hughes/search.php).

2.10 Results

2.10.1 Patterning behaviour across cell types

Cell patterning behaviour was highly heterogeneous, with adhesion to parylene-C and SiO_2 varying significantly according to cell type. The theoretical range of potential patterning behaviours can be illustrated by plotting PAI against SRI (see Figure 2-4). Figure 2-15 illustrates a similar plot showing data for all cell types tested, whilst Figure 2-16 shows the same PAI and SRI data plotted separately. Example photomicrographs for a selection of the cell types tested is shown in Figure 2-17.

LUHMES in both a differentiated or undifferentiated state did not adhere to either substrate (reflected by a SRI of almost one and PAI of almost zero: undifferentiated LUHMES: PAI 0.02±0.05, SRI 1.0±0.01 [n=27, assessed 3DIV]; differentiated LUHMES: PAI 0.0±0.0, SRI 1±0.0 [n=27, assessed 3DIV]). On the rare occasion where cell material was seen chip-bound, the cell body showed spherical morphology suggesting poor adhesion. WT and MeCP2 null ES-derived neurons similarly completely failed to adhere to either substrate (WT ES neuron: PAI 0.01±0.0, SRI 0.99±0.0; MeCP2 null ES neuron: PAI 0.01±0.01, SRI 0.99±0.01). This global chip repulsion behaviour was also seen for isolated murine anterior pituitary cells, with no adhesion seen on parylene-C or SiO_2 (murine anterior pituitary cells: PAI 0.01±0.01, SRI 1.0±0.0).

N2a, N9, mHypo-E N7, and 3T3 L1 pre adipocytes were able to grow on both substrates, consequently showing no patterning capability (N2a: PAI 0.38±0.02, SRI 0.89±0.01; N9: PAI 0.59±0.03, SRI 0.65±0.01; mHypo-E N7: PAI 0.45±0.06, SRI 0.2±0.03; 3T3 L1: PAI 0.61±0.08, SRI 0.48±0.08).

HEK 293, HBEC-5i, murine liver-derived pericytes, and all three GSC sub-types were found to have an SRI approaching 1 in combination with a high PAI (HEK 293: PAI 0.87±0.04, SRI 0.98±0.0; HBEC-5i: PAI 0.81±0.02, SRI 0.99±0.0; murine pericytes: PAI 0.85±0.04, SRI 0.97±0.0; GSC-A: PAI 0.83±0.05, SRI 0.96±0.01; GSC-B: PAI 0.99±0.0, SRI 0.96±0.01; GSC-C: PAI 0.96±0.03, SRI 0.95±0.01). This combination represents effective, discriminative cell patterning.

Figure 2-15 A plot of PAI and SRI for all cell types tested

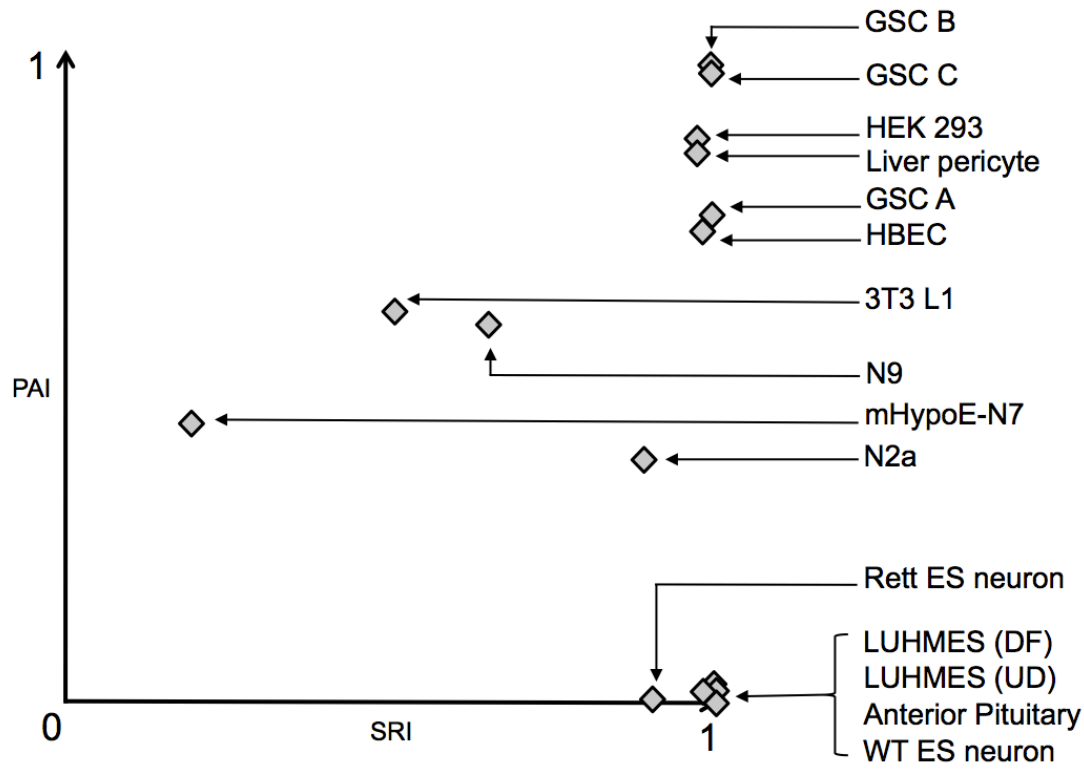

Mean parylene-C adhesion index (PAI) plotted against mean SiO_2 repulsion index (SRI) for all cell types tested. GSC cells, HEK 293 cells, pericytes, and HBEC 5i cells were found to pattern appropriately on-chip, manifesting a high SRI and high PAI. Pre-differentiated and undifferentiated LUHMES, WT ES and Rett ES neurons, and the anterior pituitary cells all found the entire chip surface repellent, adhering to neither substrate. 3T3 L1, N9, mHypoE-N7, and N2a cells were capable of adhering to both surfaces and therefore did not pattern. For SEMs, see Figure 2-16.

Figure 2-16 PAI and SRI plotted separately for all cell types tested

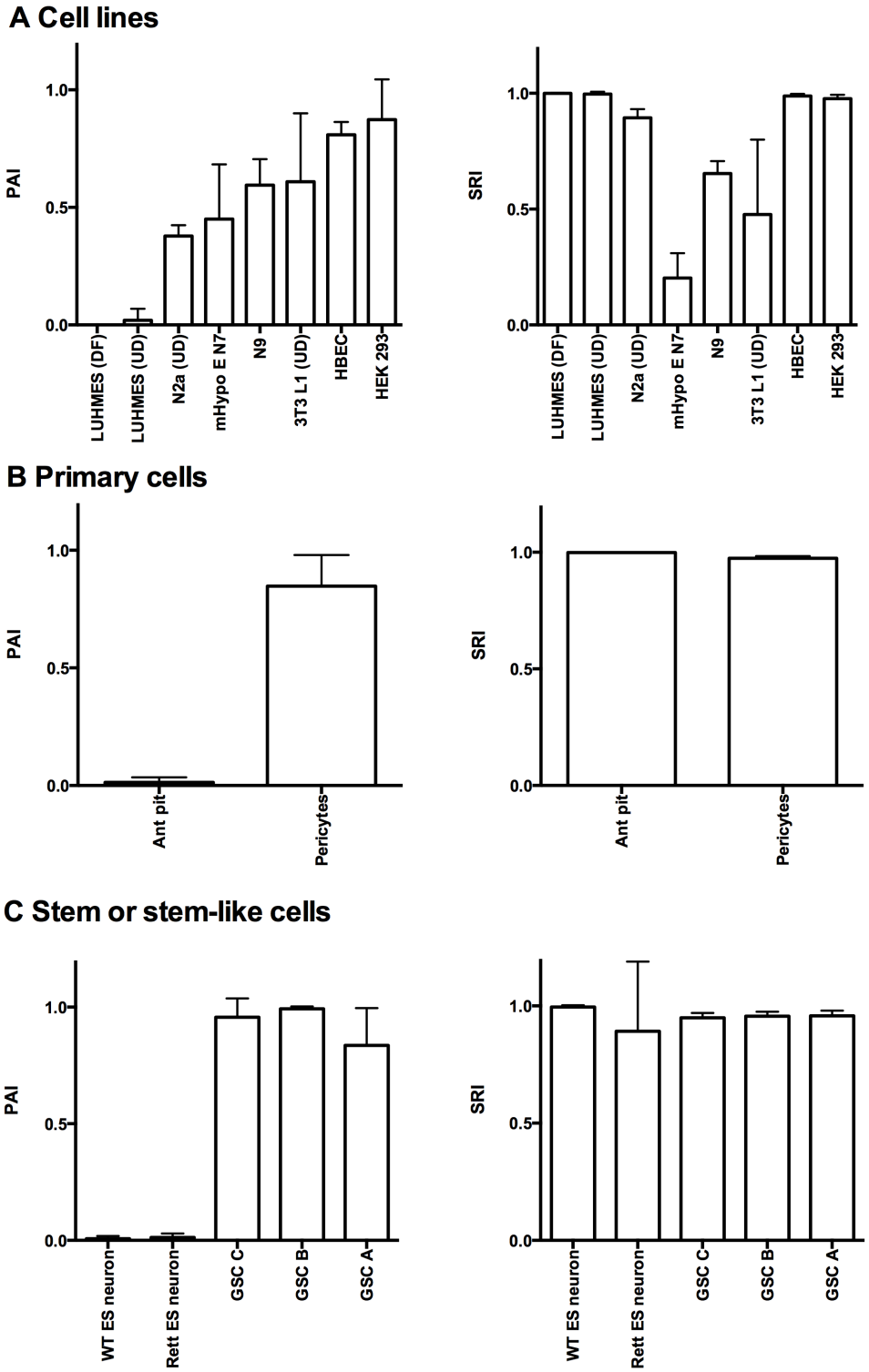

Parylene-C adhesion index (PAI) and SiO_2 repulsion index (SRI) charted separately for all cell types assessed and categorised by origin. Data is illustrated as mean±SEM. For each cell line, a minimum of 27 ROIs from 3 independent chips was assessed.

Figure 2-17 Illustrative photomicrographs of cell patterning

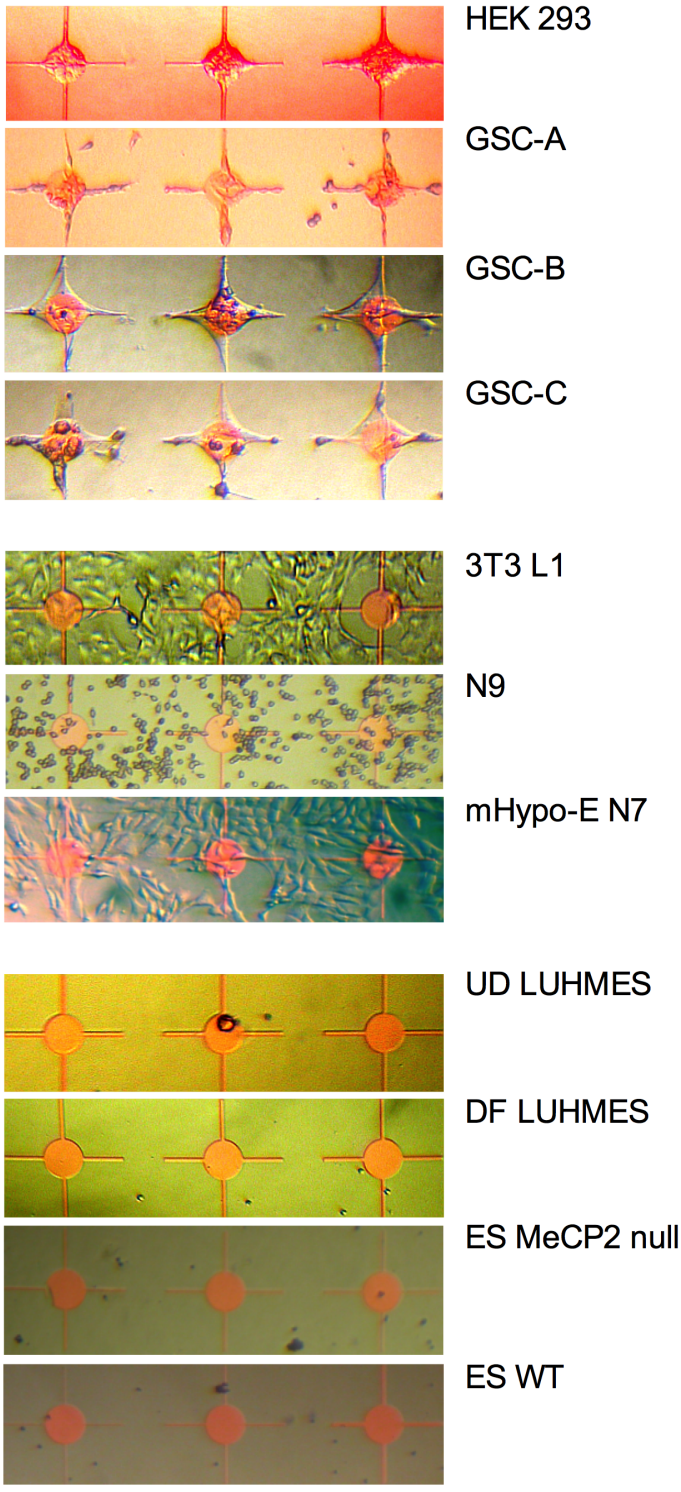

Illustrative photomicrographs showing adhesion behaviour for a selection of cell types tested. Note the markedly different behaviour across cell types; ranging from robust patterning, to undiscerning adhesion, to total repulsion from both substrates. Parylene-C nodes are 100 μm diameter in all cases and each region measures 300 μm × 1100 μm.

2.10.2 Comparison of DNA micro-array data

Appropriate DNA micro-array data was identified and consolidated for HEK 293, 3T3 L1, and N2a cell types only (see appendix 6.3 for GEO data set reference details). This very limited dataset was insufficient for identification of viable candidate genes.

2.11 Discussion:

Importantly, cell-plating densities varied somewhat across the cell types tested[§§§]. Combined with differences in both cell size and proliferation rates, this brings inherent difficulties in comparing patterning indices of different cell types. Although the numerical values are therefore not directly comparable, they have however aided categorization into three broad patterning phenotypes:

- Cells that pattern appropriately (adhere to parylene-C, repulsed completely from SiO_2): all GSC cell lines, HEK 293 cells, murine liver pericytes, and HBEC 5i cells.
- Cells that adhere to both surfaces and therefore do not pattern: 3T3 L1, N9, mHypoE-N7, and N2a cell lines.
- Cells that are globally repulsed from both surfaces: pre-differentiated and un-differentiated LUHMES, WT and Rett ES neurons, and murine anterior pituitary cells

2.11.1 Heterogeneity of patterning behaviours

Considering adhesion to parylene-C

As discussed, cell adhesion to parylene may demand that a certain integrin binds to a complimentary ligand (as presented by a non-denatured parylene-bound protein). Assessing the integrin profile of cell types with the capacity to adhere to parylene might therefore prove useful in elucidating the mechanism further. Compounding this approach, however, is the fact that most integrin receptors bind to a wide variety of ligands and many ECM proteins can also bind to multiple integrin receptors. This undiscerning binding behaviour makes identifying a key interaction difficult.

Previous protein elution studies, together with HEK 293 patterning trials using rationalised protein activation solutions, suggest a possible parylene-adhesion-promoting role for vitronectin. Integrin αVβ3 was the first identified vitronectin

[§§§] Most cell lines were plated at a density of 5×10^4 cells/mL as a 2 mL suspension. Preparation protocols for anterior pituitary cells and GSC cells generated lower numbers of cells which necessitated plating at a different density directly on-chip.

receptor. It is now clear, however, that vitronectin is able to bind to a number of other integrins (including α2bβ3, α8β1, αVβ5, and αVβ1). αVβ3 is also a particularly promiscuous integrin and is known to bind fibrinogen, fibronectin, von Willebrand's factor, osteopontin, thrombospondin-1, tenascin, nephronectin and prothrombin – as well as vitronectin (122).

HBEC-5i cells showed the capacity to adhere to parylene and to pattern on-chip. Interestingly, HBEC-5i cells have also been shown to express the integrin αVβ3 subunit (123), giving them the cell membrane machinery to engage with bound vitronectin. Analysis of the limited DNA micro-array data for HEK 293, N2a, and 3T3-L1 cells (all of which have the capacity to adhere and grow on parylene) also showed relative up-expression of the ITGAV (integrin αV) gene in all three cell types. That 3T3 L1 cells express the complete αVβ3 integrin has also been reported in the literature, in the context of IGF-1 mediated cell growth experiments (124).

Similarly, rat hepatic pericytes have been shown to express the integrins α5β1 and αVβ3 and can therefore also bind vitronectin (125). A literature search failed to provide any relevant data regarding the integrin profile of mHypoE-N7 cells.

The GSC lines were derived from three human glial tumours: one from a histologically confirmed glioblastoma (named GSC-A) and two from oligodendrogliomas (GSC-B and GSC-C). Given the previously demonstrated increased expression of vitronectin receptors in glioblastoma cells (120), these stem-like cells may too express vitronectin receptors.

Collectively, the presence of a vitronectin-binding integrin in cells that adhere to parylene is consistent with, but certainly not confirmatory of, a role for vitronectin in mediating adhesion to parylene. To explore the hypothesis further, antibodies against vitronectin receptors could be tested as a means of impeding cell adhesion to parylene-C.

On a separate note, acquiring the ability to pattern GSC, HBEC 5i, and pericytes provides an opportunity to investigate the behaviour of the cell lines themselves. For example, different parylene patterns might offer a chance to assess how (notoriously

invasive) GSC cells migrate and self organise in different, restrictive contexts. Similarly, the potential to incorporate on-chip microfluidic trenches opens the way to topographically targeted high throughput testing of potential chemotherapeutic agents.

Considering repulsion from SiO_2

Repulsion from SiO_2 domains is fundamental to effective patterning. The variability of this aspect of behaviour across cell types illustrates that repulsion is also a cell-specific phenomenon. It was hypothesised that the presence of wholly denatured proteins on SiO_2 domains (due to a surface dominated by free hydroxyl groups) may be key to enforcing cell repulsion. However, it is hard to reconcile this argument given that, of the range of cells tested, four showed indiscriminate adhesion (N2a, 3T3 L1, N9, mHypoE-N7) and the capacity to adhere *robustly* to SiO_2. One potential explanation is that such cell types are capable of secreting adhesion-mediating proteins that overwhelm an otherwise repulsive cue. 3T3 L1 pre-adipocytes, for example, secrete proteins in large quantities during differentiation (126). However, in these chip-patterning trials they were used in an undifferentiated state in which protein secretion is much less marked. Moreover, if cell-generated proteins were key to enabling adhesion on SiO_2, it would be anticipated to take time, with cells spreading from regions of established parylene-adhesion onto SiO_2 domains. In fact, this was not observed. Those cell types capable of adhering to SiO_2 did so from the *outset*. An alternative explanation is that these cells possess CAMs capable of engaging with otherwise inaccessible SiO_2-bound proteins, courtesy of a structurally different glycocalyx. Or, conversely, those cells that are repulsed from SiO_2 may in fact *possess* a membrane component that induces repulsion.

LUHMES neurons failed to adhere to either surface in either an undifferentiated or differentiated state. They found both surfaces highly repulsive. Even on the very rare occasion where LUHMES were seen to adhere, they showed no morphological evidence of differentiation into neurons. This suggests that LUHMES lack the requisite integrin to adhere to parylene-bound proteins. The same global repulsion was observed with ES-derived neurons in both the wild type and with MeCP2 null

(Rett syndrome) iterations. A search of the literature found no relevant information regarding the integrin or CAM profile for either of these cell types.

The inability of both of these neuronal cell types to engage with parylene-C paralleled an inability to morphologically differentiate into neurons. This finding re-iterates the intimation that neurons may require a glial – or other - cell type in order to adhere, pattern, and differentiate on-chip. This assertion is supported further by the observation that glial lineage GSC cells patterned very accurately.

2.11.2 Insights from micro-array analysis

Unfortunately, most of the cell lines tested had no publically available DNA micro-array data. Appropriate DNA micro-array data was identified and consolidated only for HEK 293, 3T3 L1, and N2a cell types. Relevant patterning observations with respect to these four are:

- All are capable of adhering to parylene-C.
- HEK 293 and GSC-C are avidly repulsed by SiO_2 domains.
- 3T3 L1 cells are particularly SiO_2-tolerant.
- N2a cells also show modest growth on SiO_2, though less marked.

As such, comparison of expression data from this cohort is likely to have utility only in suggesting factors that enable or disable *repulsion from SiO_2*. Either, 3T3 L1 cells express *x* (which enables adhesion to SiO_2) whilst *x* is not expressed in HEK 293 or GSC-C, or 3T3 L1 lacks expression of *y* (which prevents adhesion to SiO_2) whereas HEK 293 and GSC-CC *do* express *y* (thus ensuring repulsion from SiO_2).

However, data comparisons on this basis were fruitless and did not identify any viable candidate genes. The very limited number of datasets (relating to only four of the cell types tested) significantly restricted the usefulness of this approach. In future, running DNA micro-arrays or RNA-Seq specifically for this process, rather than relying on library data, might generate new findings. Candidates identified in this way might be validated in future by using siRNA mediated knockdown in cell types that pattern, or by over-expression of candidate genes in cells that normally do not pattern.

Importantly, this comparative DNA expression approach is also limited by the real possibility that cells may express an important adhesion-mediating receptor *in response* to being cultured on-chip. This would clearly not be reflected in the library control array datasets used here.

2.12 Conclusions and new hypotheses

The parylene-C:SiO_2 platform is not uniformly effective and is entirely dependent upon cell type. This variation is to be expected, given the large differences in CAM expression across different cell types and cell lines. LUHMES neurons, in both an undifferentiated and pre-differentiated state, failed to pattern on-chip.

Despite a systematic substrate and cell-centric exploration, the cell patterning mechanisms underpinning the parylene-C:SiO_2 platform remain unclear. Parylene-bound vitronectin may play a role in allowing cells to engage, thereby demanding the complimentary vitronectin receptor be present in the cell membrane.

A future analysis of the patterning behaviours of a broader range of cell types, in combination with assessment of each cell's proteome (with specific reference to CAM expression), may in due course allow identification of key cell membrane proteins which both facilitate parylene adhesion and, equally important, enable repulsion from SiO_2.

Chapter 3 Enabling neuronal patterning on parylene-C:SiO_2

3.1 Introduction

Despite the systematic approach described above, there remains a persisting lack of understanding regarding the mechanism of cell patterning on parylene-C:SiO_2. In the context of this uncertainty, two different approaches were taken in an effort to achieve LUHMES neuronal patterning.

3.1.1 Strategies to achieve *isolated* LUHMES patterning

Given the failure to pattern LUHMES using the established protocol, and the observation that HEK 293 patterning behaviour could be altered so significantly through modification of the chip preparation protocol, the impact of similar alterations on LUHMES behaviour was explored. Specific protocol modifications were:

- Exclusion of the piranha etch and/or serum activation stages.
- Using simplified activation solutions of either fibronectin or vitronectin or poly-L-ornithine alone[****], or fibronectin or vitronectin in combination with BSA, instead of serum.
- Using reduced concentrations of serum for chip activation, hypothesising that a potential repulsive constituent might be less overwhelming to LUHMES in lower concentrations.

3.1.2 A co-culture hypothesis to achieve neuronal adhesion

A co-culture approach was inspired by (a) the recognition that neurons *in vivo* exist in very close proximity to glia, (b) the prior successful patterning of primary hippocampal cells (predominantly glia, with some neurons) (91) (100), and (c) the

[****] Standard culture protocols for the maintenance of LUHMES neurons demand the use of culture vessels pre-treated with a combination of fibronectin and poly-L-ornithine, in order to promote healthy cell adhesion and proliferation.

finding that glial lineage GSC lines patterned extremely accurately on the parylene-C:SiO_2 platform (see Figure 2-17).

Also relevant is the recognition of extensive glia-neuron interactions that mediate neurodevelopment (127). For example, if glia are ablated during early neuronal growth, axon development is frequently found to stall (128). This suggests a role for glia in assisting neuronal axogenesis and is supported by the observation that PNS glia appear to promote expression of Futsch (a microtubule-associated protein important in extension of the axon) (129). These findings are pertinent as regards the need for undifferentiated LUHMES to morphologically differentiate, evidence of which was conspicuously absent for LUHMES on the very rare occasion that they adhered to parylene-C areas. Collectively, this thinking led to the idea of using a different, pre-patterned cell type to act as a 'pseudo-glial' cellular template for subsequent culture of neurons (see Figure 3-1).

HEK 293 cells were identified as the initial candidate for template cell, due to their robust patterning phenotype and relative ease of use. Being demonstrably *non-glial*, this also raises the interesting question of whether a supporting cell template need necessarily be of specific glial phenotype in order to enable adhesion and/or differentiation of LUHMES neurons.

Key questions:

1. Will LUHMES neurons adhere secondarily to a non-glial pre-patterned HEK 293 cell template layer?
2. If so, do they show morphological evidence of differentiation despite the absence of a glial cell type?

3.1.3 Optimising a 'pseudo-glial' template cell

Should the co-culture concept prove effective in principle, several potential issues regarding the relationship between pre-patterned cell and LUHMES neurons warrant consideration. Differentiated LUHMES are post-mitotic whereas HEK 293 cells remain proliferative with a rapid doubling time. This would inevitably lead to overgrowth of the underlying pre-patterned HEK 293 cell layer and potentially

undermine patterning, should it be found to occur. In anticipation of this problem, methods to retard or arrest HEK 293 growth were considered. One method identified involves the use of citrinin, a nephrotoxic mycotoxin, which disrupts microtubule function and has been used to induce cell cycle arrest in HEK 293 cells (130).

Key questions:

1. Can HEK 293 cell growth be retarded or arrested through exposure to citrinin?
2. Do citrinin-treated HEK 293 cells continue to pattern on-chip?

Figure 3-1 Illustration of the co-culture hypothesis

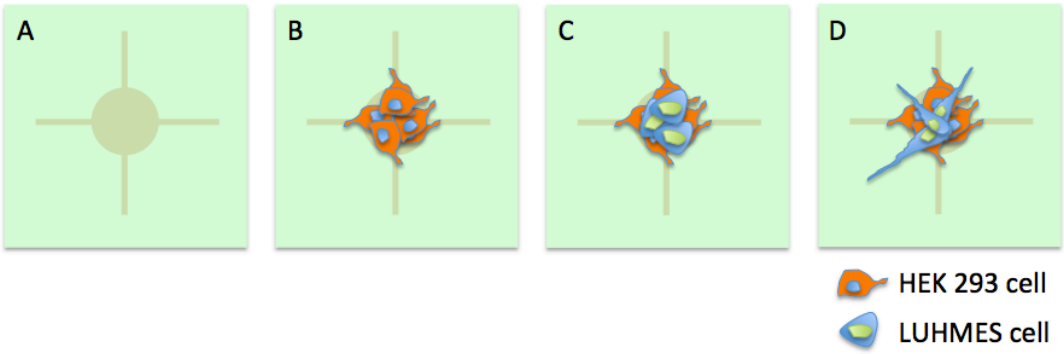

Cartoon illustration of the co-culture hypothesis, utilising HEK 293 cells as template layer. A: Region of chip after piranha and serum activation. B: After plating, and successful patterning, of HEK 293 cell suspension. C: Hypothesised secondary adhesion of undifferentiated LUHMES to the HEK 293 cellular template. D: Potential outgrowth of neurites, suggestive of morphological neuronal differentiation.

3.1.4 Human GSC as a patterning template

After HEK 293 cells, the next clear candidate template cell is the GSC group. These cells patterned accurately and are of human glial origin. In addition, their slightly slower growth profile is more favourable than that of HEK 293 cells. However, their poorly understood phenotype, tumour origin, and complex culture protocols are important less favourable characteristics. Despite a slightly longer doubling time, GSC proliferation rates would still be anticipated to quickly overwhelm any theoretical, subsequent, LUHMES neuronal patterning. In order to reduce cell turnover rate, exposure to the anti-mitotic agent cytosine-D-arabinofuranoside (Ara-C) (131) was explored as a potential means of decreasing the proliferation rates of GSCs. Ara-C, after conversion into cytosine arabinoside triphosphate, interferes with DNA synthesis and holds cells in the S phase (during which DNA is replicated). As a result, rapidly dividing cells are most affected (this being the rationale behind its use as a chemotherapeutic agent).

Key questions:

1. Will LUHMES neurons secondarily adhere to a pre-patterned 'glial' GSC template layer?
2. If so, do they show morphological evidence of differentiation?
3. Can GSC growth be retarded/arrested by adding Ara-C to growth media?
4. Do Ara-C-treated GSCs continue to pattern effectively on-chip?

3.1.5 Murine ES-derived neurons in co-culture

To explore a broader applicability of the co-culture hypothesis, an alternative (non human) neuronal cell type was tested in place of LUHMES. Murine ES-derived neurons (which were previously repulsed by both substrates when cultured in isolation, see Figure 2-17) were co-cultured after prior HEK 293 cell plating.

Key questions:

1. Will murine ES-derived neurons secondarily adhere to a pre-patterned HEK 293 template layer, thereby illustrating proof of co-culture concept with neurons from a different species?

2. If so, do they show morphological evidence of differentiation?

3.2 Methods

All experiments in this chapter utilised chip 1, with its three iterations of circular parylene nodes with a centred 'cross-hair' (node diameters 250 µm, 100 µm, and 50µm, orthogonally-orientated cross hairs measuring 450 µm in length for largest node size and 300 µm for smaller nodes) with overall chip dimension of 7.7 mm × 5.9 mm.

3.2.1 LUHMES in isolation, with protocol modifications

Impact of excluding piranha and/or serum activation

Undifferentiated LUHMES were plated as a suspension of 5×10^4 cells/mL in proliferation media on chips prepared as follows:

- No piranha treatment, no serum incubation (instead incubated overnight at 37° C in de-ionised distilled H_2O).
- Piranha acid treatment followed by no serum incubation (instead incubated overnight at 37° C in deionised distilled H_2O).
- Piranha acid treatment followed by standard serum incubation at 37° C.

Simplified activation solutions in place of serum.

Undifferentiated LUHMES were plated as a suspension of 5×10^4 cells/mL on chips that underwent standard piranha acid exposure followed by overnight incubation at 37 °C in the following alternative activation solutions:

- BSA alone (0.3 mg/ml, 3 mg/ml, 30 mg/ml dissolved in HBSS, Invitrogen).
- BSA with vitronectin (0.3 mg/ml, 3 mg/ml, 30 mg/ml BSA with 1 µg/ml vitronectin).
- BSA and fibronectin (0.3 mg/ml, 3 mg/ml, 30 mg/ml BSA with 1 µg/ml fibronectin).
- Vitronectin alone (1 µg/ml).
- Fibronectin alone (1 µg/ml).
- Poly-L-ornithine alone (50 µg/ml).
- Deionised distilled H_2O (control).

In all above experiments, cells were imaged live on day 3 *in vitro* using a Wild Heerbrugg (Switzerland) light microscope adapted for use with a Nikon Coolpix 4500 digital camera using an MDC2 relay lens. Image J (version 1.44o, National Institute for Health, USA) was used for image analysis. PAI and SRI were measured in a minimum of 18 ROIs (with equal representation of each of the three node diameters present on the chip, and data pooled). Charted data is illustrated as mean ± SEM. The Kruskal-Wallis test was again used to compare patterning indices across multiple groups (see section 2.3.6 for rationale and calculation). Prism 5 for Mac OS X (GraphPad Prism Software Inc., California, USA) was used for statistical analyses.

Impact of reduced concentration of serum

Undifferentiated LUHMES were plated as a suspension of 5×10^4 cells/mL in proliferation media on chips that had undergone standard piranha treatment followed by overnight incubation at 37 °C in FBS of concentration of 1%, 10%, and 100%. FBS was diluted as necessary in HBSS (Invitrogen).

3.2.2 LUHMES in co-culture with pre-patterned HEK 293

For all co-culture experiments, chips were prepared according to the standard piranha and serum incubation protocol (see 2.3.3).

HEK 293 cells were applied to chips as a suspension of 5×10^4 cells/ml in growth media. 24 hours later, media was removed and chips were transferred to fresh culture well. A 40 μL droplet containing 120,000 pre-differentiated LUHMES was pipetted onto the chip surface. Chips were incubated at 37 °C for 30 minutes to allow settling of cells, followed by the addition of LUHMES differentiation media. Chips were imaged daily up to 6 days *in vitro*.

HEK 293 growth retardation protocols

Citrinin treatment:

Standard HEK 293 growth media (DMEM with 10% FBS) was supplemented with citrinin (MP Biomedicals, Cambridge, UK) at a final concentration of 100 μM. The doubling time of un-patterned HEK 293 cells, growing in citrinin-doped media, was

assessed by daily measurement of percentage cell confluence. Secondly, citrinin-treated HEK 293 cells were assessed for the capacity to pattern on chips (prepared according to the standard protocol).

3.2.3 LUHMES in co-culture with pre-patterned GSCs

A 50 μL droplet containing 10,000 GSC-A cells in suspension was pipetted onto chip surfaces. Chips were incubated for 30 minutes to allow cells to settle, followed by the addition of GSC maintenance media.

72 hours later, maintenance media was removed and the chip was transferred to a fresh culture well. A 40 μL droplet containing 50,000 pre-differentiated LUHMES was pipetted onto the chip surface. Chips were then incubated at 37 °C for 30 mins, followed by addition of LUHMES differentiation media. These co-cultures were imaged alive up to 8 days *in vitro*, using a Wild Heerbrugg (Switzerland) light microscope adapted for use with a Nikon Coolpix 4500 digital camera using an MDC2 relay lens.

GSC growth retardation protocols

Growth retardation with Ara-C:

Normal GSC growth media was supplemented with Ara-C (Sigma Aldrich, Missouri, USA) at a final concentration of 0 μM, 5 μM, or 10 μM. The morphology, behaviour, and doubling time of un-patterned GSC-C growing in ara-C-containing media was assessed by daily imaging.

3.2.4 ES-derived neurons in co-culture with HEK 293

HEK 293 cells were applied to chips (prepared according to the standard piranha/serum protocol) as a suspension of 5×10^4 cells/ml in growth media. 48 hours later, media was removed and chips were transferred to fresh culture well. A 2 ml suspension (of concentration 5×10^4 wild type ES-derived neurons/mL) was added to each well. For preparation protocol, see 2.9.3. Chips were imaged daily up to 6 days *in vitro*.

3.3 Results

3.3.1 LUHMES in isolation, with protocol modifications

None of the protocol modifications enabled LUHMES to pattern appropriately on parylene-C:SiO_2.

Impact of excluding piranha and/or serum treatment

As shown in Figure 3-2, PAI remains almost zero and SRI remains almost 1 (reflecting persisting global repulsion from the chip surface) regardless of the exclusion or inclusion of piranha or serum treatment (UD LUHMES no piranha, H_2O incubation: PAI 0.01±0.0, SRI 0.97±0.01; piranha treated, H_2O incubation: PAI 0.05±0.01, SRI 0.93±0.01; piranha treated, serum incubation: PAI 0.02±0.01, SRI 1.0±0.0;).

Impact of reduced concentration of serum

Incubation in serum with concentration 10% or 100% resulted in similar, dominant cell repulsion from both parylene-C and SiO_2 (UD LUHMES piranha treated, 100% serum incubation: PAI 0.02±0.01, SRI 1.0±0.0; UD LUHMES piranha treated, 10% serum incubation: PAI 0.04±0.02, SRI 0.99±0.0). Incubation in serum diluted to a concentration of 1% resulted in attenuated repulsion from SiO_2, reflected by a significant fall in SRI (see Figure 3-3, UD LUHMES piranha treated, 1% serum incubation: PAI 0.0±0.0, SRI 0.16±0.01). In all instances, however, there was minimal or no cell adhesion to parylene domains.

Figure 3-2 Impact of exclusion of piranha acid and/or serum incubation stages on LUHMES adhesion.

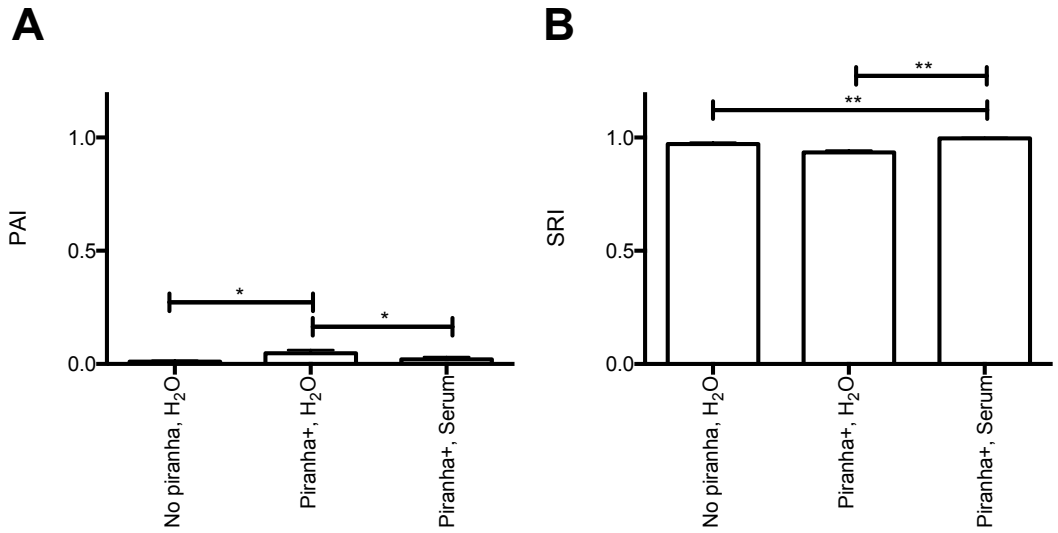

*The impact of excluding piranha acid and/or serum incubation stages upon downstream LUHMES adhesion. None of the chip preparation combinations trialled enabled cell patterning. A: PAI, parylene-C adhesion index; B: SRI, SiO_2 repulsion index. Data illustrated as mean±SEM. Kruskal-Wallis test used to compare groups, * denotes P<0.05, ** P<0.001. For each preparation, 27 ROIs from 3 independent chips were assessed.*

Figure 3-3 LUHMES adhesion indices after activation with serum of differing concentrations

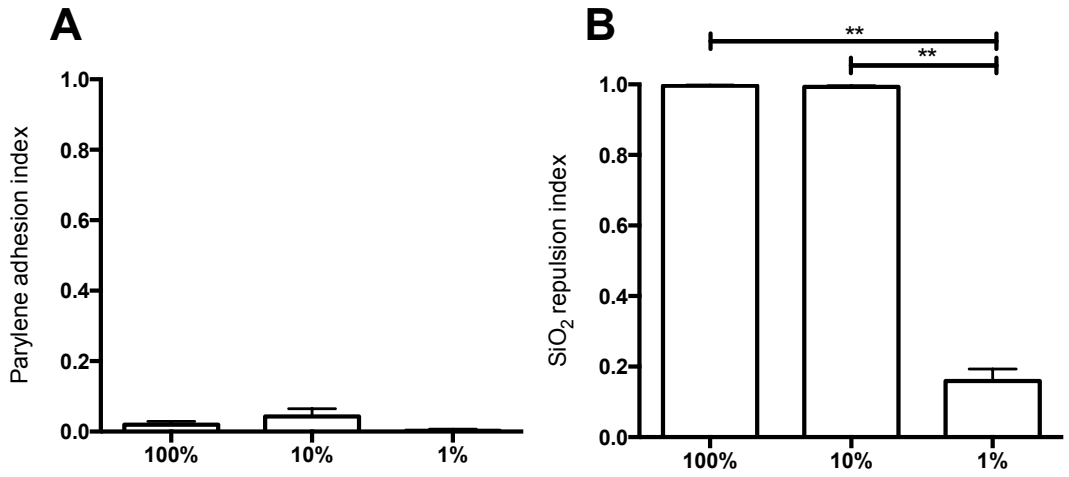

*LUHMES adhesion indices using serum concentrations of 1%, 10%, and 100%. Serum concentration of 10% or 100% results in similar, dominant cell repulsion from both parylene-C and SiO_2. Incubation in 1% serum results in attenuated repulsion from SiO_2, but persisting lack of adhesion to parylene-C. A: PAI, parylene-C adhesion index; B: SRI, SiO_2 repulsion index. Data illustrated as mean±SEM. Kruskal-Wallis test used to compare groups, * denotes P<0.05, ** P<0.001. For each serum concentration, 27 ROIs from 3 independent chips were assessed.*

Rationalized protein activation solutions in place of serum.

PAI remained almost zero for all simplified activation solutions tested, other than for PLO-treated chips. Similarly, SRI remained almost 1 for all experimental activation solutions other than PLO (BSA 0.3 mg/ml: PAI 0.00±0.0, SRI 1.0±0.0, BSA 3 mg/ml: PAI 0.00±0.0, SRI 1.0±0.0, BSA 30 mg/ml: PAI 0.00±0.0, SRI 1.0±0.0, BSA 0.3 mg/ml + vitronectin 1µg/ml: PAI 0.01±0.0, SRI 0.99±0.0, BSA 3 mg/ml + vitronectin 1µg/ml: PAI 0.00±0.0, SRI 0.99±0.0, BSA 30 mg/ml + vitronectin 1µg/ml: PAI 0.00±0.0, SRI 1.0±0.0, BSA 0.3 mg/ml + fibronectin 1µg/ml: PAI 0.01±0.0, SRI 0.99±0.0, BSA 3 mg/ml + fibronectin 1µg/ml: PAI 0.00±0.0, SRI 1.0±0.0, BSA 30 mg/ml + fibronectin 1µg/ml: PAI 0.00±0.0, SRI 1.0±0.0, vitronectin 1µg/ml alone: PAI 0.03±0.01, SRI 0.97±0.0, fibronectin 1µg/ml alone: PAI 0.02±0.01, SRI 0.98±0.0, PLO 50 µL/ml alone: PAI 0.61±0.05, SRI 0.42±0.04, see Figure 3-4).

However, in the context of activation with either vitronectin alone or fibronectin alone, there were occasional examples of LUHMES adhering to SiO_2 domains (in very small numbers) and differentiating (Figure 3-5). This contrasted with all BSA combinations, in which only cell debris could be seen on-chip. Incubation with PLO resulted in extensive but indiscriminate cell adhesion to both parylene-C and SiO_2 domains.

Figure 3-4 LUHMES adhesion after chip activation with rationalised protein activation solutions

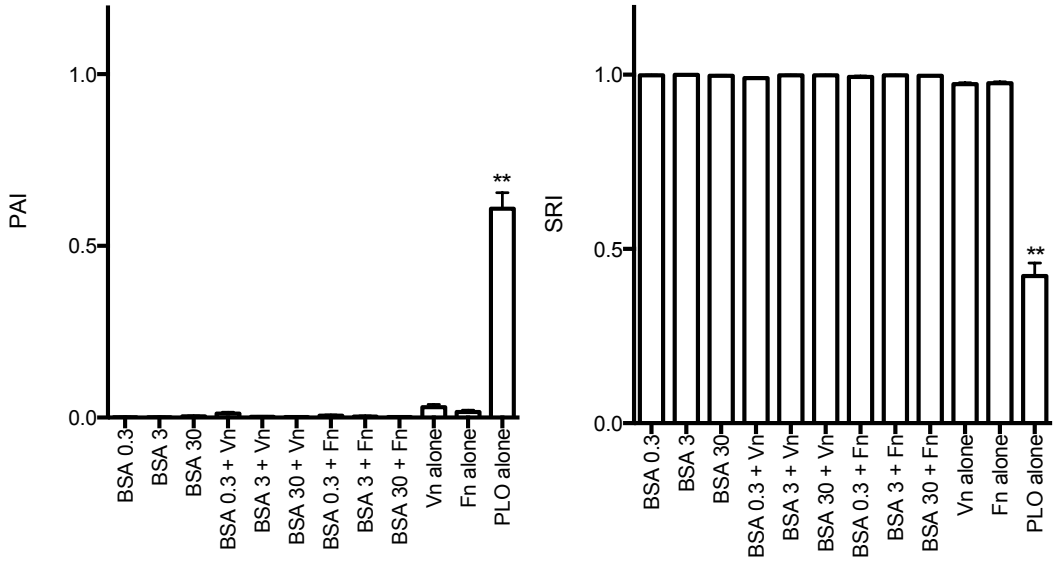

*PAI and SRI for UD LUHMES plated on chips incubated with experimental protein activation solutions. Activation with PLO alone resulted in PAI significantly greater and SRI significantly lower than for all other activation solutions. BSA: bovine serum albumin, Vn: vitronectin, Fn: fibronectin, PLO: poly-L-ornithine, PAI: parylene-C adhesion index, SRI: SiO_2 repulsion index. Data is illustrated as mean±SEM. * denotes P<0.05, ** P<0.001. For each protein solution, 27 ROIs from 3 independent chips were assessed.*

Figure 3-5 Photomicrograph of LUHMES growth on a fibronectin-activated chip

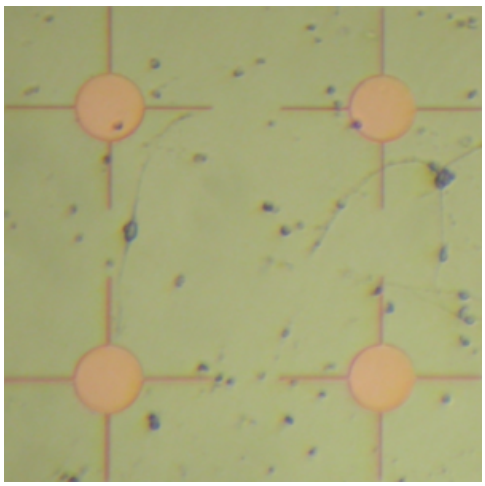

Chip prepared with standard piranha acid treatment followed by incubation with fibronectin (concentration 1 µl/ml). Plated with UD LUHMES in differentiation media and imaged after 3DIV. Note (amongst other cell debris) very occasional adhesion of viable LUHMES cells, with morphological differentiation as evidenced by projection of neurites onto surrounding SiO_2. Node diameter 100 µm.

3.3.2 LUHMES in co-culture with pre-patterned HEK 293

When pre-seeded with HEK 293 cells, secondarily plated LUHMES selectively adhere to patterned HEK 293 cell clusters. Figure 3-6 illustrates HEK 293 cells alone (sections A and B) and following secondary LUHMES co-culture (sections C-F). Pre-seeded HEK 293 cells pattern accurately, adhering only to parylene-C domains. Secondarily plated pre-differentiated LUHMES adhered only to HEK 293 cell clusters.

Importantly, these adherent neurons also showed morphological signs of differentiation, with neurites extending from parylene nodes to explore the surrounding SiO_2 environment. In some instances, neurites were seen to connect with adjacent cell clusters (see Figure 3-6E). After 4 to 5 days *in vitro*, however, cultures became unstable due to continued HEK 293 cell proliferation and cell lift-off. As such, HEK 293 cells outgrew their parylene nodes (as previously observed when cultured in isolation, see Figure 2-6). By 5 days post LUHMES plating, there was widespread culture lift-off from the chip surface.

Figure 3-6 LUHMES in co-culture with pre-patterned HEK 293 cells.

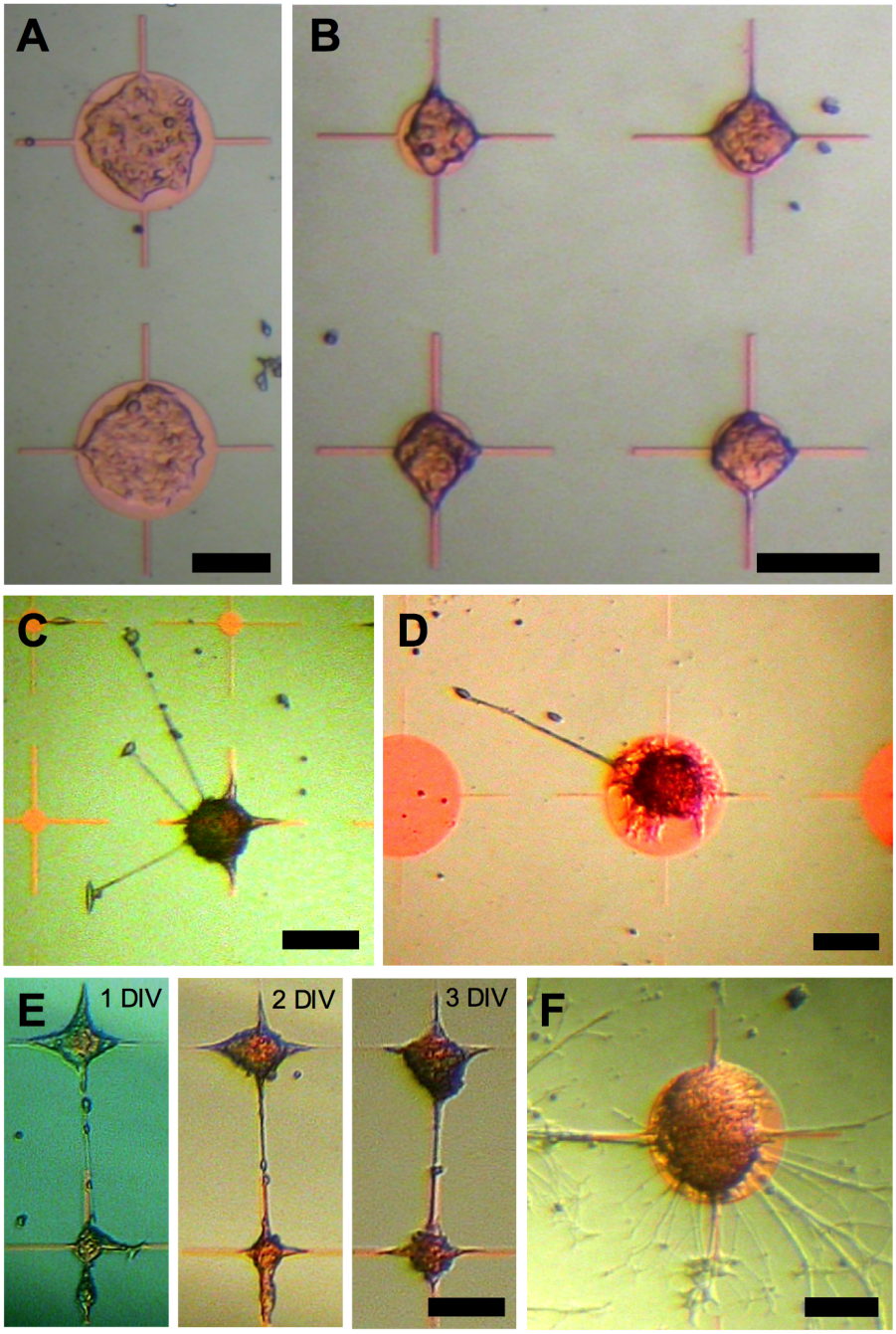

A & B: HEK 293 alone after 1DIV, on 250 μm diameter and 100 μm diameter nodes respectively. C: Two days after the addition of pre-differentiated LUHMES neurons, three neurites can be seen exploring the surrounding SiO_2. D: A 250μm diameter node following sequential co-culture with a single neurite seen extending from the cell cluster. E: Example of neurites connecting with adjacent nodes. Sequential daily imaging illustrates the continued proliferation of HEK 293 cells on parylene. F: A 250μm diameter node in which a higher density of LUHMES have successfully adhered and differentiated. Scale bar 150 μm.

Retarding HEK 293 growth with citrinin

When HEK 293 cells were grown on un-patterned polystyrene in media supplemented with 100 μM citrinin, their doubling time increased from 24.8 h to 63.4 h (see Figure 3-7). Citrinin-treated HEK 293 cells retained the ability to pattern effectively on-chip (see Figure 3-8). However, despite this reduction in doubling time, overgrowth was still pronounced by day 6 *in vitro*.

3.3.3 LUHMES in co-culture with GSC-A

When LUHMES were co-cultured on pre-patterned GSC-A, they adhered to the pre-patterned GSC-A cells and projected neurites into surrounding SiO_2. Similar to HEK 293 co-culture findings, they illustrated the capacity to extend neurites onto adjacent SiO_2 and, in some instances, connected with adjacent nodes (see Figure 3-9).

Retarding growth of GSC-A with Ara-C

Addition of Ara-C to GSC growth media resulted in a decreased rate of cell growth as measured by % confluence (see Figure 3-10). However, adherent cells developed abnormal morphology and large amounts of free-floating cell debris was noted. Crucially, when Ara-C treated GSC-A were re-plated onto chips, they failed to adhere nor pattern on-chip.

3.3.4 ES-derived neurons in co-culture with pre-patterned HEK 293

Akin to LUHMES co-cultured with HEK 293 cells, ES-derived neurons also showed the capacity to adhere to pre-patterned HEK 293 clusters. Furthermore, examples of neurites extending onto SiO_2 were also noted. On occasions, direct neurite connection between adjacent nodes was again observed (see Figure 3-11).

Figure 3-7 Impact of citrinin on HEK 293 cell proliferation rates

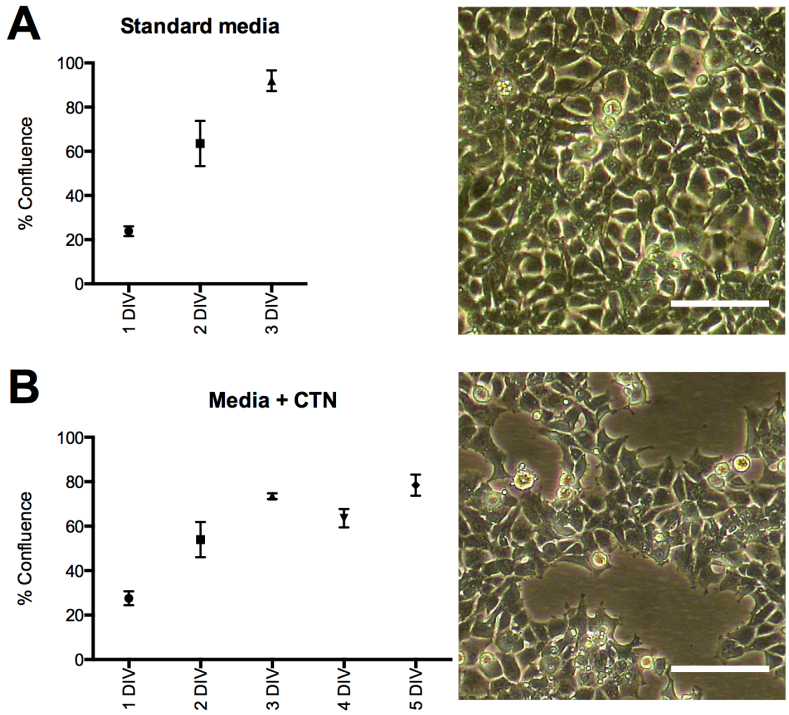

Impact of citrinin on HEK 293 cell proliferation rates, as measured by % confluence. A: Standard growth media. B: Standard media supplemented with 100 μM citrinin. Photomicrographs illustrate representative culture examples at 3 DIV; scale bar 100 μM; CTN, citrinin; DIV, days in vitro. Data is illustrated as mean±SEM. At each time point, 6 ROI (of surface area 400 × 400 μM) were assessed.

Figure 3-8 Citrinin-treated HEK 293 cells

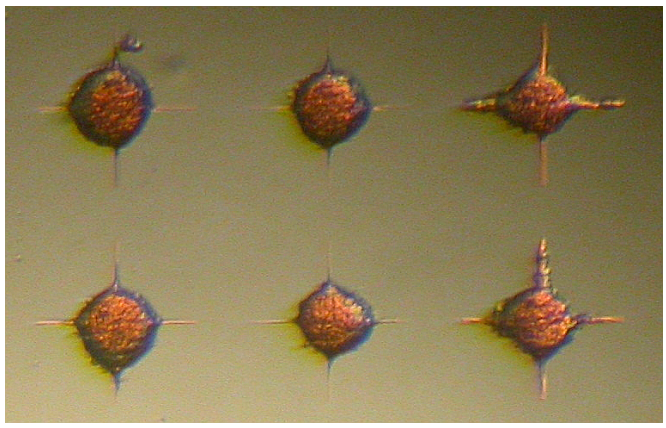

Citrinin-treated HEK 293 cells imaged after 6 days in vitro. Citrinin-treated HEK 293 cells pattern accurately but continue to proliferate beyond the margins of the parylene nodes. Area depicted shows six 100 μm diameter nodes with 'cross hairs' measuring 300 μm, total region shown measures 800 μm × 1200 μm.

Figure 3-9 LUHMES in co-culture with pre-patterned GSC-A cells.

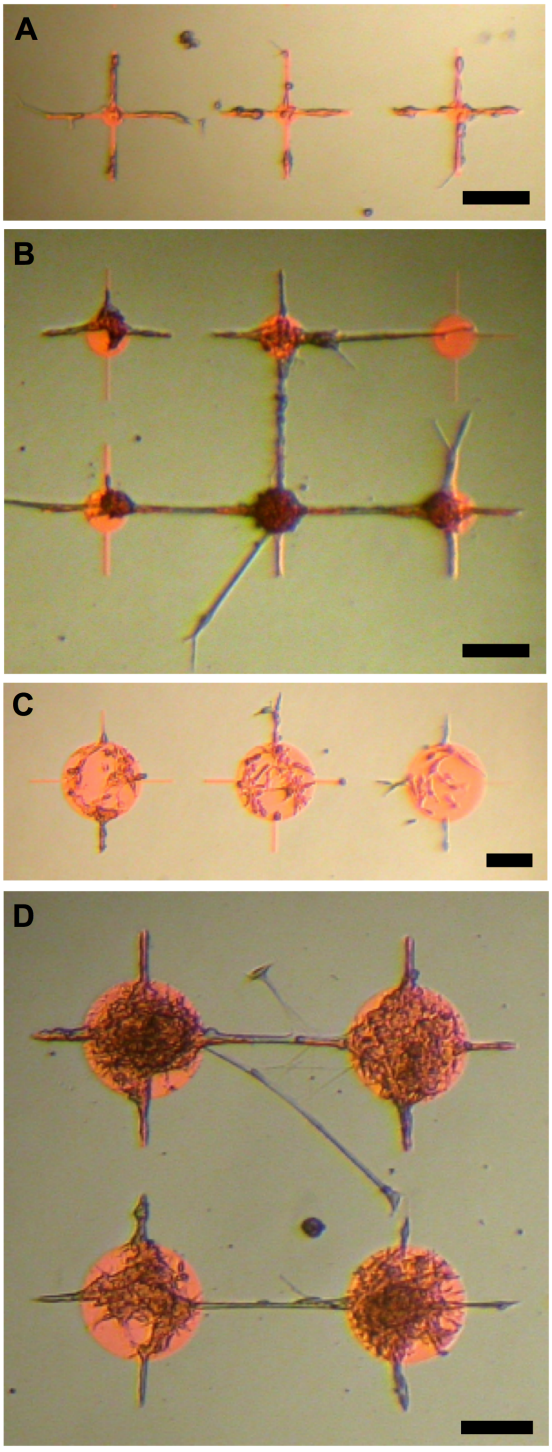

A: GSC-A alone on the smallest node design, pre-LUHMES. B: GSC-A and LUHMES in co-culture with neurites evident extending from cell clusters (after 3DIV). C: GSC-A alone on the largest node design, pre-LUHMES. D: GSC-A and LUHMES in co-culture with neurites exploring surrounding SiO_2 and occasionally connecting with adjacent nodes (after 3DIV). Scale bar 150 μm.

Figure 3-10 Effect of ara-C on GSC-A growth

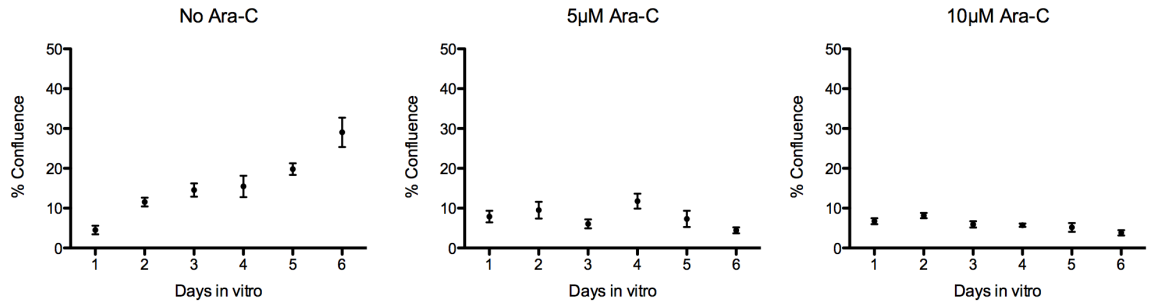

Growth profile of un-patterned GSC-A, as measured by % confluence, grown (from left to right) in: normal media, 5 μM Ara-C, and 10 μM Ara-C. Data is illustrated as mean±SEM. At each time point, 4 ROI (of surface area 400 × 400 μM) were assessed.

Figure 3-11 Wild type ES-derived neurons in co-culture with HEK 293 cells.

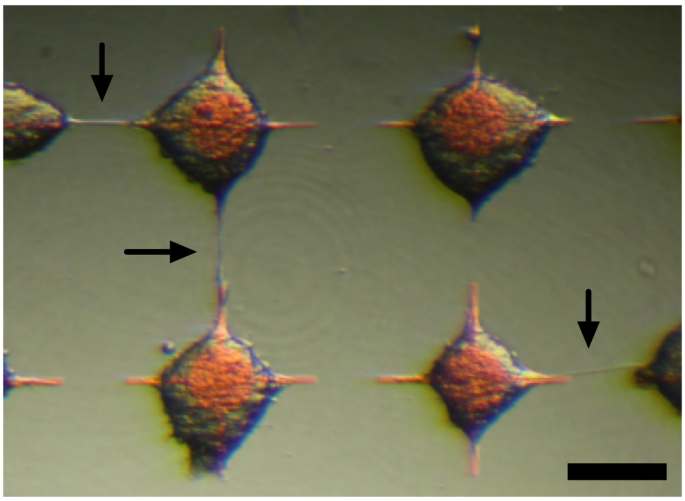

Example of WT ES-derived neurons co-cultured with HEK 293 cells. HEK 293 clusters have out-grown their underlying parylene nodes. However, occasional neurites (black arrows) are seen extending between some cell clusters, illustrating that ES-derived neurons have adhered and differentiated. Imaged at 4DIV. Scale bar 150 μm.

3.4 Discussion

3.4.1 Failure to achieve adhesion of LUHMES in isolation

Excluding piranha acid and/or serum incubation did not enable undifferentiated LUHMES to adhere to either parylene or SiO_2 domains to any meaningful extent, though there were downstream differences in adhesion indices between groups (see Figure 3-2). PAI, although statistically different across groups, remained close to 0 for all protocols tested (no piranha acid followed by water incubation, piranha acid followed by water incubation, or piranha acid followed by serum incubation). SRI remained high for all three trials. As previously discussed, absolute repulsion from SiO_2 is crucial. It was only with the combination of piranha acid treatment followed by serum incubation that the SRI was driven to 1, reflecting truly robust cell repulsion. This echoes a similar finding with HEK 293 cells, where repulsion from SiO_2 regions is achieved only with piranha acid treatment followed by serum incubation.

Reducing the concentration of serum used to activate chips did not facilitate LUHMES patterning. Serum concentrations of 10% and 100% resulted in similar global repulsion from both parylene-C and SiO_2 regions. Reducing serum concentration to 1% interestingly resulted in failure of repulsion from SiO_2 (with SRI falling to 0.16±0.01) but with persisting repulsion from parylene (PAI 0.0±0.0). One explanation is that, when diluted to 1%, protein adhesion and packing on SiO_2 is such that membrane-bound CAMs are able to engage, therefore allowing a degree of adhesion. An alternative explanation is that key repulsive component(s) in serum are so depleted as to fail to enforce repulsion. As regards parylene adhesion, LUHMES likely do not express the requisite parylene-adhesion mediating CAM(s). Therefore, regardless of serum concentration, LUHMES cannot engage with parylene-C regions.

Simplified protein activation solutions were similarly unable to induce any cell patterning. All concentrations of BSA alone or in combination with vitronectin or fibronectin resulted in a globally repulsive chip surface with PAI ~1 and SRI ~1. This contrasts with HEK 293 cell behaviour, where adhesion indices could be altered

more extensively by use of rationalised protein solutions. When activated with fibronectin or vitronectin alone, adhesion remained poor on both surfaces. However, there were occasional instances of LUHMES cell adhesion. Moreover, these adherent cells showed morphological signs of differentiation, with neurites extending out onto the chip surface. These neurites showed no apparent influence from the two different substrates, nor from surface topography, apparently growing at random on the chip surface. This illustrates that pure vitronectin or fibronectin, when not in competition with other serum proteins, is capable of coating the chip surface and enabling occasional LUHMES adhesion. Furthermore, this infers the presence of CAMs capable of engaging, all be it in small numbers, with vitronectin or fibronectin. This conflicts somewhat with the theory that the absence of a vitronectin receptor in LUHMES is responsible for their inability to bind to parylene-C regions, though a very low receptor density of the suitable integrin could explain the finding.

Poly-L-ornithine (PLO) is a synthetic amino acid chain used widely as a coating to enhance cell adhesion to plastic and glassware. Incubation of chips with PLO resulted in pronounced, but undiscerning, cell adhesion to both surfaces; likely due to a uniform coating of PLO on both parylene-C and SiO_2.

In summary, none of the alternative chip preparation and activation protocols tested enabled LUHMES to pattern effectively on-chip. For LUHMES, the patterning protocol fulfils the need to repulse from SiO_2 but fails to enable adhesion to parylene-C.

3.4.2 Achieving adhesion and differentiation by co-culture

LUHMES in co-culture with pre-patterned HEK 293

With standard chip preparation protocols, isolated LUHMES do not pattern (either in an undifferentiated or differentiated state). On the infrequent occasion in which cells are seen to adhere, they do not manifest morphological changes suggestive of differentiation (Figure 2-17). This behaviour contrasts starkly with the previous accurate patterning of primary murine hippocampal extract (7,8,9), suggesting that the presence of glia in these preparations may be key to enabling the *neuronal* component to pattern. Hypothesizing that a non-glial, but accurate-patterning, cell

type might fulfil a role analogous to glia, LUHMES were first co-cultured with pre-patterned HEK 293 cells.

When pre-differentiated LUHMES were secondarily cultured on HEK 293-patterned chips, LUHMES selectively adhered to the HEK 293 cell clusters. Neurites projected from adherent LUHMES, demonstrating morphological neuronal differentiation, and were seen to explore the surrounding SiO_2 surface. In some instances, extending neurites united with nearby cell clusters. HEK 293 cells enabled LUHMES to adhere selectively to the chip, facilitating neuronal patterning by providing a physical point of attachment. In addition, this cell:cell interaction represents an environment in which LUHMES differentiation was able to proceed, where this was not possible in isolation.

As anticipated, HEK 293 proliferation (in the face of post-mitotic arrested LUHMES growth) was troublesome. HEK 293 cells rapidly outgrew the pro-adhesive parylene nodes. As a result, 5 to 6 days after the addition of LUHMES, co-cultures were noted to lift-off from the chip and float free in growth media. The combination of HEK 293 overgrowth, and the presumed inter-node tension seen in the context of neurite-linked cell clusters, tended to cause widespread cell lift off and network obliteration by day 7 (at least) post addition of LUHMES. Critically, this is an insufficient time window for the maturation of neurons and establishment of spontaneous electrical activity in the network. In addition, it was not possible to fix these cultures for fluorescence microscopy due to network fragility. Given that spontaneous electrical activity in cultured neuronal networks only emerges after 10-12 days *in vitro*, it is key to maintain cultures for much longer periods than that allowed by HEK 293 cells in standard growth conditions.

Citrinin was found to be somewhat effective in slowing HEK 293 proliferation. Moreover, HEK 293 cells treated with citrinin maintained the capacity to pattern reliably on-chip. However, the effect was of no great practical significance as despite a modest reduction in proliferation rates, HEK 293 clusters persisted in overgrowing parylene by day 7 *in vitro*. As a consequence, citrinin-treated HEK 293 cells were not trialled with LUHMES.

LUHMES in co-culture with GSC-A

Given the successful deployment of HEK 293 cells as a glial analogue, the GSC-A line was next assessed as a potential co-culture partner. Despite their genetic aberrations, and evident ineligibility for theoretical *in vivo* downstream uses, these cultures are more readily available than primary human astrocytes and are easier to work with at this proof-of-concept stage. The slower growth profile of GSCs also potentially mitigates somewhat against problematic cell overgrowth.

All three GSC lines patterned accurately, comparable to HEK 293 cells (see Figure 2-17). Using GSC-A to pre-pattern the parylene template, successful co-culture with LUHMES was again achieved. Similar to observations from HEK 293 co-culture, LUHMES adhered to pre-patterned GSC-A clusters and neurites were seen to project out onto surrounding SiO_2. Cultures remained stable for slightly longer. However, template cell overgrowth remained problematic with cell lift-off becoming evident 7 to 8 days after the addition of LUHMES.

ES-derived neurons in co-culture with HEK 293 cells

The above work illustrates a means of dictating the point of adhesion of LUHMES neurons on-chip, using an intermediate template cell of both non-glial (HEK 293) and glial origin (GSC-A). To see whether this behaviour is LUHMES-specific, similar co-culture experiments were performed using a different neuronal cell type (ES-derived murine neurons). These cells represent both a different source and different species of neuron.

Due to logistical complexities of timing the ES-neuron preparation with HEK 293 cell culture, ES neurons were plated on chips upon which HEK 293 cells had already proliferated to a greater degree of confluence than prior experiments (for 48 hours compared with 24 hours). Additionally, as a result of being applied as a suspension, ES-derived neurons were plated at a significantly lower seeding density. Nevertheless, in this context ES-neurons were also seen to adhere to HEK 293 clusters with neurites seen extending from cell clusters. This finding suggests that the co-culture approach is more widely applicable and is not merely LUHMES-specific.

3.4.3 Resolving neuron from template cell and the challenge of controlling neurites

Behavioural differences of neurons *versus* template cell

The results illustrated above involve light microscopy of live co-cultures. There is therefore no capacity to fully resolve LUHMES neurons from underlying template cell. The presence of neurites is the key factor in confirming the presence and adherence of LUHMES cells, also illustrating the capacity for cells to morphologically differentiate. However, it is important to better resolve the two cell types. Differential immunofluorescence labelling is one option, provided that cultures remain stable enough for fixation procedures. Theoretically, neuron specific β-3 tubulin is a good marker for demarcating LUHMES (101), whilst glial fibrillary acidic protein (GFAP) may be appropriate for GSC lines. With improved resolution, it should become possible to better define the interface between template cell and differentiating LUHMES.

Furthermore, there is as yet no functional data regarding the behaviour of patterned neurons. It is important to ensure that patterned neurons are capable of becoming spontaneously electrically active and of forming synapses with adjacent cells, in the context of this artificial on-chip network. The impact of their relationship with the underlying 'glial' template is also undefined. Though enabling targeted adhesion and neuronal differentiation, the current constructs may in other ways be counter-productive to functional neuronal network function.

Achieving control of neurite behaviour

Co-culture work illustrated that LUHMES neurons adhere and differentiate when cultured on a template cell line of either HEK 293 cells or GSC-A. However, the forces governing the behaviour (especially direction of growth) of neurites are as yet unexplored. Key questions involve the potential impact of parylene-C itself (possibly capable of imparting a haptotactic guidance cue on advancing neurites) or whether a secreted chemotactic agent (akin to netrin, for example) is the dominant factor guiding neurite trajectory. Chapter 4 explores factors that influence neurite directionality, utilising the different domains on chip 1 to identify changes in

network configuration that are induced by different parylene-C node designs. Only with such factors identified, along with a means of promoting long-term network survival, will better-defined and polarised neuronal networks become a viable prospect.

3.5 Conclusions

Efforts to induce LUHMES to pattern in isolation, by altering chip preparation protocols, were unsuccessful. LUHMES can, however, adhere and differentiate in a co-culture environment. In the context of an intermediate cell type, LUHMES adhere and show signs of morphological differentiation, as evidenced by projection of neurites on-chip.

HEK 293 cells fulfil a template cell role and, in doing so, perform a function analogous to glia. However, HEK 293 overgrowth (and ultimately cell lift-off) compromise long-term culture viability. Human GSC-A also enables spatially defined secondary adhesion of human LUHMES neurons and morphological differentiation. Similar co-culture behaviour was observed for murine ES-derived neurons co-cultured with pre-patterned HEK 293. This suggests a broader, cross-species, principle in action.

Chapter 4 Refining network architecture

4.1 Introduction

A sequential co-culture approach has enabled targeted adhesion of LUHMES to pre-patterned template cells, with subsequent morphological evidence of neuronal differentiation. Important next questions are:

1. Can neurite outgrowth trajectory now be manipulated so as to gain better control of network topography and potentially even neuronal polarity?
2. Can LUHMES neurons be better resolved from the underlying template layer?

4.1.1 Controlling neurite directionality

Equipped with a method to dictate the location of adhesion of neuronal cell bodies, the next challenge is to control the direction of growth of neuronal processes. For the creation of networks capable of meaningful interrogation, neurite growth direction, connectivity, and polarity needs to be controllable. Chip 1 was designed with arrays of nodes of three different diameters, all with orthogonally arranged 'spokes' extending at 0º, 90º, 180º, and 270º (see Figure 4-1). This provides the opportunity to assess how size and spacing of parylene nodes impacts neurite organisation.

The 'spoke' projections were included as a potential haptotactic cue, intended to guide growing neurites along the parylene track. With co-culture protocols optimised (with respect to cell plating density and timing), repeat experiments were performed using HEK 293 cells and pre-differentiated LUHMES neurons, to specifically assess how neurite directionality varies according to underlying parylene node size and configuration. The primary alternative to haptotactic guidance is a chemotactic cue, with neurites growing towards (or perhaps away from) a chemotactic gradient. As such, a diffusible compound secreted from HEK 293/LUHMES cell clusters may be the dominant signal governing neurite growth.

To challenge these two alternative guidance mechanisms, a third chip was designed and fabricated (see Figure 4-2). Here, parylene node morphology was varied once again; with either a single or double spoke, or a single or double teardrop design.

Nodes were positioned such that those with a double spoke or double teardrop morphology 'aimed' towards the nearest neighbouring node, whilst single spoke and single teardrop nodes instead aimed towards a more distant node.

If a chemotactic cue (originating from nearby cell clusters) dominates, it is hypothesized that neurites will tend to grow towards the nearest neighbouring node *despite* the presence of a parylene track directing growth in a different direction. Identifying the dominant neurite guidance mechanism theoretically opens the door to manipulation of both network topography and potentially network polarity, a key goal.

Key questions:

1. Beyond directing the attachment of neuronal cell bodies (via an intermediate template cell) can parylene haptotactically influence the direction of growth of extending neurites during differentiation?
2. If not under haptotactic control, what rules instead dominate neurite arrangement and direction? Can these be extrapolated and utilized to enhance topographic control of the network?

Figure 4-1 Schematic illustration of node configuration on chip 1

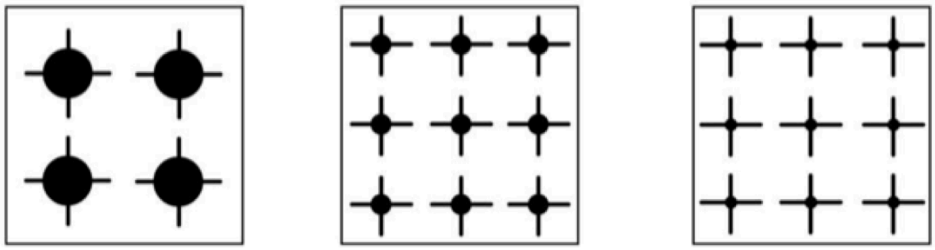

Node diameters are 250 µm, 100 µm, and 50 µm with orthogonally-orientated 'spokes' measuring 100 µm in length for the large and medium sized nodes and 125 µm for smallest node). Overall chip dimensions are 7.7 mm × 5.9 mm. A distance of 100 µm separates the end of one cross hair from the beginning of the next in all cases.

Figure 4-2 Schematic illustration of node configuration on chip 3-1

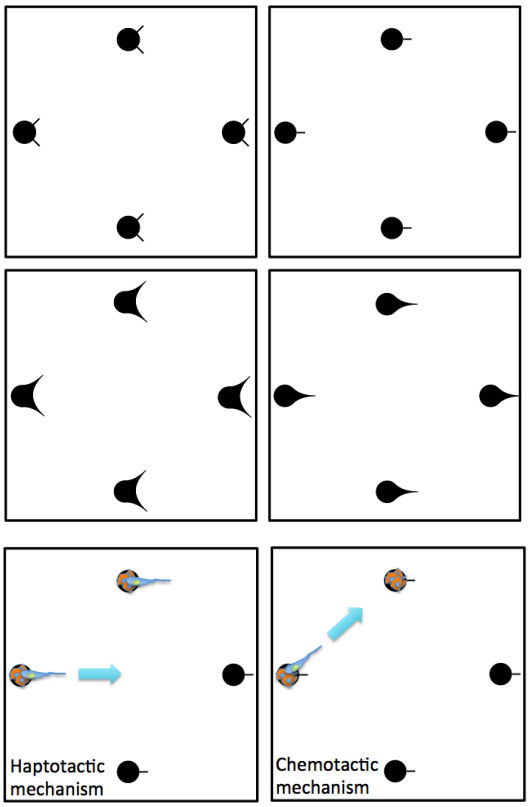

Four different node morphologies are shown, with identical inter-node spacing. Node diameter is 50 µm for all, with either a single or double spoke (20 µm long and 2 µm wide) or a single or double teardrop (20 µm long, tapering). Nearest neighbouring nodes are positioned at 45° and 135° with respect to one another. For single spoke/single teardrop nodes the intended (haptotactic) target is orientated at 90°, towards a node 400 µm away. For double spoke/double teardrop nodes, intended growth direction is towards the nearest nodes, 247.5 µm away.

4.1.2 Resolving neurons from the template cell

Behavioural differences

Several downstream optical methods to assess the electrophysiological activity of patterned neurons rely on being able to resolve exactly where neuronal material (rather than template cell) resides. The co-culture process means that parylene nodes contain a combination of both template cell and differentiating LUHMES neurons. However, SiO_2 regions between nodes – where no prior attachment of template cell occurs – ought to contain neurites only.

To further explore this perceived behavioural difference between neuron and pre-patterned glial cell, another parylene node configuration was created (constituting a separate region of chip 3) with parylene tracks extending between adjacent nodes (see Figure 4-3). If GSC-A template cells are unable to connect with adjacent nodes, unless provided with this parylene track, support is added to the theory that any cell matter that *is* capable of doing so is neuronal.

Immunofluorescence labelling

Light microscopy of co-cultures confirmed the presence of adherent neurons by the visualisation of neurites extending onto SiO_2. Unfortunately, HEK 293 co-cultures proved difficult to fix for immunofluorescence microscopy, due to cell lift-off obliterating cultures either before or during fixation. However, GSC-A/LUHMES co-cultures appeared more robust and may tolerate fixation procedures.

Immunofluorescence techniques offer the possibility of labelling the two different cell types. Neuron-specific β-3 tubulin has previously been used to reliably stain LUHMES neurons (101), as shown in Figure 4-4. This marker labels a microtubule element of the neuronal cytoskeleton. As such, β-3 tubulin was assessed as a means of labelling the neuronal component of the co-culture, whilst glial fibrillary acidic protein (GFAP) was assessed as a means of staining GSC-A cell lines. GFAP is an intermediate cytoskeleton filament, considered a specific marker for glia.

Figure 4-3 Schematic illustration of node configuration on chip 3-2

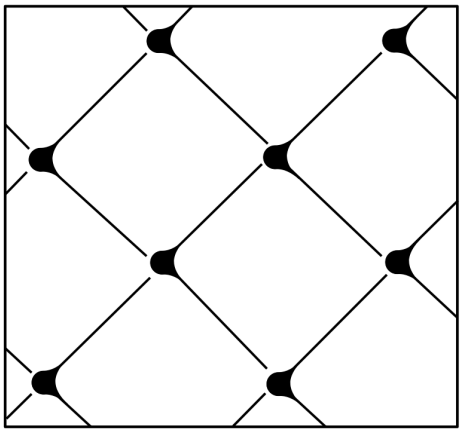

Array of 50 µm diameter nodes arranged such that a 400 µm distance separates nodes vertically and horizontally. Two parylene tracks (2 µm wide) extend from each node nodes at trajectories of 45° and 135°.

Figure 4-4 Immunofluorescence staining of LUHMES neurons

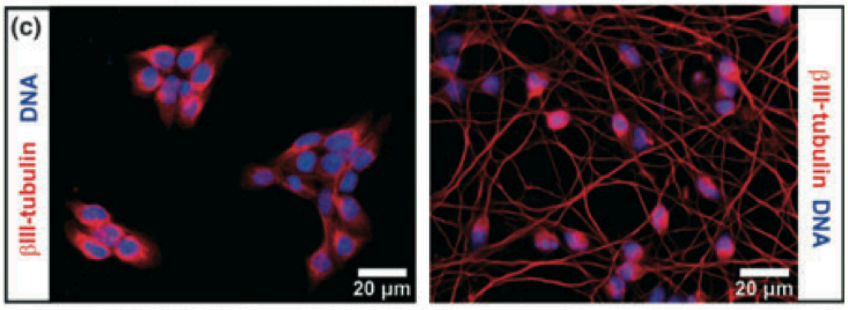

β-3 tubulin immunostaining (red) of pre-differentiation (left) and 5 days post induction of differentiation (right) LUHMES neurons. Nuclei are labelled with H-33341 dye (blue). Adapted from Scholz et al. (101).

4.2 Methods

4.2.1 Assessment of neurite directionality

Co-cultures of HEK 293 and LUHMES were generated using chip 1 and chip 3 as follows:

HEK 293 cells were applied to chips (prepared according to the standard piranha then serum protocol) as a suspension of 5×10^4 cells/ml in growth media. 24 h later, media was removed and chips were transferred to fresh culture well. A 40μL droplet containing 120,000 pre-differentiated LUHMES was pipetted onto the chip surface. Chips were incubated for 30 mins to allow settling of cells, followed by the addition of LUHMES differentiation media. Cultures were imaged daily up to 7 days *in vitro*.

Chip 1:

To quantify the impact of the parylene node morphology and configuration upon neurite orientation, neurites in co-culture experiments were traced manually using Image J (version 1.44o, National Institute for Health, USA). All neurites in a region of interest were tracked from a start point (centred on a parylene node) to an end point (defined either as branching point, termination, or the point of encountering another cell body). Traced segments were divided into 100 μm sub-segments. A tangent was taken to each sub-segment and the angle, θ, of each segment measured and categorized into 11.25° bins (354.375° to 5.625°, 5.625° to 16.875°, 16.875° to 28.125°, etc). Entries in bins 180° apart were summed, as the aim was to assess for neurite growth between the orthogonally arranged parylene nodes.

A radial plot illustrating the frequency of θ values, according to their 11.25° bins, reveals the orientation of neurite segments. This process was conducted for areas encompassing each of the three different node configurations on chip 1, and also for differentiated LUHMES cultured in isolation on a polystyrene surface treated to promote homogenous, un-patterned cell adhesion (with 50 μg/ml poly-L-ornithine and 1 μg/ml fibronectin in H_2O for 3 hrs). 12 independent chip experiments using chip 1 enabled acquisition and measurement of 200 neurite sub-segments (each of 100 μm length) representing each of the four different culture environments. Datasets

derived for each of the four environments were compared using the Kolmogorov-Smirnov test[††††].

Chip 3

For each of the four different node design regions (single spoke, double spoke, single teardrop, double teardrop), neurites were traced manually using Image J, segmented, and categorized into 11.25° bins (as above). 8 independent chip experiments using chip 3 enabled acquisition and measurement of a total of 220 neurite sub-segments (each of 100 μm length). A radial plot illustrating the frequency of θ values, according to their 11.25° bins, reveals the orientation of neurite segments. Datasets derived for each environment were compared using the Kolmogorov-Smirnov test.

4.2.2 Behavioral and immunofluorescence assessment of cultures

LUHMES and GSC-A cells were maintained as previously described (see 2.9.1).

GSC-A imaged in isolation with GFAP:

A 50μL droplet containing 10,000 GSC-A cells in suspension was pipetted onto the chip surface (chip 3, prepared according to standard piranha/serum protocol). Chips were incubated for 30 mins to allow cells to settle, followed by addition of GSC maintenance media. For immunocytochemistry, cultures were fixed (on day 7 *in vitro*) with phosphate-buffered saline (PBS)/4% paraformaldehyde for 15 min at 20° C, washed, permeabilized with PBS/0.2% Triton X-100 and pre-incubated with PBS/1% BSA (Sigma Aldrich, Missouri, USA) for 1 h at 20° C. After blocking, chips were incubated with anti-GFAP Alexa Fluor® 488 monoclonal antibody (Invitrogen) at a 1:50 dilution in blocking buffer for 3 hours at room temperature.

[††††] This is a non-parametric test of the equality of one-dimensional probability distributions. The null hypothesis is that the samples are drawn from the same distribution. The Kolmogorov-Smirnov statistic, *D*, represents the distance between the empirical distribution functions of two samples.

Co-culture of LUHMES and GSC-A, labelled with β-3 tubulin:

A 50μL droplet containing 10,000 GSC-A cells in suspension was pipetted onto the chip surface (chip 1, prepared according to standard piranha then serum protocol), incubated for 30 mins, followed by addition of maintenance media. 72 hrs later, a 40 μL droplet containing 50,000 pre-differentiated LUHMES was pipetted onto the chip surface, incubated for 30 mins, followed by addition of LUHMES differentiation media. Cells were fixed on day 7 post-addition of LUHMES. For immunocytochemistry, cultures were fixed with PBS/4% paraformaldehyde for 15 min at 20° C, washed, permeabilized with PBS/0.2% Triton X-100 and pre-incubated with PBS/1% BSA (Sigma Aldrich, Missouri, USA) for 1 h at 20° C. After blocking, chips were incubated with anti-Neuron-specific β-III Tubulin-NL637 conjugated antibody (R&D Systems, Minnesota, USA) at a 1:10 dilution in blocking buffer for 3 hours at room temperature.

Fluorescently labelled chips were attached to glass slides using a small droplet of Fluorsave reagent (Calbiochem, Merck Millipore). A cover slip was mounted on the chip surface using Fluorsave reagent. Chips were imaged with a Zeiss Axioskop microscope (Göttingen, Germany), using a ×10 oil objective with NA of 0.3. Image processing was carried out with Image J software (version 1.44o, National Institute for Health, USA).

4.3 Results

4.3.1 Assessing neurite directionality

Chip 1 – altered node size and configuration

Orientation of neurite growth is shown in radial plots in Figure 4-5, illustrating each of the four different patterning environments (the three different node designs on chip 1 and an un-patterned polystyrene surface treated to promote homogenous and therefore random cell adhesion).

Neurite orientation differs significantly according to parylene node configuration (Kolmogorov-Smirnov tests: un-patterned *vs* 250 μm diameter nodes D=0.20, P=0.001; 250 μm *vs* 100 μm nodes D=0.20, P=0.001; 100 μm *vs* 50 μm nodes D=0.15, P=0.03). There is a trend towards increasingly orthogonal growth as parylene configuration changes from 250 μm to 100 μm to 50 μm diameter nodes.

Chip 3 – altered node morphology

Radial plots showing the directionality of neurites on corresponding regions of chip 3 are shown in Figure 4-6. Regardless of different node morphology, the dominant orientation of neurites is in the bins centred on 45º (39.375º to 50.625º) and 135º (129.375º to 151.875º). This corresponds to the two nearest neighbouring nodes.

There is no significant difference between the distributions of data for single spoke *vs* double spoke and for single teardrop *vs* double teardrop (Kolmogorov-Smirnov tests: single spoke *vs* double spoke D=0.18, P=0.29, single teardrop *vs* double teardrop D=0.18, P=0.29).

4.3.2 Behavioral and immunofluorescence assessment

GSC-A cells do not possess the capacity to grow between nodes of parylene-C, as shown in Figure 4-7D & 4-7E. However, in the presence of a parylene track connecting adjacent nodes, GSC-A cells are able to extend and form reticular networks (see 4-7B & 4-7C). This contrasts with the behaviour observed for LUHMES neurons in co-culture (Figure 4-8), where neurites 'bridge the gap' between adjacent parylene nodes in the absence of an intervening track.

Figure 4-5 Directionality of neurite growth on chip 1

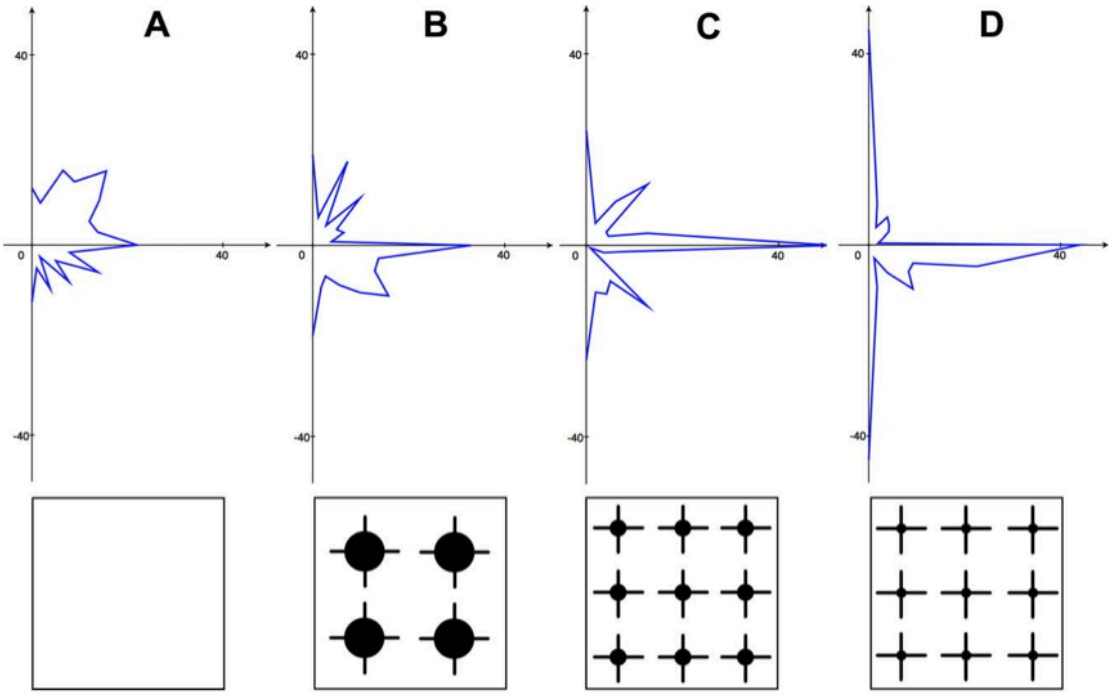

Radial plots illustrating the directionality of neurite growth for different regions of chip 1 and for plain polystyrene, with a schematic illustration of corresponding parylene design below each plot. (A) LUHMES on plain polystyrene, (B) co-culture on 250 μm diameter parylene nodes, (C) co-culture on 100 μm diameter nodes, (D) co-culture on 50 μm diameter nodes.

Figure 4-6 Directionality of neurite growth on chip 3-1

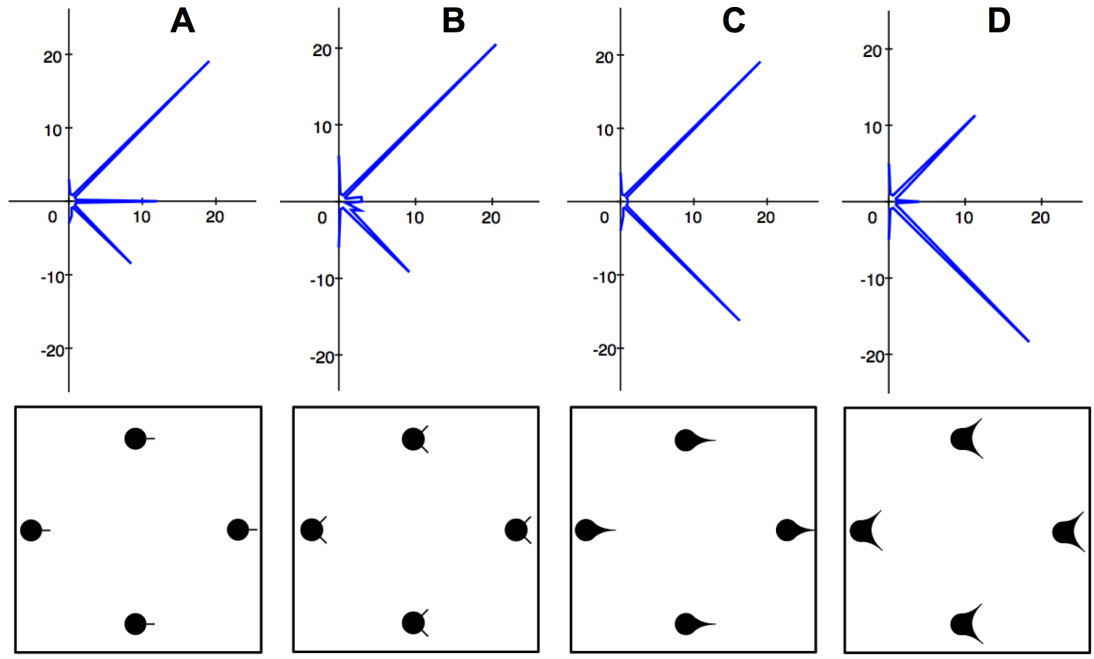

Radial plots illustrating the directionality of neurite growth for four regions of chip 3, with schematic representation of corresponding parylene configuration below plot.

Figure 4-7 GSC-A cells require a parylene path to connect adjacent nodes

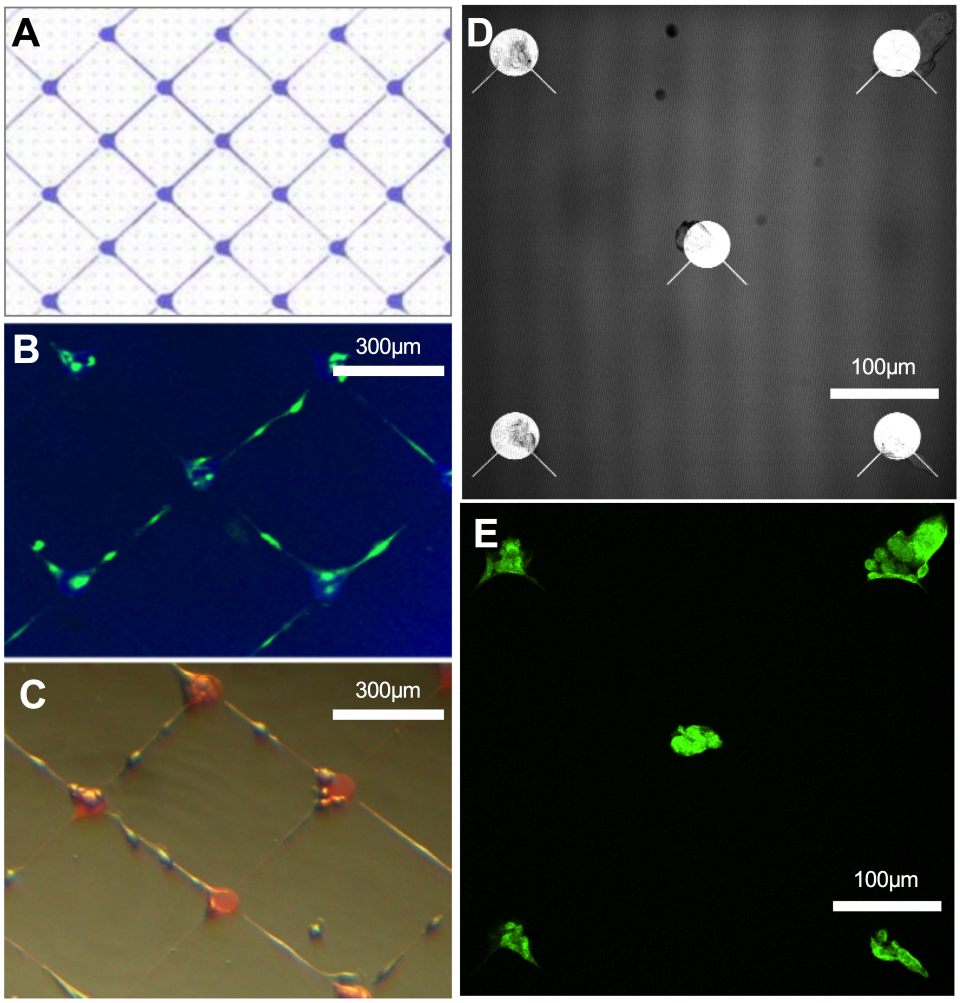

GSC-A cell line cultured on-chip in isolation. (A) Schematic of parylene pattern imaged in B & C. (B) GSC-A fixed and stained with glial fibrillary acidic protein. (C) Light micrograph of GSC-A imaged at 3DIV. (D) Reflectance image showing parylene pattern in figure E. (E) GSC-A cells fixed and stained with glial fibrillary acidic protein.

Figure 4-8 Co-cultured LUHMES and GSC-A on chip 1

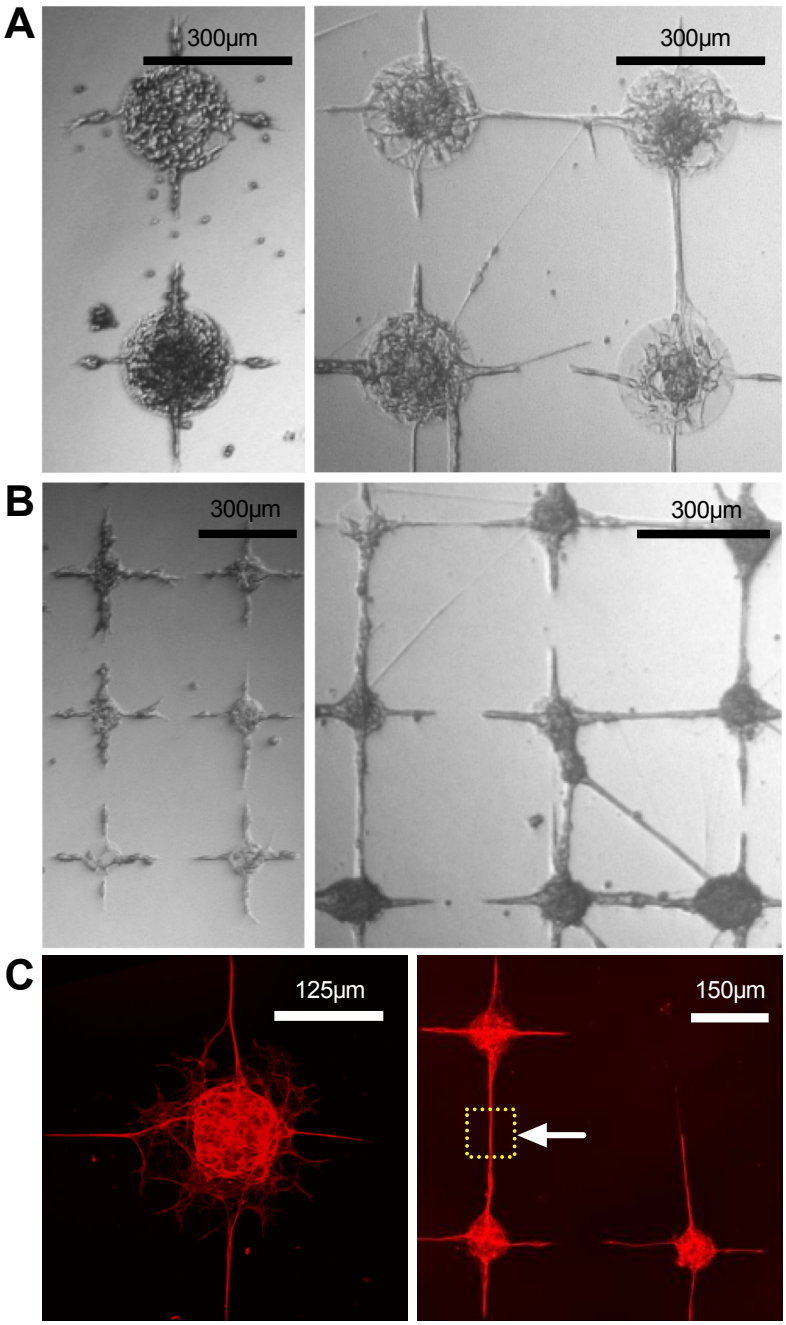

A and B: Glioblastoma-derived line GSC-A in isolation (left) and in co-culture with pre-differentiated LUHMES (right). Node diameter 250 µm in A and 100 µm in B. (C) Neuron-specific β-III tubulin stained co-culture of pre-differentiated LUHMES with glioblastoma-derived glial cell GSC-A. Fixed after 7DIV. The dashed square marked by the arrowhead demarcates a theoretical neurite-only region of interest.

As a control, GSC-A in isolation were also fixed and stained with neuron-specific β-3 tubulin, after culture on chip 1. Unexpectedly, GSC-A also labelled with β-3 tubulin (see Figure 4-9). Again, however, there was no evidence of GSC-A cells extending off parylene regions.

Figure 4-9 GSC-A aberrantly expresses 'neuron-specific' with β-3 tubulin

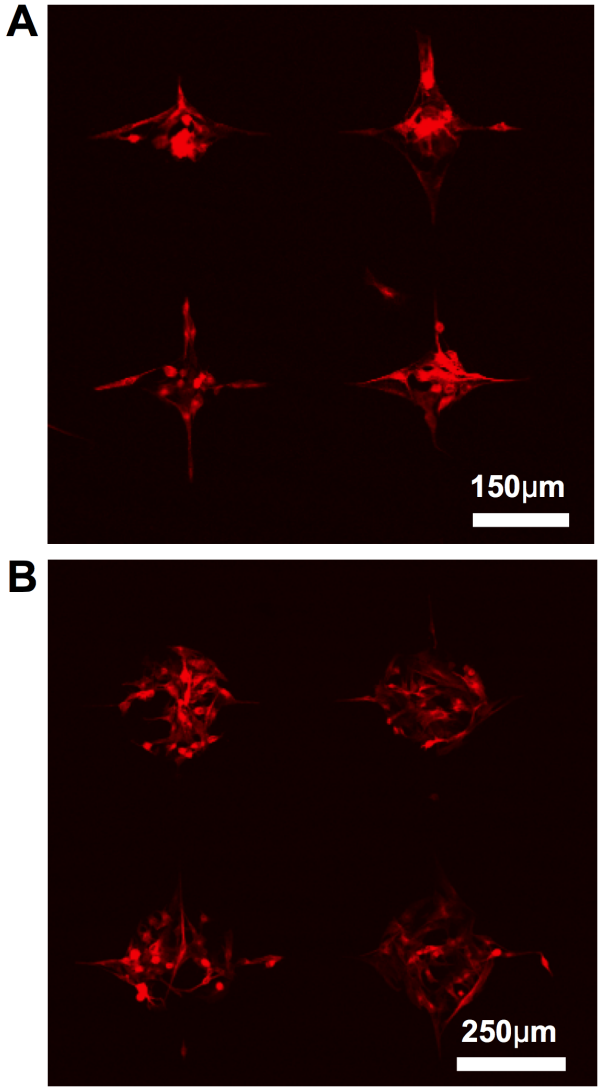

GSC-A cultured alone on chip 1. Fixed and immuno-stained with β-3 tubulin. A: node diameter 100 µm. B: node diameter 250 µm.

4.4 Discussion

4.4.1 Refining control of network topography

Establishing orthogonal network growth

Radial plots allowed comparison of neurite orientation. Using chip 1, and having optimised the co-culture protocol, it was possible to grow orthogonally arranged neuronal networks using both HEK 293 and GSC-A cells. Each of the three node sizes/configurations promoted some degree of orthogonal growth (compared with the random growth observed on un-patterned polystyrene) but accuracy improved from largest (250 μm diameter) to smallest (50 μm diameter) node.

Growth was most orthogonal for the configurations in which parylene nodes were more closely packed. A chemotactic process potentially explains this finding, where the closer proximity of secreting cell clusters results in a more powerful chemotactic gradient. Importantly, however, the parylene designs on chip 1 (with all parylene 'spokes' directing towards adjacent, nearest nodes) are not able to reliably distinguish between a chemo- or hapto-tactic guidance mechanism, as both mechanisms would theoretically result in the orthogonal neurite growth pattern observed. That said, it was noteworthy that neurites in co-culture experiments were sometimes seen to extend off parylene nodes *away* from the spoke tracks, suggesting that the neuronal growth cone was undiscerning with respect to the 'underfoot' substrate.

Disregard for node morphology

Data from chip 3 constitutes further evidence supporting the dominance of a chemotactic mechanism. Here, regardless of the morphology of the underlying parylene node, neurites were seen to organise themselves in a configuration suggesting a vector of growth that sought out the nearest neighbouring node. Both of the node designs with morphology attempting to haptotactically direct neurites towards a more distant node (singe spoke and single teardrop) were unable to exert influence. Hence, for all node designs, the overwhelming neurite direction was towards the nearest neighbouring node orientated at 45° and 135°.

However, it is important to note some limitations. The parylene node itself rapidly becomes overgrown with template HEK 293 cells (an issue noted previously). As a consequence, overlying LUHMES growth cones may not in fact be greatly exposed to parylene-C, but instead interact with the more amorphous profile of the underlying template cell. In addition, both of these directionality experiments are limited by the fact that advancing growth cones were measured at a single point in time, with no dynamic data measuring the true vector of neurite growth. This could be achieved in future using time-lapse imaging. Furthermore, multiple neurites running together in close proximity are difficult to resolve using light microscopy. As such, some data may have been lost.

Considering the chemotactic hypothesis further, questions arise regarding the character, origin, and distance of action of the diffusible agent. If one assumes that parylene regions acquire a population of patterned cells proportionate to their surface area, and that a given chemotactic substance is secreted in proportion to the volume of cells, an opportunity arises to mathematically model the system. If a chemotactic cue is secreted from cell clusters, an explanation is also needed for neurites not being compelled to return or reside at their 'home' node, given that the concentration will be highest in this location. One explanation is that the growth cone requires a certain amount of time in order to become sensitive to the purported chemotactic agent (contingent upon reaching a certain stage of neuronal maturation). As such, after initially heading off at random, relevant receptor expression becomes up-regulated, the growth cone becomes responsive to the diffusible cue, and the vector of growth changes so as to seek out the nearest cell cluster.

4.4.2 Behavioral and immunofluorescence assessment

The critical behavioural difference between cell types is that the neurite growth cone, in contrast with GSC and HEK 293 cells, is able to adhere to and traverse bare SiO_2. For future work, it becomes important to integrate techniques that allow assessment of electrical and synaptic activity in the patterned network. This capacity of neurites to 'jump the gap' between parylene nodes represents an opportunity to interrogate a neurite-only region of interest. By focusing on a parylene-free, inter-node space (see

Figure 4-8C, demarcated by dashed yellow box) one can be confident that neurites alone will be interrogated.

Immunofluorescence staining of the network was complicated by the fact that GSC-A was found to aberrantly express 'neuron-specific' β-3 tubulin. Tubulin is a major constituent of microtubules, which play key roles in chromosome segregation, intracellular transport, ciliary and flagellar bending, and structural support of the cytoskeleton. β-3 tubulin is abundant in the CNS and PNS, being particularly prominently expressed during fetal & postnatal development. In adult tissues, the distribution of β-3 tubulin is almost exclusively neuronal. However, on reviewing the literature, it is apparent that altered patterns of expression have previously been noted in cancer (132), with aberrant expression seen in some glial tumours. Evidently, the tumour from which GSC-A was isolated is one such glial tumour. Co-staining with GFAP and β-3 tubulin would enable the two different cell types to be resolved. Alternatively, another truly neuron-specific marker could be employed. Some preliminary work using neurofilament-L has illustrated its capacity to reliably stain LUHMES neurons and not GSC-A (see Figure 4-10).

The issue of template cell overgrowth persists, despite use of the slightly slower growing GSC-A. It is confounded by the fact that neurites, after encountering another node, apparently straighten up under tension. That growth cones of developing neurons generate tensile forces is well-described (133) and this behaviour has been observed before in the context of carbon-nanotube patterned substrates (134). For long-term neuronal cultures, the current construct is unsuitable. A post-mitotic template cell line might enable prolonged viability of co-cultures. However, the issue of neurite tension might nevertheless result in cell cluster lift-off.

Thinking beyond the initial motivations for the creation of neuronal networks, this lift-off phenomenon might theoretically be useful for neuro-regenerative purposes. For example, it represents a method of defining a neuronal network *in vitro* on-chip that then detaches (see Figure 4-11) and which might then be implanted with the intention of *in vivo* nervous system repair.

Figure 4-10 Neurofilament-L labels LUHMES but not GSC-A

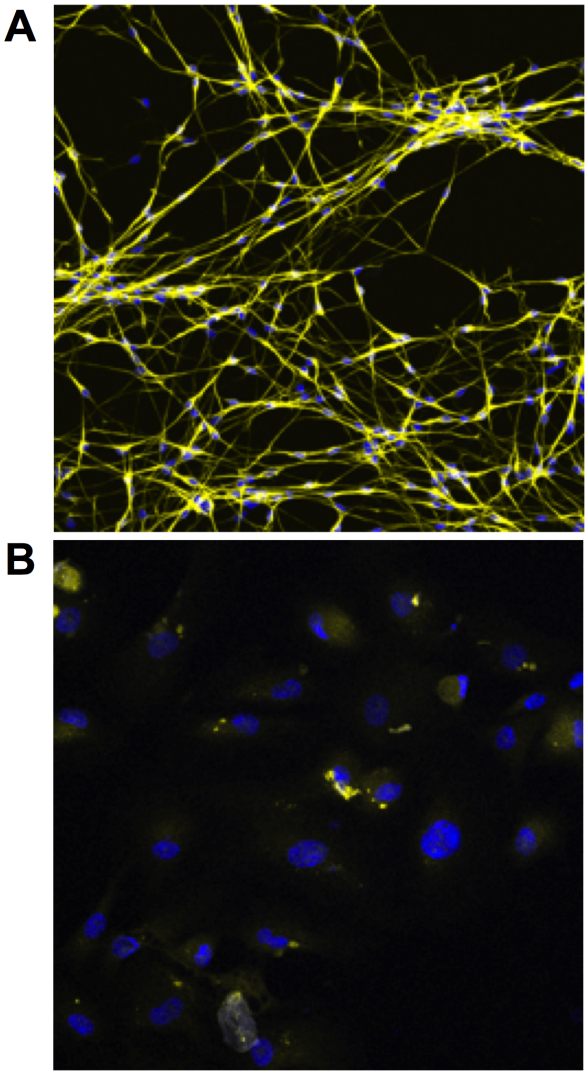

A: Un-patterned LUHMES cultured on a glass coverslip, fixed and stained with neurofilament L (yellow) and DAPI (blue). Region shown measures ~600 µm ×600 µm. B: Un-patterned GSC-A cultured on glass coverslip, fixed and stained with neurofilament-L (yellow) and DAPI (blue). Region shown measures ~150 µm ×150 µm. The LUHMES neuron cytoskeleton is well demarcated by neurofilament-L, compared with minimal expression in GSC-A.

Figure 4-11 HEK 293-LUHMES culture lift-off

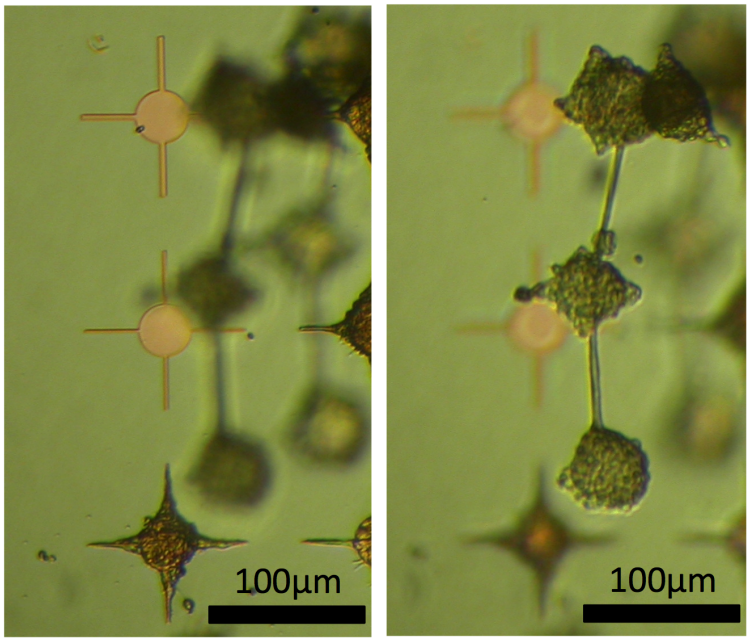

HEK 293 cells co-cultured with pre-differentiated LUHMES. A linear network lifts off from the chip surface after 6DIV (left and right image are the same chip region imaged at two different depths of focus).

4.4.3 Future work

Polarity

The apparent growth of neurites towards their nearest neighbouring cell cluster presents an opportunity to create a polarised, linear network. By constructing a linear array of parylene nodes which become progressively more closely spaced (from left to right), growing neurites ought be induced to grow from left to right, due to the chemotactic influence of their nearest neighbouring node (see Figure 4-12).

To test this hypothesis, time-lapse imaging of co-cultures could be used to assess neurite behaviour. This technique could be enhanced by combination with a live fluorescence cell visualization platform. For example CellTracker™ dyes (Life Technologies, CA, USA) pass through the cell membrane freely whereupon they are transformed in a cell impermeable products. This allows cellular movement to be tracked. Also from a fluorescence imaging perspective, dendritic compared with axonal components can also be differentially stained in LUHMES neurons. Tau-1 labels axons whilst MAP2 labels dendritic proteins (101). Staining with these two markers in fixed cultures could help to assess for the establishment of appropriate overall neuronal polarity, beyond the directionality of growing neurites.

Figure 4-12 Proposal for chip 4

Chip 4. Proposed linear node array. 50 µm diameter nodes are separated as shown, becoming progressively more close-packed from right to left. The chemotactic influence of each node's nearest neighbour will theoretically induce neurites to grow from left to right.

Action potential generation and synaptic transmission

Looking forward, a fundamental question is whether co-cultured LUHMES neuronal networks are forming functional synapses with adjacent neurons. Additionally, given

sufficient time to mature, is this context one in which LUHMES will become spontaneously electrically active? Potential strategies to address these questions are discussed in section 5.2.

4.5 Conclusion

In co-culture experiments, the size and spatial configuration of parylene nodes informed neurite organisation. Specifically, reticular networks of neurons can be generated using an orthogonally arranged node-and-spokes parylene design. Direction of growth of the neurite does not appear to be influenced by parylene. Neurites instead seek out nearby cell clusters, regardless of underlying parylene node morphology. A chemotactic guidance mechanism could explain this behaviour.

GSC-A cells are unable to grow between nodes of parylene-C unless a parylene track is provided. LUHMES neurites, however, possess the capacity to traverse bare SiO_2. This key behavioural difference allows neurite-only ROIs to be identified on-chip. Aberrant expression of beta-3 tubulin in GSC-A cells precludes its use as a means of selectively labelling LUHMES in co-cultures. However, neurofilament-L shows promise as a selective marker. Overgrowth of the template cell remains problematic, with the current protocol presenting insufficient time for functional maturation of LUHMES neurons.

Chapter 5 Conclusions

5.1 Summary

Initial project aims were to:

- Investigate the mechanisms of cell patterning on parylene-C:SiO_2, using both a cell and substrate centric approach.
- Achieve reliable patterning of neuronal cells on parylene-C:SiO_2.
- Establish finer control over neuronal morphology, with respect to axo-dendritic processes, in order to create topographically defined networks.
- Explore techniques to stimulate and record from patterned networks, so as to ensure that patterned neurons retain a viable and functional phenotype.
- Construct and stimulate simple, appropriately polarised, poly-neuronal reflex arcs.

The first three of these aims have largely been achieved and a strategy to address the final goal has been proposed. However, less progress has been made in developing and incorporating tools that evaluate functional characteristics of patterned neuronal networks.

5.1.1 Cell patterning on parylene-C:SiO_2

The parylene-C:SiO_2 platform has been explored from both a substrate and cell centric perspective. Whilst the overarching mechanism of action remains elusive, several important (and previously unexplored) aspects have been identified and investigated.

Chip fabrication processes have a profound impact upon surface characteristics. At the outset, the importance (and cell specificity) of repulsion from SiO_2 was significantly underestimated. Absolute repulsion from SiO_2 domains is *fundamental* to effective cell patterning. As such, piranha treatment (previously considered merely a cleaning step) has been shown to be key to enabling SiO_2 domains to exert downstream cell repulsion after serum incubation. Piranha acid treatment results in both a decrease in contact angle and also a change in surface roughness on SiO_2

regions. However its impact is transient, meaning that serum incubation must occur immediately after piranha treatment. The key components of serum that ultimately impart each substrate with its respective cyto-repulsive or cyto-adhesive character remain unknown. However, parylene-bound vitronectin may play a role in allowing cells to engage, demanding the presence of complimentary vitronectin receptors in the cell membrane. These findings go some way to explain why the parylene-C:SiO_2 patterning platform is not universally effective, with only a subset of cell types patterning reliably (likely a consequence of variation in their CAM expression).

The persisting uncertainty regarding the mechanism of action of the parylene-C:SiO_2 construct restricts its utility as a broad-spectrum cell patterning platform, as there is no way of knowing whether a given cell type will pattern effectively. As such, further work is needed to understand the platform more fully (see 5.2).

5.1.2 Engineering neuronal networks

LUHMES neurons, the neuronal cell model chosen for this project, failed to pattern on-chip in isolation, in either an undifferentiated and pre-differentiated state. All efforts to induce LUHMES to pattern by altering chip preparation protocols were ineffective. This demanded an indirect approach to generating neuronal networks, reliant upon the presence of a pseudo-glial template cell. In the context of a pre-patterned intermediate cell type, LUHMES adhered and showed signs of morphological differentiation. Interestingly, HEK 293 cells (demonstrably non-glial) can fulfil a cellular template role. However, continued HEK 293 proliferation (and ultimately cell lift-off) significantly reduced the lifespan of such co-cultures. A human glioma-derived stem like cell line (GSC-A) also enabled spatially defined secondary adhesion of human LUHMES neurons and morphological differentiation. Similar co-culture behaviour was observed for murine ES-derived neurons co-cultured with pre-patterned HEK 293 cells. These findings demonstrate that the co-culture principle operates both for different types of neurons and also across different species.

Reticular networks of neurons were generated using an orthogonally arranged node-and-spokes parylene design. Neurite behaviour appears to be influenced not by

underlying parylene but by a diffusible chemotactic guidance cue. The recognition of this dominant cue to neurite organisation theoretically offers the potential to create a polarised, linear network. In contrast to template cell, LUHMES neurites possess the capacity to traverse bare SiO_2. This allows neurite-only ROIs to be identified on-chip that may, in due course, facilitate use of tools to assess network functionality. Overgrowth of the pseudo-glial template cell remains problematic and the current protocol provides an insufficient time window for electrophysiological maturation of LUHMES neurons.

Though this platform has enabled patterning of neurons, and has (via harnessing innate neurite growth behaviours) allowed a degree of specific network connectivity to be asserted, it has involved a somewhat circuitous progression. This process has highlighted some interesting concepts (particularly the need, in this context, for an intermediate cell), but has also made some of the core aims of the project more difficult to achieve. For example, the need for a template cell currently limits neuronal network lifespan and impedes on-chip cellular recording strategies. Neurite growth and connectivity also remains largely autonomous (though this may in fact be a strength).

Certain of these challenges are seen in other contemporary neuronal network engineering tools, with some platforms excelling with respect to a given technical aspect but being compromised in another. Arguably at the forefront, Boehler *et al.* (135) have successfully developed a platform capable of recording from patterned hippocampal neurons for up to 21 days. However, this construct involves alignment of a PDMS stamp (inked with polylysine) with a separate MEA-incorporated substrate. Echoing some of the challenges identified in the parylene-C platform, this team faced problems ensuring that MEA substrate fabrication processes remained sympathetic to the core cell patterning strategy. However, once refined, they achieved reliable patterning of neuronal networks with specified connectivity (see Figure 5-1). Crucially, the underlying MEA electrodes also allowed recording of spike activity in the network. It was observed that spike rates were constant regardless of pattern complexity (4, 6, or 8 connections), suggesting that neurons may be optimised for a state of spike rate homeostasis. Identifying such emergent

neuronal network properties exemplifies the potential of topographically defined neuronal networks. This platform would, however, be improved by combining the two-stage print process and removing the need for secondary MEA alignment. An optimised parylene-C:SiO_2 platform could theoretically facilitate similar experiments at a more complex scale and with higher through-put.

Another important issue is the conflict between defining topography to an extent that allows comparison and analysis, versus allowing an appropriate degree of physiological self-organisation. Li *et al.* (136) have recently designed a platform that defines the location of the cell body but intentionally does not restrict neurite outgrowth or dendritic branching and arborisation (the 'NeuroArray', see Figure 5-2). This is reminiscent of the parylene-C:SiO_2 method in the sense that it similarly does not restrict neurite behaviour. The NeuroArray enables a spatially defined, well-connected, and spontaneously active network to be cultured and assessed (via calcium imaging to characterise activity). However, this method does not integrate recording technology into the patterning construct, being based on a PDMS stencil rather than constructed on silicon.

Figure 5-1 Patterned, long-term hippocampal networks integrated with MEAs. Adapted from (135).

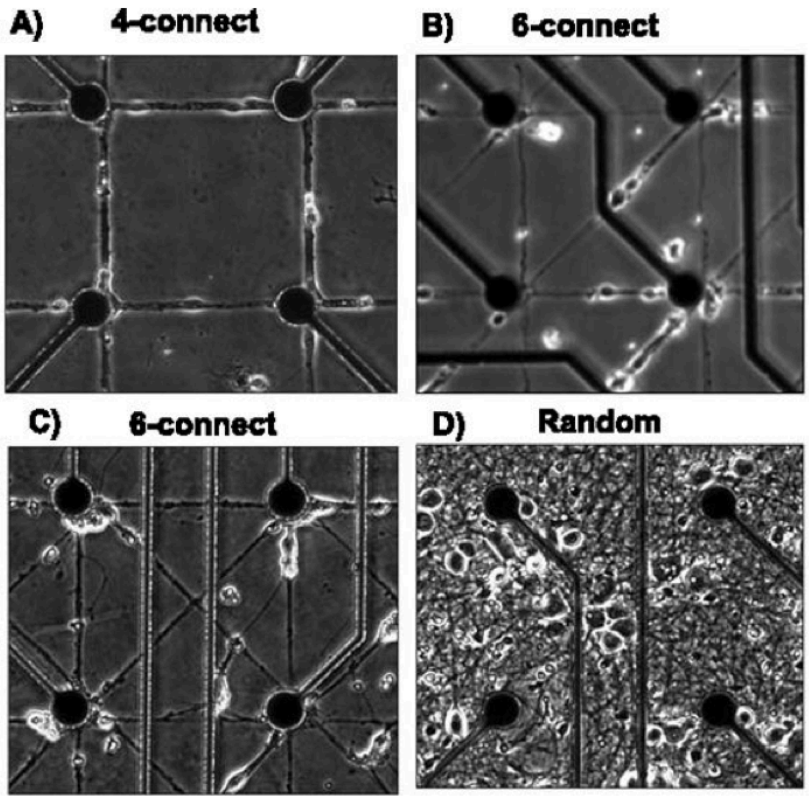

A PDMS print is 'inked' with polylysine and aligned with a background substrate containing embedded MEA electrodes. Hippocampal neurons grow according to the print pattern which here has defined three different levels of connectivity. A: 4 connections, B: 6 connections, C: 8 connections, D: Random growth. MEA electrodes are separated by 200 μm vertically and horizontally.

Figure 5-2 Schematic illustration of the 'NeuroArray' platform, adapted from (136)

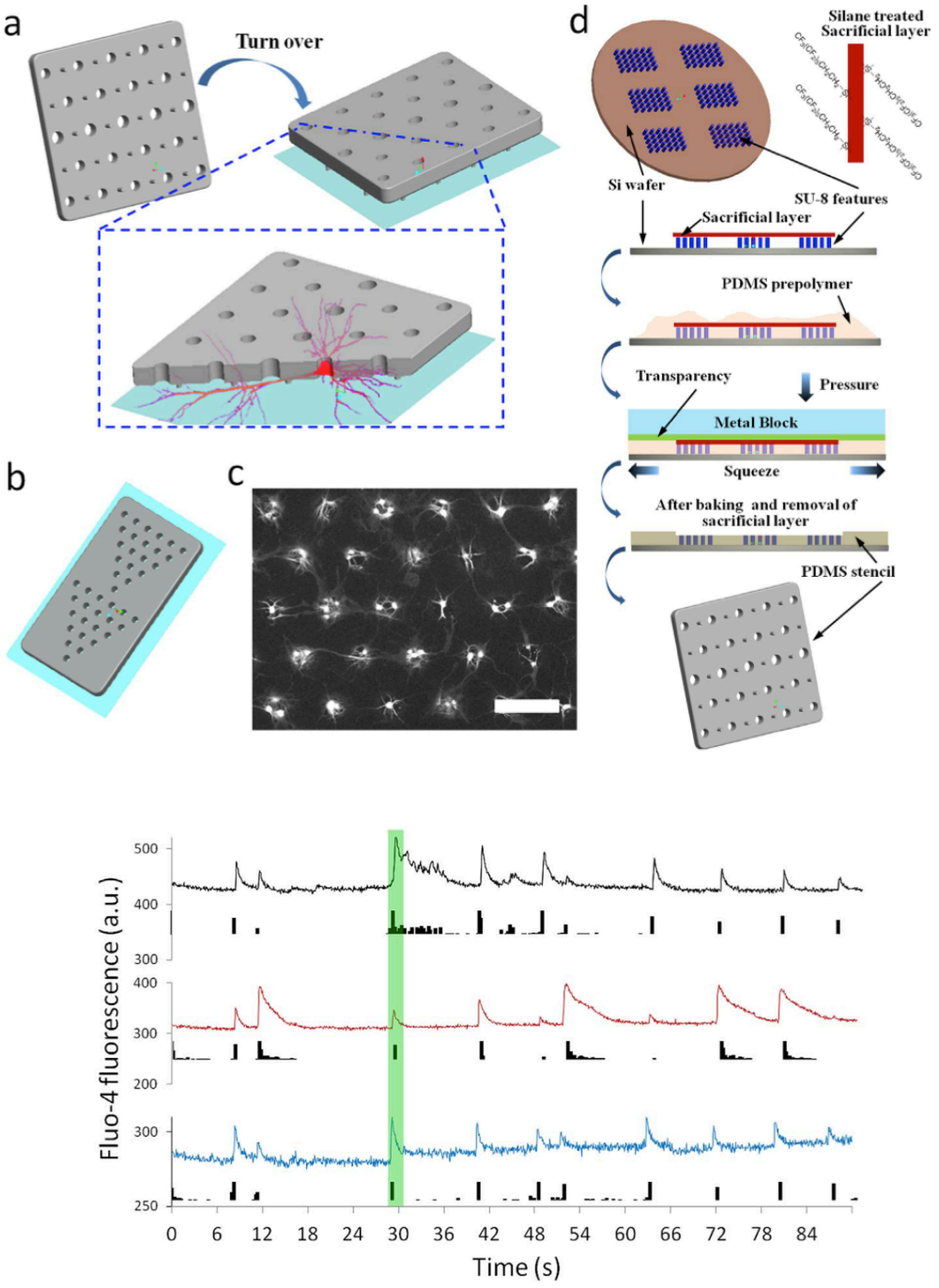

Schematic illustration of 'NeuroArray' technology. Top: A: Design and working principle. B: Example of patterned configuration of through-holes for pattering neural network. C: Representative fluorescence (β-3 tubulin) image of neurons cultured for 4 days, scale bar, 100 μm. D: Fabrication procedures using sacrificial-layer-protected PDMS molding. Bottom: Traces of calcium fluctuation of three neurons showing their spiking activities.

5.2 Future work and ideas

Cell patterning mechanism

Unambiguously defining the mechanism of action of patterning on parylene-S:SiO_2 remains a key challenge. Performing more cell patterning trials and running specific DNA micro-arrays (or RNA-Seq) may generate new findings that illuminate the key CAM and ligand (in the context of serum activation).

An alternative approach is to trial other rationalised protein solutions, the constituents of which are informed specifically by Vroman-mediated binding dynamics. Given the dynamic binding behaviours of proteins in solution, it is conceivable that the use of specific solutions for defined durations may allow targeted and controlled protein binding to the two substrates. Removing the need for serum is critical to removing a large component of the uncertainty that currently limits the utility of the platform.

Engineering neuronal networks

As regards neuronal network engineering, a major rate-limiting step of the co-culture protocol is overgrowth of the template cell. A different, post mitotic cell that patterns accurately is required to allow full maturation and long-term survival of patterned networks. However, even if that is achieved, the issue of neurite tension causing network lift-off may yet remain problematic.

The current hypothesis regarding LUHMES neurite directionality is that a secreted chemotactic agent induces growth towards the nearest neighbouring cell cluster. The proposed design of chip 4, combined with time-lapse imaging and immuno-labelling of different neuronal compartments, offers a means of assessing both neurite growth and the impact upon cellular polarity.

Incorporating on-chip tools to assess functionality

Useful engineered neuronal networks must have appropriate neurophysiological functionality; forming synapses, generating action potentials, and remaining viable

for weeks to months. Otherwise, they arguably run the risk of merely representing microscopic neuronal art.

Several potential methods exist for *in vitro* assessment of neurophysiological characteristics. The on-chip environment presents novel opportunities for certain techniques whilst for others it may be restrictive. Specifically, the parylene-C:SiO_2 construct represents an opportunity to incorporate MEM technologies as a means of cell interrogation. Future work to assess functionality may therefore involve techniques that (i) incorporate bespoke interfacing components into chip fabrication or (ii) use 'traditional' *in vitro* neuronal interrogation techniques.

CNTs represent an interesting potential material for use as an on-chip electrode. As discussed in 1.5.2, CNTs are cylindrical carbon allotropes which have been demonstrated as a biocompatible and electrically conducting substrate to which neurons adhere (30,86). The challenge is to develop a means of targeted CNT generation on-chip that is compatible with the current photolithographic processes.

Optogenetic techniques are another potential tool for assessing activity in patterned neuronal networks and would not require significant alteration of the chip fabrication process. Optogenetics involves the use of light to control neurons that have been genetically modified with light sensitive proteins. Light-gated ion channels (such as channelrhodopsin or halorhodopsin) are the optogenetic actuators whilst recording can be achieved using genetically encoded sensors of calcium or voltage. Theoretically, patterned LUHMES neurons transfected with an appropriate light-gated ion channel could be targeted in this way, with very fine spatial and temporal resolution.

Evolutionary game theory to inspire network design

Once tools for patterning, interacting and recording from engineered neuronal networks reach appropriately high fidelity (on this platform or others), a fundamental question arises regarding the type of network to engineer, and why. One interesting approach involves the application of evolutionary game theory (EGT).

Game theory is a study of strategic decision-making. Its aim is to mathematically

determine the optimal strategy in situations of conflict and cooperation between intelligent rational decision makers. Originally conceived to analyse economic processes, game theory rapidly found utility in biological contexts (for example regarding survival, a competitive strategy, and reproduction, which involves investment, risk, and return). Evolutionary game theory (EGT), advocates that Darwinian evolution does not lead to fitness optimization, but rather that evolution yields solutions to games. EGT helps to define a framework of contests, strategies, and analytics by focusing on the dynamics of strategy change. With respect to Darwinian evolution, players in the game are proteins or cells or whole organisms. The rules are those of inheritance, phenotypic variation, and natural selection. Strategies are the value of phenotypic traits (e.g. anatomy, acuity of perception). The reward is fitness. EGT has also proven useful in explaining some complex, and superficially counter-intuitive, aspects of biology (such as altruism).

The nervous system is under selective pressure to generate adaptive behaviour but is restricted by energy costs. Maintenance of the neuronal membrane potential is a particularly metabolically demanding process, as is vesicle loading and transmitter recycling. This conflict demands the development of energy efficient wiring schemes and computational processes. As such, perhaps there is role for EGT as a tool to inspire the design *and interpretation* of engineered, topographically defined neuronal networks. This approach may aid the identification of emergent properties or mechanisms underpinning neural communication and organization. Nervous systems have been considered theoretically in the context of EGT mechanics before (137,138). Here, however, the aim here would be to build a specific network with the intention of testing a given ‘game’ inspired by the EGT framework that relies on players, rules, and strategies:

- Players in the game are the individual firing neurons
- Rules would include those of dynamic polarisation, long-term potentiation/depression, or other core aspects of neuronal function.
- Strategy might be the firing rate of a neuron, or its connectivity as measured by synaptic formation or pruning.

- Reward is more difficult to envisage but might relate to energy efficiency or reaching equilibrium of network activity.

This approach also provides a framework in which to mathematically model a proposed collection of rules and strategies, from which data can be compared to that generated in real engineered *in vitro* networks.

Chapter 6 Appendix

6.1 Parylene-C material properties

Table 5 Material properties of different types of commercially available parylene.

Property	Parylene-C	Parylene-N	Parylene-D
Density (g/cm^3)	1.289	1.11	1.418
Refractive index	1.639	1.661	1.669
Melting point (ºC)	290	420	380
Dielectric constant (60 Hz)	3.15	2.65	2.84
Tensile modulus (GPa)	3.2	2.4	2.84
Elongation to break (%)	200	30	10
Static coefficient of friction	0.29	0.25	0.31
Dynamic coefficient of friction	0.29	0.25	0.31
Water absorption (% in 24 h)	<0.1	<0.1	<0.1
Oxygen gas permeability (cc.mm)/(m^2.day)	2.8	15.4	12.6
Water vapour transmission rate (g.mm)/(m^2.day)	0.08	0.59	0.09
Water contact angle	87º	79º	97º

Data from Tan et al. (93).

6.2 Raman spectroscopy data

Figure 6-1 Raman spectroscopy results.

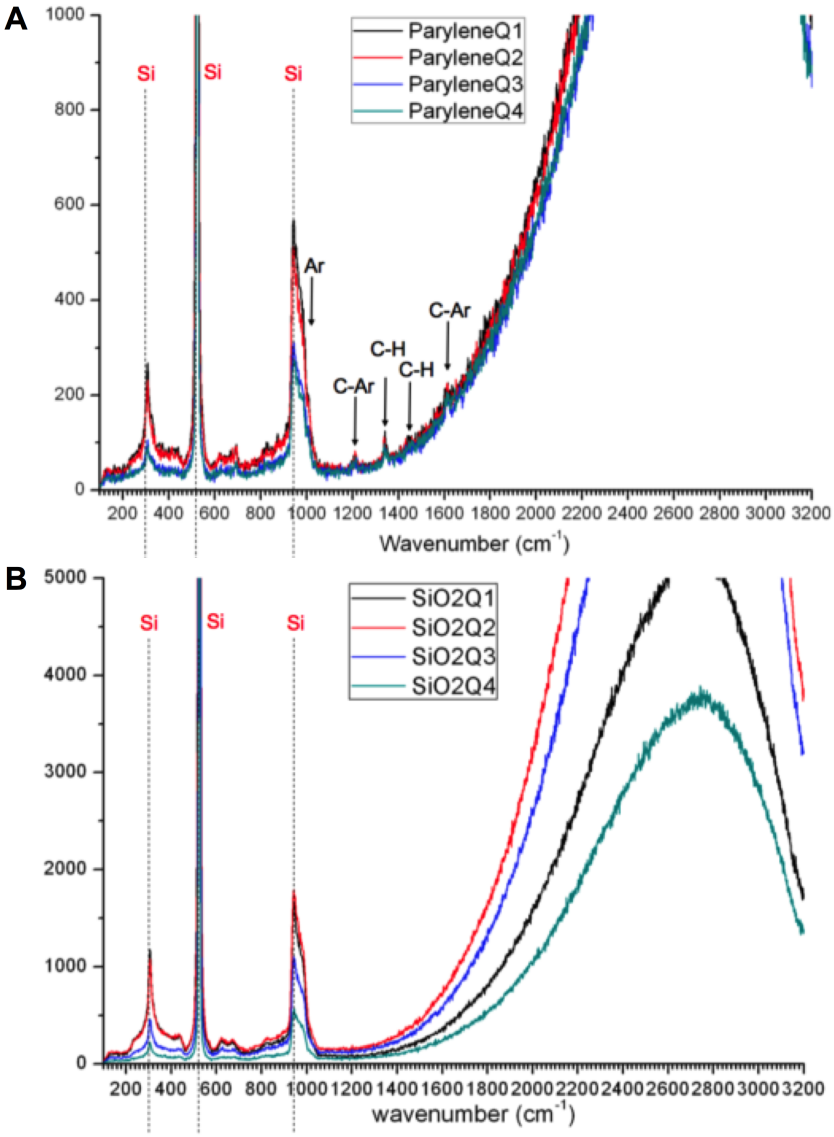

A ParyleneQ1: plain parylene, untreated with piranha solution or serum. ParyleneQ2: plain parylene, treated for 10 mins with piranha solution but no serum. ParyleneQ3: plain parylene, treated with piranha and incubated with serum. ParyleneQ4: plain parylene, untreated with piranha but incubated with serum. 'Ar' refers to an aromatic ring. B SiO2Q1: plain SiO_2, untreated with piranha solution or serum. SiO2Q2: plain SiO_2, treated for 10 mins with piranha solution but no serum. SiO2Q3: plain SiO_2, treated with piranha and incubated with serum. SiO2Q4: plain SiO_2, untreated with piranha but incubated with serum. For parylene surfaces, large silicon peaks dominate whilst the presence of parylene is just discernible. The cause of the large broad peak at 2900cm^{-1} is unknown but could be an artefact in the Raman system, from luminescence of silicon, and or due to heating of the sample. This signal obliterates any peaks that might be attributable to adherent organic material on serum-incubated substrates.

6.3 DNA micro array data sources

Table 6 Gene expression omnibus references and specific data sets used for DNA micro-array comparisons.

Cell line	Gene Expression Omnibus reference
HEK293 (human)	GSE1676 (6 samples GSM28627→28632, uninfected controls). PLATFORM: Affymetrix Human HG-Focus Target Array GSE1822 (2 samples GSM31805→6). PLATFORM: Affymetrix Human Genome U133A Array GSE35226 (4 samples GSM864208→864211) HEK293-WT-1 to 4). PLATFORM Affymetrix Human Gene 1.0 ST Array GSE10241 (1 sample GSM258516 normal control). PLATFORM: Illumina human-6 v2.0 expression beadchip GSE35084 (2 samples GSM861810 and GSM861810). PLATFORM: Affymetrix Human Genome U133 Plus 2.0
N2a (mouse)	GSE17494 (1 sample GSM436142). PLATFORM: Affymetrix Mouse Genome 430 2.0 Array GSE30190 (8 control samples GSM747388-747395). PLATFORM: Agilent-026655 Whole Mouse Genome Microarray 4x44K v2 (Feature Number version)
3T3 L1 (mouse)	GSE20696 (2 samples GSM519581 and GSM519582. PLATFORM: Affymetrix Mouse Genome 430 2.0 Array GSE1458 (3 samples GSM24459→61 control). PLATFORM: Affymetrix Murine Genome U74 Version 2 Array GSE6794 (2 samples GSM156862→3, pre-confluent and confluent). PLATFORM: Affymetrix Murine 11K SubA Array

6.4 Peer-reviewed papers

Hughes MA, Bunting A, Brennan PM, Cameron K, Murray AF & Shipston MJ. (2014) Patterning human neuronal networks on photo-lithographically engineered silicon dioxide substrates functionalized with glial analogues. *J Biomed Mat Res A*. 102(5): 1350-60.

Hughes MA, Bunting A, Brennan PM, Shipston MJ & Murray AF. (2014) Cell patterning on photolithographically-defined parylene-C/SiO2 substrates. *J Vis Exp*. 85: e50929, doi:10.3791/50929.

Hughes MA, Bunting A, Cameron K, Murray AF, & Shipston MJ. (2013) Modulating patterned adhesion and repulsion of HEK 293 cells on micro-engineered parylene-C/SiO_2 substrates. *J Biomed Mat Res A*. 101(2): 349-57.

Hughes MA, Murray AF & Shipston MJ. Toward a "Siliconeural" Computer: Technological Successes and Challenges. *Phil. Trans. Roy. Soc. A*. Invited article, submitted.

6.5 Oral and poster presentations

Hughes MA, Bunting A, Brennan PM, Murray AF & Shipston MJ. (2014) Patterning neuronal networks on photolithographically-defined parylene:silicon substrates. Experimental Biology, San Diego, [Oral presentation].

Hughes MA, Bunting A, Brennan PM, Murray AF & Shipston MJ. (2014) Engineering neuronal networks on photolithographically defined, biologically activated silicon substrates. Academy of Medical Sciences Spring Meeting, London. Proceedings: *The Lancet* AMS Supplement 2014 [Poster].

Hughes MA, Bunting A, Brennan PM, Murray AF & Shipston MJ (2014). Towards regenerative neurosurgery: Interfacing neuronal networks with silicon-based microelectronics. Society of Academic and Research Surgery (SARS) annual meeting, Cambridge. Proceedings: *British Journal of Surgery* [Oral presentation].

Hughes MA, Murray AF, & Shipston MJ. (2013) Patterning neurons and informing neurite geometry on photolithographically defined parylene-C coated SiO_2. International Union of Physiological Sciences (IUPS) Congress, Birmingham [Poster].

Hughes MA, Murray AF, & Shipston MJ. (2012) Progress towards merging neuronal network engineering with semiconductor microelectronics technology: tools for neuroscience and neurosurgery. Society of British Neurological Surgeons (SBNS) Annual Conference, Aberdeen. Proceedings: *British Journal of Neurosurgery* 2012; 26(2): 132–174.

Hughes MA, Bunting A, Murray AF, & Shipston MJ (2012). Patterning human dopaminergic neurons on photolithographically engineered silicon dioxide wafers functionalized with pre-adhered HEK 293 cells. PC 237. Physiology Congress, Edinburgh [Poster].

6.6 Prizes

Winner of Society of Academic and Research Surgeons (SARS) Academic Clinical Lecturer future projects prize. SARS annual meeting, Cambridge, 2014.

Winner of British Journal of Neurosurgery Prize for best abstract, SBNS conference, Aberdeen, 2012.

Winner of EUSci (student-run science communication group) Scientific Photography Competition 2012 (for image of patterned co-culture of LUHMES and glioma-derived stem-like cell line entitled “A Neuronal Celtic Cross”).

6.7 References

1. Lin P, Lin C-W, Mansour R, Gu F. (2013) Improving biocompatibility by surface modification techniques on implantable bioelectronics. *Biosensors and Bioelectronics.* 15;47: 451–60.

2. Lutz R, Pataky K, Gadhari N, Marelli M, Brugger J, Chiquet M. (2011) Nano-Stenciled RGD-Gold Patterns That Inhibit Focal Contact Maturation Induce Lamellipodia Formation in Fibroblasts. *PLoS ONE*. 27:6(9): e25459.

3. Guillotin B, Guillemot F. (2011) Cell patterning technologies for organotypic tissue fabrication. *Trends in Biotechnology.* 1:29(4): 183–90.

4. Marconi E, Nieus T, Maccione A, Valente P, Simi A, Messa M, et al. (2012) Emergent Functional Properties of Neuronal Networks with Controlled Topology. *PLoS ONE.* 6:7(4): e34648.

5. Biffi E, Piraino F, Pedrocchi A, Fiore GB, Ferrigno G, Redaelli A, et al. (2012) A microfluidic platform for controlled biochemical stimulation of twin neuronal networks. *Biomicrofluidics*. 2012:6(2): 024106.

6. Lebedev MA, Tate AJ, Hanson TL, Li Z, O'Doherty JE, Winans JA, et al. (2011) Future developments in brain-machine interface research. *Clinics*. 66:25–32.

7. Daly JJ, Wolpaw JR. (2008) Brain–computer interfaces in neurological rehabilitation. *The Lancet Neurology.* 1:7(11): 1032–43.

8. Demming A, Gimzewski JK, Vuillaume D. (2013) Synaptic electronics. *Nanotechnology*. 24(38): 380201.

9. Bacakova L, Filova E, Parizek M, Ruml T, Svorcik V. Modulation of cell adhesion, proliferation and differentiation on materials designed for body implants. (2011) *Biotechnology Advances.* 3: 1–29.

10. Sackmann E, Bruinsma RF. (2002) Cell adhesion as wetting transition? *Chem Phys Chem.* 3(3): 262–9.

11. Humphries JD. (2006) Integrin ligands at a glance. *Journal of Cell Science.* 119: 3901–3.

12. Diamond MS, Springer TA. (1994) The dynamic regulation of integrin adhesiveness. *Current Biology.* 4(6): 506–17.

13. Streuli CH, Akhtar N. (2009) Signal co-operation between integrins and other receptor systems. *Biochem J.* 418(3): 491-506.

14. Schwartz MA, Schaller MD, Ginsberg MH. (1995) Integrins: emerging paradigms of signal transduction. *Annual review of cell and developmental biology.* 11(1): 549–99.

15. García AJ. (2005) Get a grip: integrins in cell–biomaterial interactions. *Biomaterials*. 26(36): 7525–9.

16. Zhang Z, Vuori K, Wang H-G, Reed JC, Ruoslahti E. (1996) Integrin activation by R-ras. *Cell*. 85(1): 61–9.

17. Clark EA, Brugge JS. (1995) Integrins and signal transduction pathways: the road taken. *Science*. 268(5208): 233–9.

18. Takeichi M. (2006) The cadherin superfamily in neuronal connections and interactions. *Nat Rev Neurosci.* 8(1): 11–20.

19. Probstmeier RR, Pesheva PP. (1999) Tenascin-C inhibits beta1 integrin-dependent cell adhesion and neurite outgrowth on fibronectin by a disialoganglioside-mediated signaling mechanism. *Glycobiology*. 9(2): 101–14.

20. Stoeckli ET. (2010) Neural circuit formation in the cerebellum is controlled by cell adhesion molecules of the Contactin family. *Cell Adhesion & Migration.* 4(4): 523–6.

21. Freeman S, Allison LA, Black M, Podgorski G, Quillin K, Taylor E. (2014) *Biological Science.* London: Pearson Education.

22. Humphries JD. (2000) Molecular Basis of Ligand Recognition by Integrin alpha 5beta 1. *Journal of Biological Chemistry.* 275: 20337–45.

23. Tang LL, Wu YY, Timmons RBR. (1998) Fibrinogen adsorption and host tissue responses to plasma functionalized surfaces. *J Biomed Mater Res.* 42(1): 156–63.

24. Groth T, Altankov G, Kostadinova A, Krasteva N, Albrecht W, Paul D. (1999) Altered vitronectin receptor (alpha v integrin) function in fibroblasts adhering on hydrophobic glass. *J Biomed Mater Res.* 44(3): 341–51.

25. Hynes RO. (2002) Integrins: bidirectional, allosteric signaling machines. *Cell*. 110(6): 673–87.

26. Amiji M, Park K. (1993) Surface modification of polymeric biomaterials with poly(ethylene oxide), albumin, and heparin for reduced thrombogenicity. *J Biomater Sci Polym Ed.* 4(3): 217–34.

27. Sammons RL, Lumbikanonda N, Gross M, Cantzler P. (2005) Comparison of osteoblast spreading on microstructured dental implant surfaces and cell behaviour in an explant model of osseointegration. A scanning electron microscopic study. *Clin Oral Implants Res.* 16(6): 657–66.

28. Kriparamanan R, Aswath P, Zhou A, Tang L, Nguyen KT. (2006) Nanotopography: Cellular Responses to Nanostructured Materials. *Journal of Biomedical Nanotechnology.* 6(7): 1905–19.

29. Martínez E, Engel E, Planell JA, Samitier J. (2009) Effects of artificial micro- and nano-structured surfaces on cell behavio*ur. Annals of Anatomy.* 191(1): 126–35.

30. Bekyarova E, Ni Y, Malarkey EB, Montana V, McWilliams JL, Haddon RC, et al. (2005) Applications of Carbon Nanotubes in Biotechnology and Biomedicine. *Journal of Biomedical Nanotechnology.* 1(1):3–17.

31. Curran JM, Stokes R, Irvine E, Graham D, Amro NA, Sanedrin RG, et al. (2010) Introducing dip pen nanolithography as a tool for controlling stem cell behaviour: unlocking the potential of the next generation of smart materials in regenerative medicine. *Lab Chip.* 10(13): 1662-70.

32. Engler A, Bacakova L, Newman C, Hategan A. (2004) Substrate Compliance versus Ligand Density in Cell on Gel Responses. *Biophysical Journal.* 86: 617-28.

33. Wang N, Naruse K, Stamenović D, Fredberg JJ, Mijailovich SM, Tolić-Nørrelykke IM, et al. (2001) Mechanical behavior in living cells consistent with the tensegrity model. *PNAS.* 98(14): 7765-70.

34. Engler AJ, Sen S, Sweeney HL, Discher DE. (2006) Matrix Elasticity Directs Stem Cell Lineage Specification. *Cell*. 126(4): 677–89.

35. Nikukar H, Reid S, Tsimbouri PM, Riehle MO, Curtis ASG, Dalby MJ. Osteogenesis of Mesenchymal Stem Cells by Nanoscale Mechanotransduction. *ACS Nano.* 2013 Mar 26;7(3):2758–67.

36. Crick F. *The Astonishing Hypothesis: The Scientific Search for the Soul.* London: Simon and Schuster.

37. Bullock TH. (2005) The Neuron Doctrine, Redux. *Science*. 310(5749): 791–3.

38. Cajal S. (1995) *Histology of the nervous system of man and vertebrates.* Oxford: Oxford University Press.

39. Bullock TH. (1959) Neuron Doctrine and Electrophysiology: A quiet revolution has been taking place in our concepts of how the nerve cells

act alone and in concert. *Science*. 129(3355): 997–1002.

40. Merighi A, Salio C, Ferrini F, Lossi L. (2011) Neuromodulatory function of neuropeptides in the normal CNS. *Journal of Chemical Neuroanatomy*. 42(4): 276–87.

41. Sanes JN, Donoghue JP. (2000) Plasticity and Primary Motor Cortex. *Annu Rev Neurosci.* 23(1): 393–415.

42. Wickman K, Clapham DE. (1995) Ion channel regulation by G proteins. *Physiol Rev.* 75(4): 865-885.

43. Levitan IB. (1994) Modulation of Ion Channels by Protein Phosphorylation and Dephosphorylation. *Annu Rev Physiol.* 56(1): 193–212.

44. Perea G, Araque A. (2010) Glia modulates synaptic transmission. *Brain Research Reviews.* 63(1-2): 93-102.

45. Rizo J, Rosenmund C. (2008) Synaptic vesicle fusion. *Nat Struct Mol Biol.* 15(7): 665–74.

46. Südhof TC. (2013) Neurotransmitter Release: The Last Millisecond in the Life of a Synaptic Vesicle. *Neuron*. 80(3): 675-90.

47. White JG, Southgate E, Thomson JN. (1983) Factors that determine connectivity in the nervous system of Caenorhabditis elegans. *Cold Spring Harb Symp Quant Biol.* 48(2): 633-40.

48. Toga AW, Clark KA, Thompson PM, Shattuck DW, Van Horn JD. (2012) Mapping the Human Connectome. *Neurosurgery*. 71(1): 1–5.

49. Azevedo FAC, Carvalho LRB, Grinberg LT, Farfel JM, Ferretti REL, Leite REP, et al. (2009) Equal numbers of neuronal and nonneuronal cells make the human brain an isometrically scaled-up primate brai*n. J Comp Neurol.* 513(5): 532–41.

50. Tang Y, Nyengaard JR, De Groot DMG, Gundersen HJRG. (2001) Total regional and global number of synapses in the human brain neocortex. *Synapse*. 41(3):258–73.

51. Reynolds CW. (1997) Flocks, Herds, and Schools: A Distributed Behavioral Model. *Computer Graphics.* 21(4): 25-34.

52. Chen X, Leischner U, Varga Z, Jia H, Deca D, Rochefort NL, et al. (2012) LOTOS-based two-photon calcium imaging of dendritic spines in vivo. *Nature Protocols.* 7(10): 1818–29.

53. Williams SCP, Deisseroth K. (2013) Optogenetics. P*roceedings of the National Academy of Sciences.* 110(41): 16287–7.

54. Ogura A, Takahashi K. (1976) Artificial deciliation causes loss of calcium-dependent responses in Paramecium. *Nature*. 264(5582): 170–2.

55. Vreeling FW, Houx PJ, Jolles J. (1995) Primitive reflexes in Alzheimer's disease and vascular dementia. *Journal of Geriatric Psychiatry and Neurology.* 8(2): 111-7.

56. Sanz-Arigita EJ, Schoonheim MM, Damoiseaux JS. (2010) Loss of 'small-world'networks in Alzheimer's disease: graph analysis of FMRI resting-state functional connectivity. *PLoS ONE.* 5(11): e13788.

57. Woodward KE, Gaxiola-Valdez I, Goodyear B, Federico P. (2013) Frontal Lobe Epilepsy Alters Functional Connections within the Brain's Motor Network: A Resting-state fMRI Study. *Brain Connectivity.* 4(2): 91-9.

58. Akil H, Brenner S, Kandel E, Kendler KS, King MC, Scolnick E, et al. (2010) The Future of Psychiatric Research: Genomes and Neural Circuits. *Science*. 327(5973): 1580–1.

59. Hochberg LR, Serruya MD, Friehs GM, Mukand JA, Saleh M, Caplan

AH, et al. (2006) Neuronal ensemble control of prosthetic devices by a human with tetraplegia. *Nature*. 442(7099): 164–71.

60. Hochberg LR, Bacher D, Jarosiewicz B, Masse NY, Simeral JD, Vogel J, et al. (2012) Reach and grasp by people with tetraplegia using a neurally controlled robotic arm. *Nature*. 485(7398): 372–5.

61. Santhanam G, Linderman MD, Gilja V. (2007) HermesB: A Continuous Neural Recording System for Freely Behaving Primates. *IEEE Transactions Biomedical Engineering.* 54(11): 2037-2050.

62. Winslow BD, Tresco PA. (2010) Quantitative analysis of the tissue response to chronically implanted microwire electrodes in rat cortex. *Biomaterials*. 31(7): 1558-67.

63. Bartels J, Andreasen D, Ehirim P, Mao H, Seibert S, Wright EJ, et al. (2008) Neurotrophic electrode: Method of assembly and implantation into human motor speech cortex. *Journal of Neuroscience Methods.* 174(2): 168–76.

64. Hughes MA. (2014) Engineering brain-computer interfaces: past, present and future. *J Neurosurg Sci.* 58(2): 117–23.

65. Indiveri G. (2011) Neuromorphic silicon neuron circuits. *Frontiers in Neuroscience.* 5(73): 1–23.

66. Li JL, Cai YL, Guo YL, Fuh JYH, Sun J, Hong GS, et al. (2013) Fabrication of three-dimensional porous scaffolds with controlled filament orientation and large pore size via an improved E-jetting technique. *J Biomed Mater Res.* 102(4):651-658.

67. Tong HD, Zwijze AF, Berenschot JW, Wiegerink RJ. (2001) Platinum patterning by a modified lift-off technique and its application in a silicon load cell. *Sensors and Materials.* 13(4): 235-246.

68. Hartmann JT, Lipp H-P. (2003) Toxicity of platinum compounds. *Expert Opin Pharmacother.* 4(6): 889–901.

69. Schmid RS, Anton ES. (2003) Role of integrins in the development of the cerebral cortex. *Cereb Cortex.* 13(3):219–24.

70. Nadarajah B, Alifragis P, Wong R. (2002) Ventricle-directed migration in the developing cerebral cortex. *Nat Neuroscience.* 5(3): 218 - 224.

71. Letinic K, Rakic P. (2001) Telencephalic origin of human thalamic GABAergic neurons. *Nat Neurosci.* 4(9): 931-6.

72. Kennedy TE. (2006) Axon Guidance by Diffusible Chemoattractants: A Gradient of Netrin Protein in the Developing Spinal Cord. *Journal of Neuroscience.* 26(34): 8866–74.

73. Arimura N, Kaibuchi K. (2007) Neuronal polarity: from extracellular signals to intracellular mechanisms. *Nat Rev Neurosci.* 8(3): 194–205.

74. Rasband MN. (2010) The axon initial segment and the maintenance of neuronal polarity. *Nat Rev Neurosci.* 11(8): 552–62.

75. Barnes AP, Polleux F. (2009) Establishment of Axon-Dendrite Polarity in Developing Neurons. *Annu Rev Neurosci.* 32: 347-81.

76. Thomas CA, Springer PA, Loeb GE. (1972) A miniature microelectrode array to monitor the bioelectric activity of cultured cells. *Exp Cell Res.* 74(1): 61-6.

77. Pine J. (1980) Recording action potentials from cultured neurons with extracellular microcircuit electrodes. *Journal of Neuroscience Methods.* 2(1): 19-31.

78. Gross GW. (1979) Simultaneous single unit recording in vitro with a photoetched laser deinsulated gold multimicroelectrode surface. Biomedical Engineering. *IEEE Transactions on Biomedical*

Engineering. 26(5): 273-279.

79. Roth EA, Xu T, Das M, Gregory C, Hickman JJ, Boland T. (2004) Inkjet printing for high-throughput cell patterning. *Biomaterials*. 25(17): 3707-15.

80. Sanjana N. A fast flexible ink-jet printing method for patterning dissociated neurons in culture. *Journal of Neuroscience Methods.* 136(2): 151–63.

81. Csucs G, Michel R, Lussi JW, Textor M, Danuser G. Microcontact printing of novel co-polymers in combination with proteins for cell-biological applications. *Biomaterials*. 24(10): 1713–20.

82. Belkaid W, Thostrup P, Yam PT, Juzwik CA, Ruthazer ES, Dhaunchak AS, et al. (2013) Cellular response to micropatterned growth promoting and inhibitory substrates. *BMC Biotechnology.* 13(86).

83. Zeck GN, Fromherz P. (2001) Noninvasive neuroelectronic interfacing with synaptically connected snail neurons immobilized on a semiconductor chip. *PNAS*. 98(18): 10457-62.

84. Xie C, Hanson L, Xie W, Lin Z, Cui B, Cui Y. (2010) Noninvasive Neuron Pinning with Nanopillar Arrays. *Nano Lett.* 2010. 10(10): 4020–4.

85. Dowell-Mesfin NM, Abdul-Karim M-A, Turner AMP, Schanz S, Craighead HG, Roysam B, et al. (2004) Topographically modified surfaces affect orientation and growth of hippocampal neurons. *J Neural Eng.* 1(2): 78–90.

86. Gabay T, Ben-David M, Kalifa I, Sorkin R, Abrams ZR, Ben-Jacob E, et al. (2007) Electro-chemical and biological properties of carbon nanotube based multi-electrode arrays. *Nanotechnology*. 18(3): 035201.

87. Sorkin R, Greenbaum A, David-Pur M, Anava S, Ayali A, Ben-Jacob E, et al. (2008) Process entanglement as a neuronal anchorage mechanism to rough surfaces. *Nanotechnology*. 2008 20(1): 015101.

88. Scotchford CA, Ball M, Winkelmann M, Vörös J, Csucs C, Brunette DM, et al. (2003) Chemically patterned, metal-oxide-based surfaces produced by photolithographic techniques for studying protein-and cell-interactions. *Biomaterials*. 24(7): 1147–58.

89. Morin F, Nishimura N, Griscom L, LePioufle B, Fujita H, Takamura Y, et al. (2006) Constraining the connectivity of neuronal networks cultured on microelectrode arrays with microfluidic techniques: A step towards neuron-based functional chips. *Biosensors and Bioelectronics.* (7): 1093–100.

90. Kim DH, Kim PSS, Lee K, Kim J, Kim MJ. (2013) Galvanotactic behavior of Tetrahymena pyriformisunder electric fields. *J Micromech Microeng.* 23(12): 125004.

91. Delivopoulos E, Murray AF, MacLeod NK, Curtis JC. (2009) Guided growth of neurons and glia using microfabricated patterns of parylene-C on a SiO2 background. *Biomaterials*. 30(11): 2048–58.

92. Delivopoulos E. (2004) *Patterned cultures of neurons and glia on silicon with the use of lithography and photo-resist materials.* Thesis (MSc), School of Informatics, University of Edinburgh.

93. Tan CP, Craighead HG. (2010) Surface Engineering and Patterning Using Parylene for Biological Applications. *Materials*. 3(3): 1803–32.

94. Tan CP, Cipriany BR, Lin DM, Craighead HG. (2010) Nanoscale Resolution, Multicomponent Biomolecular Arrays Generated By Aligned Printing With Parylene Peel-Off. *Nano Lett.* 10(2): 719–25.

95. Ilic B, Czaplewski D, Zalalutdinov M, Schmidt B, Craighead HG.

(2002) Fabrication of flexible polymer tubes for micro and nanofluidic applications. *J Vac Sci Technol B*. 20(6): 2459.

96. Hermansson K, Lindberg U, Hok B, Palmskog G. (1991) Wetting properties of silicon surfaces. *IEEE Solid-state Sensors and Actuators*. 193–6.

97. Price PJ, Gregory EA. (1982) Relationship between in vitro growth promotion and biophysical and biochemical properties of the serum supplement. *In Vitro*. 18(6): 576–84.

98. Fabrizius-Homan DJ, Cooper SL. (1992) A comparison of the adsorption of three adhesive proteins to biomaterial surfaces. *J Biomater Sci Polym Ed*. 3(1):27–47.

99. Delivopoulos E, Murray AF. (2011) Controlled Adhesion and Growth of Long Term Glial and Neuronal Cultures on Parylene-C. *PLoS ONE*. 6(9): e25411.

100. Delivopoulos E, Murray AF, Curtis JC. (2010) Effects of parylene-C photooxidation on serum-assisted glial and neuronal patterning. *J Biomed Mater Res*. 94(1): 47–58.

101. Scholz D, Pöltl D, Genewsky A, Weng M, Waldmann T, Schildknecht S, et al. (2011) Rapid, complete and large-scale generation of post-mitotic neurons from the human LUHMES cell line. *Journal of Neurochemistry*. 119(5): 957–71.

102. Graham FL, Smiley J, Russell WC, Nairn R. (1977) Characteristics of a human cell line transformed by DNA from human adenovirus type 5. *Journal of General Virology*. 36(1): 59–72.

103. Bodary SC, McLean JW. (1990) The integrin beta 1 subunit associates with the vitronectin receptor alpha v subunit to form a novel vitronectin receptor in a human embryonic kidney cell line. *Journal of Biological*

Chemistry. 265(11):5938–41.

104. Shaw G. (2002) Preferential transformation of human neuronal cells by human adenoviruses and the origin of HEK 293 cell*s*. *The FASEB Journal*. 16(8): 869-71.

105. Zhu G, Zhang Y, Xu H, Jiang C. (1998) Identification of endogenous outward currents in the human embryonic kidney (HEK 293) cell line. *Journal of Neuroscience Methods*. 81(1-2): 73–83.

106. Gorbunov BZ, Safatov AS. (1982) Determination of the concentration of surface hydroxyl groups on silicon dioxide particles by the method of IR spectroscopy. *J Appl Spectrosc.* 36(3):328–32.

107. Boyd NA, Bradwell AR, Thompson RA. Quantitation of vitronectin in serum: evaluation of its usefulness in routine clinical practice. *Journal of Clinical Pathology*. 46(11): 1042–5.

108. Grinnell F, Feld MK. (1982) Fibronectin adsorption on hydrophilic and hydrophobic surfaces detected by antibody binding and analyzed during cell adhesion in serum-containing medium. *Journal of Biological Chemistry*. 257(9): 4888–93.

109. Unsworth CP, Delivopoulos E, Gillespie T, Murray AF. (2011) Isolating single primary rat hippocampal neurons & astrocytes on ultra-thin patterned parylene-C/silicon dioxide substrates. *Biomaterials*. 32(10): 2566–74.

110. Unsworth CP, Graham ES, Delivopoulos E, Dragunow M, Murray AF. (2010) First human hNT neurons patterned on parylene-C/silicon dioxide substrates: Combining an accessible cell line and robust patterning technology for the study of the pathological adult human brain. *Journal of Neuroscience Methods.* 194(1): 154–7.

111. Frantz C, Stewart KM, Weaver VM. (2012) The extracellular matrix at a

glance. *Journal of Cell Science.* 123(24): 4195–200.

112. Righi M, Mori L, Libero GD, Sironi M. (1989) Monokine production by microglial cell clones. *European Journal of Immunology.* 19(8): 1443-48.

113. Tremblay RG, Sikorska M, Sandhu JK, Lanthier P, Ribecco-Lutkiewicz M, Bani-Yaghoub M. (2010) Differentiation of mouse Neuro 2A cells into dopamine neurons. *Journal of Neuroscience Methods.* 186(1): 60–7.

114. Zebisch K, Voigt V, Wabitsch M, Brandsch M. (2012) Protocol for effective differentiation of 3T3-L1 cells to adipocytes. *Analytical Biochemistry.* 425(1): 88–90.

115. Dorovini-Zis K, Prameya R, Bowman PD. (1991) Culture and characterization of microvascular endothelial cells derived from human brain. *Lab Invest.* 64(3): 425–36.

116. Khaw LT, Ball HJ, Golenser J, Combes V, Grau GE. (2013) Endothelial Cells Potentiate Interferon-γ Production in a Novel Tripartite Culture Model of Human Cerebral Malaria. *PLoS ONE.* 8(7): e69521.

117. Belsham DD, Cai F, Cui H, Smukler SR, Salapatek AMF, Shkreta L. (2004) Generation of a Phenotypic Array of Hypothalamic Neuronal Cell Models to Study Complex Neuroendocrine Disorders. *Endocrinology*. 145(1): 393–400.

118. Goffin D, Zhou Z. (2012) The neural circuit basis of Rett syndrome. *Front Biol.* 7(5): 428–35.

119. Pollard SM, Yoshikawa K, Clarke ID, Danovi D, Stricker S, Russell R, et al. (2009) Glioma Stem Cell Lines Expanded in Adherent Culture Have Tumor-Specific Phenotypes and Are Suitable for Chemical and Genetic Screens. *Cell Stem Cell*. 4(6): 568–80.

120. Gladson CL, Cheresh DA. Glioblastoma expression of vitronectin and the alpha v beta 3 integrin. Adhesion mechanism for transformed glial cells. *J Clin Invest.* 1991. 88(6): 1924-32.

121. Schnabl B. (2001) TAK1/JNK and p38 have opposite effects on rat hepatic stellate cells. *Hepatology*. 2001. 34(5): 953–63.

122. Clegg DO, Wingerd KL, Hikita ST, Tolhurst EC. (2003) Integrins in the development, function and dysfunction of the nervous system. *Front Biosci.* 8: 723-50.

123. Claessens A. (2010) *How Plasmodium falciparum malaria parasites bind to human brain endothelial cells.* Thesis (PhD). School of Medicine and Veterinary Medicine, University of Edinburgh.

124. Sekimoto H, Eipper-Mains J, Pond-Tor S, Boney CM. (2005) αvβ3 Integrins and Pyk2 Mediate Insulin-Like Growth Factor I Activation of Src and Mitogen-Activated Protein Kinase in 3T3-L1 Cells. *Molecular Endocrinology*. 19(7): 1859–67.

125. Iwamoto H, Sakai H, Nawata H. (1998) Inhibition of integrin signaling with Arg-Gly-Asp motifs in rat hepatic stellate cells. *J Hepatol.* 29(5): 752–9.

126. Kratchmarova I. (2002) A Proteomic Approach for Identification of Secreted Proteins during the Differentiation of 3T3-L1 Preadipocytes to Adipocytes. *Molecular & Cellular Proteomics.* 1(3): 213–22.

127. Auld V. (1999) Glia as mediators of growth cone guidance: studies from insect nervous systems. *Cellular and Molecular Life Sciences.* 55(11): 1377–85.

128. Sepp KJ, Auld VJ. (2003) Reciprocal interactions between neurons and glia are required for Drosophila peripheral nervous system development. *J Neurosci.* 2003. 23(23): 8221–30.

129. Hummel T, Krukkert K, Roos J, Davis G, Klämbt C. (2000) Drosophila Futsch/22C10 is a MAP1B-like Protein Required for Dendritic and Axonal Development. *Neuron*. 26(2): 357–70.

130. Chang CH, Yu FY, Wu TS, Wang LT, Liu BH. (2010) Mycotoxin Citrinin Induced Cell Cycle G2/M Arrest and Numerical Chromosomal Aberration Associated with Disruption of Microtubule Formation in Human Cells. *Toxicological Sciences.* 119(1): 84–92.

131. Rhodes KE, Moon LDF, Fawcett JW. (2003) Inhibiting cell proliferation during formation of the glial scar: effects on axon regeneration in the CNS. *Neuroscience*. 120(1): 41–56.

132. Katsetos CD, Herman MM, Mörk SJ. (2003) Class III β-tubulin in human development and cancer. *Cell motility and the cytoskeleton.* 55(2): 77–96.

133. Lowery LA, Van Vactor D. (2009 The trip of the tip: understanding the growth cone machinery. *Nat Rev Mol Cell Biol.* 10(5): 332–43.

134. Shein Idelson M. (2011) Engineered neuronal circuits: a new platform for studying the role of modular topology. *Front Neuroeng.* 4(10): 1–8.

135. Boehler MD, Leondopulos SS, Wheeler BC, Brewer GJ. (2012) Hippocampal networks on reliable patterned substrates. *Journal of Neuroscience Methods.* 203(2): 344–53.

136. Li W, Xu Z, Huang J, Lin X, Luo R, Chen C-H, et al. (2014) NeuroArray: A Universal Interface for Patterning and Interrogating Neural Circuitry with Single Cell Resolution. *Sci Rep.* 4: 4784.

137. Schuster A, Yamaguchi Y. (2010) Application of Game Theory to Neuronal Networks. *Advances in Artificial Intelligence.* 2010: 521606.

138. Cohen Y, Cohen JY. (2009) Evolutionary game theory and the evolution

of neuron populations, firing rates, and decision making. *Nature Precedings.* Available at: http://hdl.handle.net/10101/npre.2009.3373.1.